

AD-A252 575



DOCUMENTATION PAGE

Form Approved
OMB No. 0704-0188

This document is a report of work performed by the Department of Defense, including the time for preparation, distribution, and dissemination of information. It is not to be distributed outside the Department of Defense without the approval of the Director of Defense Research and Engineering. Send comments regarding this document to the Director of Defense Research and Engineering, 1215 Jefferson Davis Highway, Arlington, VA 22202-4302. Send comments regarding this document to the Director of Defense Research and Engineering, 1215 Jefferson Davis Highway, Arlington, VA 22202-4302.

2. REPORT DATE
19923. REPORT TYPE AND DATES COVERED
THESIS/DESSERTATION

4. TITLE AND SUBTITLE

An in Vitro Corrosion Study of Two Implant Materials
Using Electrochemical Impedance Spectroscopy and
Potentiodynamic Polarization

5. FUNDING NUMBERS

6. AUTHOR(S)

Martin Williams Kerber, Captain

7. PERFORMING ORGANIZATION NAME(S) AND ADDRESS(ES)

AFIT Student Attending: University of Alabama

8. PERFORMING ORGANIZATION
REPORT NUMBER

AFIT/CI/CIA- 92-023

9. SPONSORING/MONITORING AGENCY NAME(S) AND ADDRESS(ES)

AFIT/CI
Wright-Patterson AFB OH 45433-6583

10. SPONSORING/MONITORING
AGENCY REPORT NUMBER

11. SUPPLEMENTARY NOTES

12a. DISTRIBUTION AVAILABILITY STATEMENT

Approved for Public Release IAW 190-1
Distributed Unlimited
ERNEST A. HAYGOOD, Captain, USAF
Executive Officer

12b. DISTRIBUTION CODE

13. ABSTRACT (Maximum 200 words)

DTIC
ELECTE
JUL 09 1992
S A D

92-17929



14. SUBJECT TERMS

15. NUMBER OF PAGES

147

16. PRICE CODE

17. SECURITY CLASSIFICATION
OF REPORT18. SECURITY CLASSIFICATION
OF THIS PAGE19. SECURITY CLASSIFICATION
OF ABSTRACT

20. LIMITATION OF ABSTRACT

AN IN VITRO CORROSION STUDY OF TWO IMPLANT MATERIALS USING
ELECTROCHEMICAL IMPEDANCE SPECTROSCOPY AND POTENTIODYNAMIC
POLARIZATION

by

MARTIN WILLIAMS KERBER



A THESIS

Accession For	
NTIS GRA&I	<input checked="" type="checkbox"/>
DTIC TAB	<input type="checkbox"/>
Unannounced	<input type="checkbox"/>
Justification	
By	
Dist. Data	
Availability Codes	
Dist	ST
A-1	

Submitted in partial fulfillment of the requirements for
the degree of Master of Science in the Department of
Materials Science and Engineering in the Graduate School,
The University of Alabama at Birmingham.

BIRMINGHAM, ALABAMA

1992

ABSTRACT

In vitro corrosion evaluations of commercially pure titanium (CP-Ti) and Ti-6Al-4V samples with different surface treatments were conducted using potentiodynamic polarization and electrochemical impedance spectroscopy (EIS). The different surface treatments tested were as-polished, nitric acid passivated (ASTM F86), and anodized. The test solution consisted of oxygenated 0.9 normal NaCl buffered to a pH of 7.3 at 37 °C. The corrosion properties were shown to be similar for the two metals in the polished and passivated condition. The CP-Ti was found to be more corrosion resistant than the Ti-6Al-4V in the anodized condition. For both metals, the anodized condition was much more corrosion resistant than the passivated condition which was more corrosion resistant than the as-polished condition. The oxide layer on both metals in the as-polished and passivated conditions as well as on the CP-Ti in the anodized condition was composed of non-porous TiO_2 . The protection provided by this layer was found to be related to its thickness. The oxide on the anodized Ti-6Al-4V was composed of a porous layer of hydrated TiO_3 on top of a nonporous layer of TiO_2 . Although this layer was thicker than that on the anodized CP-Ti, it did not provide as much protection against corrosion.

ACKNOWLEDGEMENTS

I would like to first thank my advisor Dr. Doug Rigney for his guidance throughout my Master's program, for free lunches and shuttle rides from Boligee.

Second, I would like to thank the faculty of "Juvenile Hall" for much comradery and intriguing political and philosophical debates and also because they make up 3/4 of my committee and I want to butter them up.

Next I would like to thank the Earle and Marion Nutter Scholarship trust for funding my graduate studies and the U.S. Air Force Academy Association of Graduates for administering this trust.

To the two men who's lack of faith in my abilities pushed me to prove them wrong I simply say, "Ha! Take that!"

Finally, to my wife, for enduring the lonely nights when I was 1000 miles away in the other room, and for listening patiently and acting interested even when you were clueless as to the meaning of all that engineering gibberish I was mumbling, I say thank you and I love you. Lets put this show on the road.

Its workin' out so far...

TABLE OF CONTENTS

	<u>Page</u>
ABSTRACT	ii
ACKNOWLEDGEMENTS	iii
LIST OF TABLES	vi
LIST OF FIGURES	vii
CHAPTER	
I. INTRODUCTION	1
Objective	3
Materials Selection	4
Analysis Techniques	5
A. Potentiodynamic Polarization	5
B. Electrochemical Impedance Spectroscopy	9
C. Energy Dispersive Spectroscopy (EDS)	18
D. Auger Electron Spectroscopy (AES)	19
II. LITERATURE REVIEW	21
Surface Treatments	21
Corrosion Measurement Techniques	22
Equivalent Circuit Models	25
Studies on Related Materials	33
III. EXPERIMENTAL PROCEDURE	36
Sample Preparation	36
Solution Preparation	41
Cell Setup	42
Water Bath	43
Potentiodynamic Polarization	46
Electrochemical Impedance Spectroscopy	47
Test Matrix	48
Energy Dispersive Spectroscopy	49
Auger Electron Spectroscopy	49
IV. RESULTS	51
Anodization Treatment	51

TABLE OF CONTENTS (Continued)

	<u>Page</u>
Potentiodynamic Polarization	52
Electrochemical Impedance Spectroscopy . . .	58
Energy Dispersive Spectroscopy	81
Auger Electron Spectroscopy	84
V. DISCUSSION	94
Anodization Treatment	94
Potentiodynamic Polarization	99
Electrochemical Impedance Spectroscopy . . .	107
Auger Electron Spectroscopy	135
Summary	137
VI. CONCLUSIONS	141
REFERENCES	145

LIST OF TABLES

<u>Table</u>	<u>Page</u>
1 Compositional Allowances for CP-Ti ³ and Ti-6Al-4V ⁴ .	4
2 Impedance for Various Circuit Elements	10
3 Test Matrix	48
4 Oxide Layer Thicknesses	93
5 Potentiodynamic Polarization Values	101
6 Circuit Element Values for EIS Circuit Model . . .	115
7 Circuit Element Values for the Anodized Ti-6Al-4V Circuit Model	132
8 Summary of Corrosion Results	138

LIST OF FIGURES

<u>Figure</u>	<u>Page</u>
1. Typical potentiodynamic polarization curve showing R_p and i_{corr} extrapolation. ⁵	7
2. Typical Bode plot with both the magnitude and phase angle plotted against the same frequency axis, showing how various circuit model values can be extrapolated. ⁷	12
3. Typical Nyquist plot showing how various circuit model values can be extrapolated. ⁷	13
4. Randle's circuit which is most basic circuit model for corroding interfaces.	14
5. Double layer at the surface of a metal in a solution which results from a charge differential across a thin film of non-charged solvent molecules ⁷	16
6. Equivalent circuit typically used to model the corrosion behavior of a coated metal.	17
7. Equivalent circuit model for a metal with a single non-porous surface layer.	27
8. Equivalent circuit model for a metal with a single porous surface layer.	28
9. Equivalent circuit model for a metal with two non-porous surface layers.	29
10. Equivalent circuit model for a metal with a porous surface layer on top of a non-porous surface layer.	30
11. Equivalent circuit model for a metal with two porous surface layers.	31

LIST OF FIGURES (Continued)

<u>Figure</u>	<u>Page</u>
12. Equivalent circuit which models pores in a surface layer as semi-infinite transmission lines where Z is the impedance per unit length between the pore wall and the solution within the pore. ¹⁰	32
13. Schematic drawing of the surface of anodized aluminum along with several different equivalent circuit models. ²³	34
14. Sample mounting technique.	39
15. Corrosion cell components and electrical connections.	44
16. Water bath and reservoir used to maintain the desired temperature without affecting the EIS measurements.	45
17. Potentiodynamic polarization curve obtained with the modified mounting procedure compared with the ASTM standard curve. ²⁸	53
18. Typical potential versus time trend during equilibration for the polished samples.	54
19. Various potential versus time trends during passivation for the passivated samples.	55
20. Various potential versus time trends during equilibration for the passivated samples.	57
21. Typical potential versus time trends during equilibration for the anodized samples.	59
22. Average potentiodynamic polarization curves for the polished CP-Ti and the polished Ti-6Al-4V.	60
23. Average potentiodynamic polarization curves for the passivated CP-Ti and the passivated Ti-6Al-4V.	61
24. Average potentiodynamic polarization curves for the anodized CP-Ti and the anodized Ti-6Al-4V.	62

LIST OF FIGURES (Continued)

<u>Figure</u>	<u>Page</u>
25. Average potentiodynamic polarization curves for the CP-Ti in the polished, passivated and anodized conditions. Error bars are given for the average E_{corr} on each curve.	63
26. Average potentiodynamic polarization curves for the Ti-6Al-4V in the polished, passivated and anodized conditions. Error bars are given for the average E_{corr} on each curve.	64
27a. Average Bode magnitude curves for the polished CP-Ti and the polished Ti-6Al-4V.	66
27b. Average Bode phase angle curves for the polished CP-Ti and the polished Ti-6Al-4V.	67
28. Average Nyquist curves for the polished CP-Ti and the polished Ti-6Al-4V.	68
29a. Average Bode magnitude curves for the passivated CP-Ti and the passivated Ti-6Al-4V.	69
29b. Average Bode phase angle curves for the passivated CP-Ti and the passivated Ti-6Al-4V.	70
30. Average Nyquist curves for the passivated CP-Ti and the passivated Ti-6Al-4V.	71
31a. Average Bode magnitude curves for the anodized CP-Ti and the anodized Ti-6Al-4V.	72
31b. Average Bode phase angle curves for the anodized CP-Ti and the anodized Ti-6Al-4V.	73
32. Average Nyquist Curves for the anodized CP-Ti and the anodized Ti-6Al-4V.	74
33a. Average Bode magnitude curves for the CP-Ti in the polished, passivated and anodized conditions.	75
33b. Average Bode phase angle curves for the CP-Ti in the polished, passivated and anodized conditions.	76

LIST OF FIGURES (Continued)

<u>Figure</u>	<u>Page</u>
34. Average Nyquist curves for the CP-Ti in the polished, passivated and anodized conditions.	77
35a. Average Bode magnitude curves for the Ti-6Al-4V in the polished, passivated and anodized conditions.	78
35b. Average Bode phase angle curves for the Ti-6Al-4V in the polished, passivated and anodized conditions.	79
36. Average Nyquist curves for the Ti-6Al-4V in the polished, passivated and anodized conditions.	80
37. Energy dispersive spectroscopy spectrum for the CP-Ti sample showing only the characteristic titanium peaks.	82
38. Energy dispersive spectroscopy spectrum for the Ti-6Al-4V sample showing the characteristic peaks for titanium, as well as aluminum and vanadium.	83
39. Auger electron spectroscopy surface spectra for the CP-Ti (a) and the Ti-6Al-4V (b), revealing the presence of vanadium in the Ti-6Al-4V sample.	85
40. AES depth profile for the polished CP-Ti.	87
41. AES depth profile for the polished Ti-6Al-4V.	88
42. AES depth profile for the passivated CP-Ti.	89
43. AES depth profile for the passivated Ti-6Al-4V.	90
44. AES depth profile for the anodized CP-Ti.	91
45. AES depth profile for the anodized Ti-6Al-4V.	92
46a. Potential - pH equilibrium diagram for titanium in water at 25 °C, considering Ti_2O_3 and TiO_2 as the derivatives of tri- and tetravalent titanium. ²⁹	97

LIST OF FIGURES (Continued)

<u>Figure</u>	<u>Page</u>
46b. Potential - pH equilibrium diagram for titanium in water at 25 °C, considering $\text{Ti}(\text{OH})_3$ and $\text{TiO}_2 \cdot \text{H}_2\text{O}$ as the derivatives of tri- and tetravalent titanium. ²⁹	98
47. Equivalent circuit used to model the polished and the passivated CP-Ti and Ti-6Al-4V and the anodized Ti-6Al-4V as having a single layer of non-porous TiO_2	113
48a. Bode magnitude plot comparing the average measured values to the calculated equivalent circuit values for polished CP-Ti.	116
48b. Bode phase angle plot comparing the average measured values to the calculated equivalent circuit values for polished CP-Ti.	117
49a. Bode magnitude plot comparing the average measured values to the calculated equivalent circuit values for polished Ti-6Al-4V.	118
49b. Bode phase angle plot comparing the average measured values to the calculated equivalent circuit values for polished Ti-6Al-4V.	119
50a. Bode magnitude plot comparing the average measured values to the calculated equivalent circuit values for passivated CP-Ti.	120
50b. Bode phase angle plot comparing the average measured values to the calculated equivalent circuit values for passivated CP-Ti.	122
51a. Bode magnitude plot comparing the average measured values to the calculated equivalent circuit values for passivated Ti-6Al-4V.	122
51b. Bode phase angle plot comparing the average measured values to the calculated equivalent circuit values for passivated Ti-6Al-4V.	123
52a. Bode magnitude plot comparing the average measured values to the calculated equivalent circuit values for anodized CP-Ti.	124

LIST OF FIGURES (Continued)

<u>Figure</u>	<u>Page</u>
52b. Bode phase angle plot comparing the average measured values to the calculated equivalent circuit values for anodized CP-Ti.	125
53. Equivalent circuit used to model the anodized Ti-6Al-4V as having a porous layer of $\text{TiO}_3 \cdot 2\text{H}_2\text{O}$ over a non-porous layer of TiO_2	131
54a. Bode magnitude plot comparing the average measured values to the calculated equivalent circuit values for anodized Ti-6Al-4V.	133
54b. Bode phase angle plot comparing the average measured values to the calculated equivalent circuit values for anodized Ti-6Al-4V.	134

CHAPTER I

INTRODUCTION

There is considerable concern over the release of metallic ions from implant materials into the body.¹ This concern stems from the fact that some of these ions are known to be harmful to human tissue and other ions are suspected to be harmful.

The rate at which metallic ions are released is analogous to the corrosion rate. Therefore, by reducing the corrosion rate, the number of metallic ions released into the body would be decreased. One way to reduce the corrosion rate of implants is to apply a protective coating to the implant material that reduces the corrosion rate of the base metal.

Two common metals used for implants today are commercially pure, or grade two, titanium (CP-Ti) and titanium alloyed with six percent aluminum and four percent vanadium (Ti-6Al-4V). Commercially pure titanium has the lower yield strength of the two, but it has very good corrosion resistance in the body, and its corrosion products are considered to be non-harmful.² The Ti-6Al-4V has much greater strength, but there is concern over the release of aluminum and vanadium into the body.²

Both of these materials are active/passive metals. This means that they oxidize but in doing so they form an adherent, protective oxide layer on their surface which decreases the oxidation rate of the parent material underneath. This protective coating can be enhanced by passivation in which a corrosive media (such as an acid) is used to rapidly oxidize the surface, thereby protecting it. Passivation typically produces a thicker oxide layer than would form naturally and therefore offers additional corrosion protection. The oxide can be further enhanced by anodization which consists of oxidizing the surface by driving a current through the material while it is in a corrosive media. The affects of these different surface treatments can be evaluated electrochemically.

Electrochemical techniques for corrosion analysis are based on either direct current (DC) or alternating current (AC). Direct current techniques have been around longer than AC techniques and provide results that are easy to interpret. This study uses the DC technique of potentiodynamic polarization in order to determine corrosion rates for the different materials and surface treatments. Alternating current techniques, more specifically electrochemical impedance spectroscopy (EIS), are fairly new to corrosion science and are therefore still open to interpretation. These techniques, however, offer insight into not only bulk corrosion rates but also into the kinetics occurring at the corroding interface. EIS techniques are therefore used to

evaluate the protective nature of the oxide layers formed on the materials.

Objective

The objective of this study was to analyze the corrosion mechanisms that occur on the surfaces of orthopedic implant materials that had been subjected to surface preparations designed to increase their corrosion resistance through enhancement of their native oxide. A further objective of this study was to compare and contrast the corrosion information obtained from two different analysis techniques: potentiodynamic polarization and electrochemical impedance spectroscopy. The following hypotheses were developed and evaluated in this study:

1. For the same surface preparation, CP-Ti will be more corrosion resistant than Ti-6Al-4V.
2. For the same material, the anodized condition will be more corrosion resistant than the passivated condition, which will be more corrosion resistant than the polished condition.
3. For the same material, the oxide layer on the anodized sample will be thicker than the oxide layer on the passivated sample, which will be thicker than the oxide layer on the polished sample.
4. A thicker oxide coating will correspond to a lower corrosion current density as determined from potentiodynamic polarization.

5. The polarization resistance obtained from the EIS will be equal to the polarization resistance as determined from the potentiodynamic polarization.

6. The resistance calculated from the applied current and potential during anodization will be the same as that calculated from the equilibrium current and potential.

7. The impedance data for the different materials and surface preparations will behave as analogous electrical circuits.

8. A thicker oxide coating will correspond to higher pore resistances and higher coating capacitances as determined from EIS.

Materials Selection

The two materials selected for this study, CP-Ti and Ti-6Al-4V, have compositional tolerances defined by ASTM F67³ and ASTM F136⁴, respectively, as given in Table 1.

TABLE 1
Compositional Allowances for CP-Ti³ and Ti-6Al-4V⁴

ELEMENT	COMPOSITION %	
	CP-Ti	Ti-6Al-4V
Nitrogen, max	0.03	0.05
Carbon, max	0.10	0.08
Hydrogen, max	0.0125	0.012
Iron, max	0.30	0.25
Oxygen, max	0.25	0.13
Aluminum	---	5.5 - 6.50
Vanadium	---	3.5 - 4.5
Titanium	balance	balance

Samples of each of these two materials were prepared from commercially available 5/8 inch diameter bar stock. In each case the bar had been drawn to final shape. The 5/8 inch diameter was chosen to coincide with commercially available corrosion test samples. The sample preparation is covered in the procedure section which follows.

Conditions in the body were simulated by using a 0.9 normal sodium chloride (NaCl) solution that was buffered to normal body pH (7.3), saturated with oxygen and heated to normal body temperature (37 °C).

Analysis Techniques

Electrochemical corrosion is so named because there is both an electrical and a chemical component. The chemical breakdown of a metal produces free ions and electrons. This in turn results in a potential that is characteristic to the particular metal/solution system and a current density that is indicative of the rate at which ions are leaving the surface (i.e., the corrosion rate). On any corroding surface, there are areas of local anodic and local cathodic activity. Because of this, the net current density of the system is zero. Consequently, the corrosion current density cannot be measured directly, but must be determined by a specialized corrosion measurement technique such as potentiodynamic polarization.

A. Potentiodynamic Polarization

Potentiodynamic polarization is a direct current technique which is conducted by forcing the corrosion system

away from its equilibrium potential by driving a current through the system. The current is adjusted so that the potential scans through a specified range at a specified rate. The potentials as well as the current densities applied to produce them are recorded at set intervals. The potential is driven first in the cathodic (more negative) direction, and then in the anodic (more positive) direction. The anodic portion follows the cathodic test because it induces increased corrosion of the sample, thereby damaging the surface.

Very near the corrosion potential, where the net current density approaches zero, the slope of the potential versus current density curve is linear. The slope of this line determines the polarization resistance, R_p , or the resistance of the material to corrosion as a result of an induced potential. The potential versus current density is linear only over a small potential range, usually about 10 mV on either side of the corrosion potential. Therefore, the calculation for R_p must be made within this linear polarization range which is indicated in Figure 1.

The value can easily and accurately be determined by computer. This is done by conducting a linear regression fit to the potentiodynamic polarization data within 10 mV of the corrosion potential. Since this technique depends on a narrow potential range, it is necessary that the corrosion potential be fairly stable and that there be little noise around the corrosion potential.⁶ If there is too much

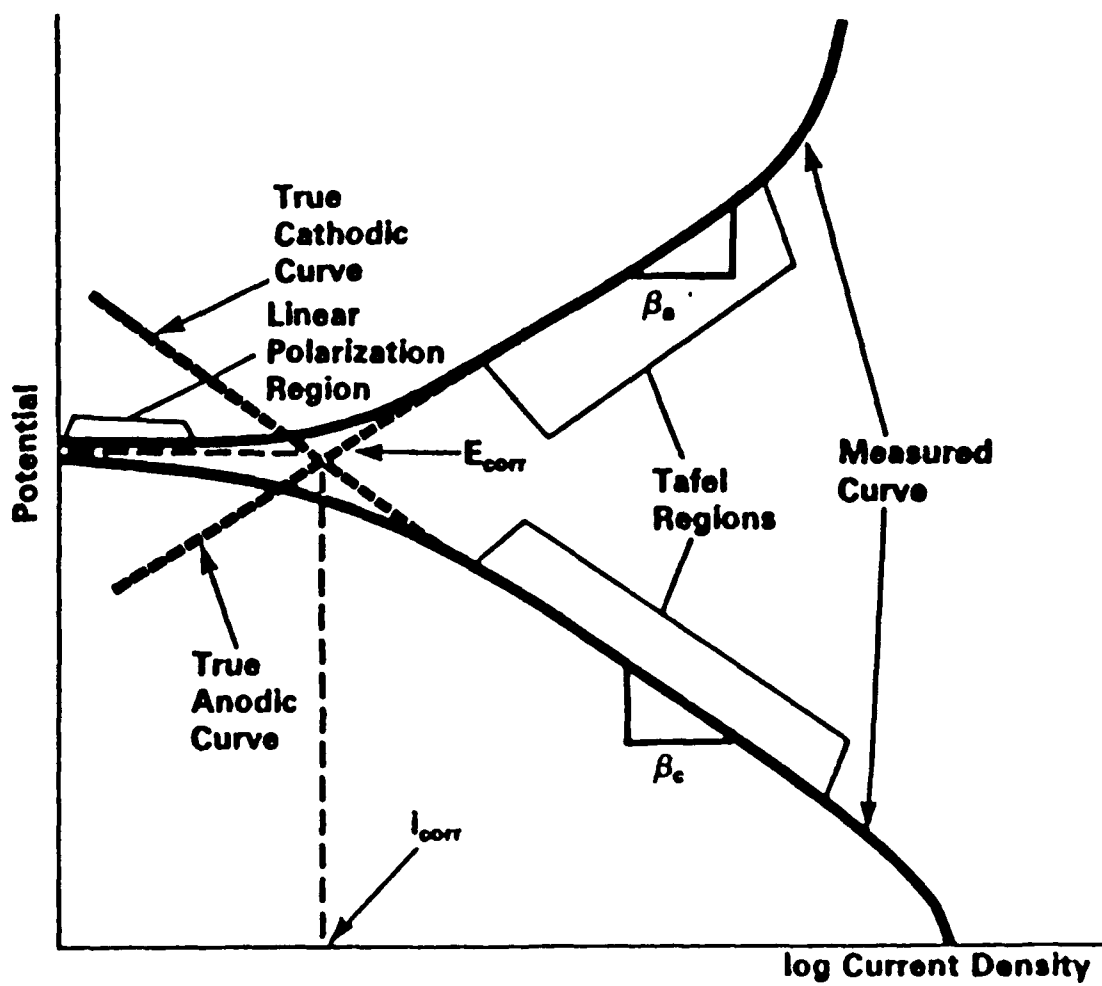


FIGURE 1. Typical potentiodynamic polarization curve showing R_p and i_{corr} extrapolation.⁵

curvature within a close potential range, the computer cannot perform the linear regression. If there is too much scatter in the data, the computer will perform the calculation but the correlation between the linear regression and the measured data will be low. The correlation can sometimes be improved by choosing a wider potential range, but this must be done with care so that the regression does not extend past the linear region of the curve.

While the calculation of R_p requires that the current densities be plotted linearly, potentiodynamic polarization data is usually plotted versus the log of the current density. This semi-log plot is used due to the wide range of current density values typically measured in a potentiodynamic polarization test. Furthermore, when plotted in this fashion, the plot shows two linear regions, called the Taffel regions as shown in Figure 1.

This plot of potential versus log current density is used to determine the corrosion current density, i_{corr} . This can be done manually by extrapolating the linear portion of the cathodic and anodic curves back to the equilibrium corrosion potential, E_{corr} , as shown in Figure 1. Some materials have a tendency to passivate, which is the formation of a protective oxide film. This causes the anodic curve to show a lower current density due to the protective nature of the layer. Therefore, if the material of interest passivates, then the anodic portion of the curve can not be used in the extrapolation process. Since all of the

materials used in this study passivate, only the cathodic curves will be extrapolated.

Besides this manual extrapolation technique, there are computer aided techniques to determine the corrosion current. These techniques, however, have some difficulty with passivated systems, particularly in systems with low corrosion current densities. Therefore, this data should not be used without verifying it against the manual extrapolation technique.




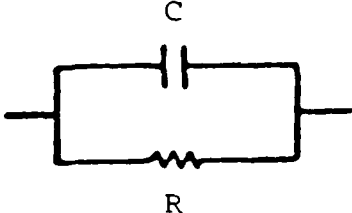
Direct current electrochemical measurement techniques have been in use for some time and are useful in determining bulk corrosion rates. These techniques, however, do not provide any information on the corrosion mechanisms occurring at the corroding interface nor do they allow any mechanistic analysis of protective coatings other than changes in the bulk corrosion rate of the coated material. The newer technique of electrochemical impedance spectroscopy (EIS) can be used not only to obtain corrosion rates of implant materials but also to evaluate the protective nature of applied coatings.

B. Electrochemical Impedance Spectroscopy

Electrochemical impedance spectroscopy, EIS, is an alternating current (AC) technique. In AC circuits, the current flow is impeded not only by resistors as in DC circuits, but also by capacitors and inductors. Furthermore, both the current and the potential are frequency dependent so the impedance has both a magnitude, $|Z|$, and a phase angle,

Θ. This gives the impedance both a real (Z') and an imaginary (Z'') component. Purely resistive elements are not dependent on frequency and have only real impedance components. Capacitors and inductors are dependent on frequency and have only imaginary components. The impedances of these circuit elements are given in Table 2.

TABLE 2
Impedance for Various Circuit Elements

Circuit Element	Impedance Equation	
<p>R</p> 	$Z = R + 0j$	$j = \sqrt{-1}$
<p>C</p> 	$Z = 0 - \frac{j}{\omega C}$	$\omega = 2\pi f$
<p>L</p> 	$Z = 0 + j\omega L$	$\omega = 2\pi f$
<p>C</p>  <p>R</p>	$Z = \frac{R}{1 + \omega^2 C^2 R^2} - \frac{j\omega C R^2}{1 + \omega^2 C^2 R^2}$	

EIS tests are conducted by applying a small sinusoidal waveform about the equilibrium corrosion potential of a test sample. The amplitude of the perturbations is small enough (about 5 to 10 mV) so that no permanent damage is done to the

test surface. The frequency is varied in order to obtain the full range of responses. Ideally, the low frequency end is low enough to approximate a zero frequency (or direct current), and the high frequency end is high enough to approximate an infinite frequency. After gathering impedance data for the frequency range selected, the data is plotted, typically in one of two formats.

The Bode plot (Figure 2) is a polar representation of the impedance data which gives both the magnitude, $|Z|$, and the phase shift, Θ , of the impedance versus the frequency. The magnitude curve will reach a plateau and the phase angle curve will approach zero as they approach both the zero and the infinite frequency conditions. The Nyquist plot (Figure 3) is a rectangular representation of the EIS data which shows the imaginary, Z'' , versus the real, Z' , component of the impedance. The imaginary component of this plot will approach zero as the frequency approaches both the zero and infinite conditions.

One of the advantages of EIS is that the data can be used to model the corrosion interface as an equivalent circuit. The Randle's circuit shown in Figure 4 is often used to model corrosion systems.⁷ In this model, R_Ω is the uncompensated resistance of the test solution. The C_{DL} term is the double layer capacitance which describes the adsorption and desorption occurring at the surface of the corroding material.⁸ The double layer forms when cations leave the surface of the metal, leaving a negative charge on

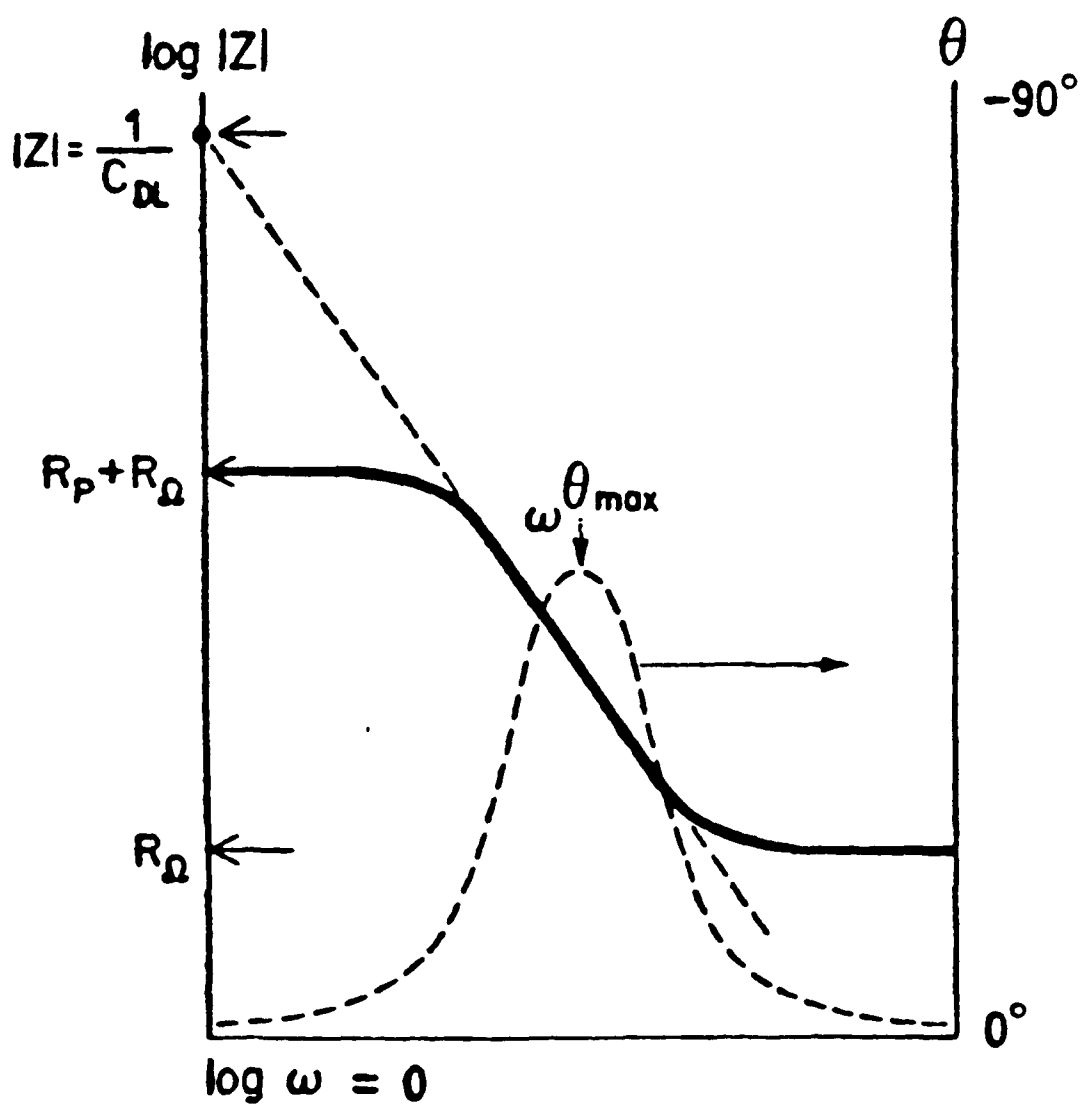


FIGURE 2. Typical Bode plot with both the magnitude and phase angle plotted against the same frequency axis, showing how various circuit model values can be extrapolated.⁷

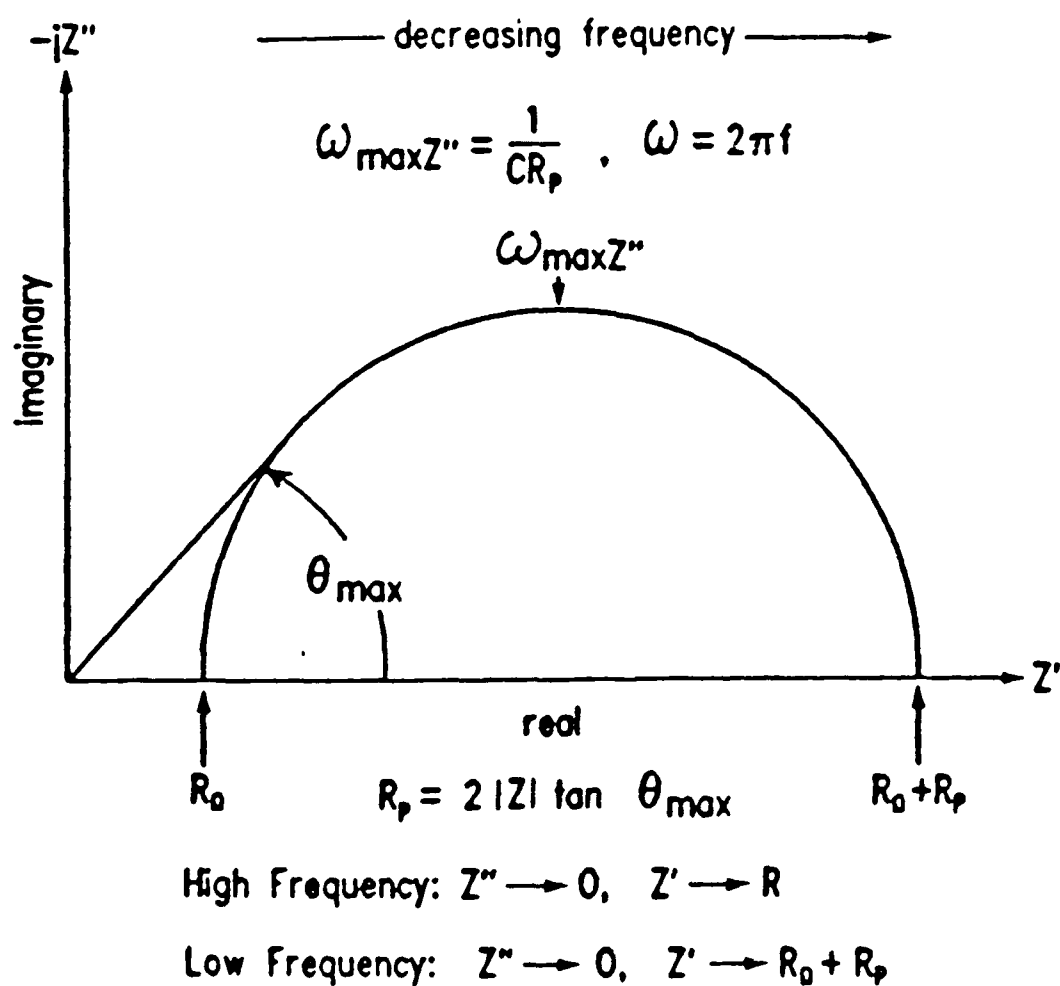


FIGURE 3. Typical Nyquist plot showing how various circuit model values can be extrapolated.⁷

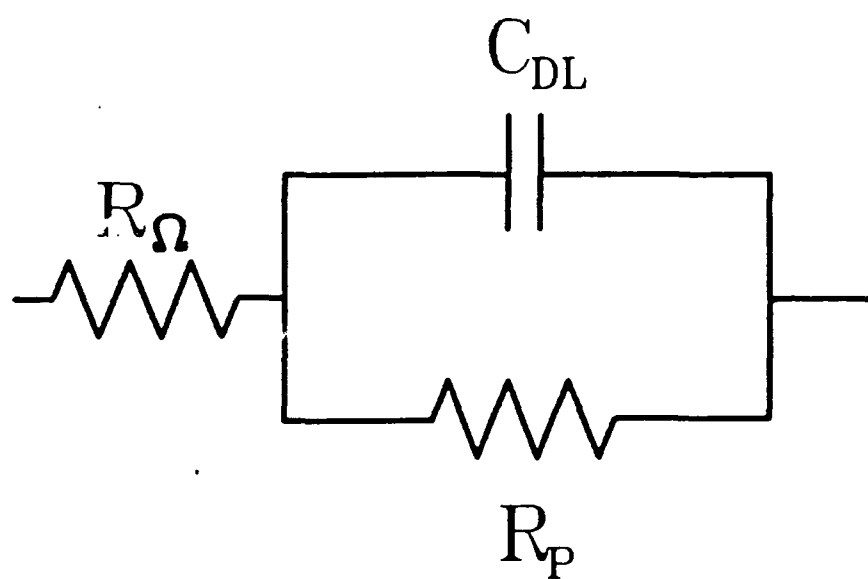


FIGURE 4. Randle's circuit which is most basic circuit model for corroding interfaces.

the metal. This results in a charge differential⁷ across a thin film of solution, which acts as a capacitor as shown in Figure 5. The R_p element is the polarization resistance which is the charge-transfer resistance at the sample/solution interface.⁸ This resistance results when the cations leaving the surface and the anions going to the surface interfere with each other, thus limiting the rate of charge transfer and the corrosion rate.

From the impedance relations given in Table 2 it can be seen that as the frequency approaches infinity, the capacitor in the Randle's circuit approaches a short circuit and the total impedance is equal to that of R_0 . Similarly, as the frequency approaches zero, the capacitor approaches an open circuit and the total impedance is equal to the sum of R_0 and R_p . The values of these circuit elements as well as the double layer capacitance, C_{DL} , can be obtained from either the Bode plot (Figure 2) or the Nyquist plot (Figure 3) as long as the frequency range was adequate to approximate both the zero and infinite frequency conditions.

For a metal with a porous, nonconductive coating such as an oxide film, a more complicated equivalent circuit such as the one shown in Figure 6 may be necessary.⁷ In this case the coating capacitance, C_c , is the capacitance across the nonconductive coating, and the pore resistance, R_{po} , is the resistance to diffusion through the coating.⁹ Models such as this one, that are more complex than the Randle's circuit, cannot be solved directly from the Bode and Nyquist plots.

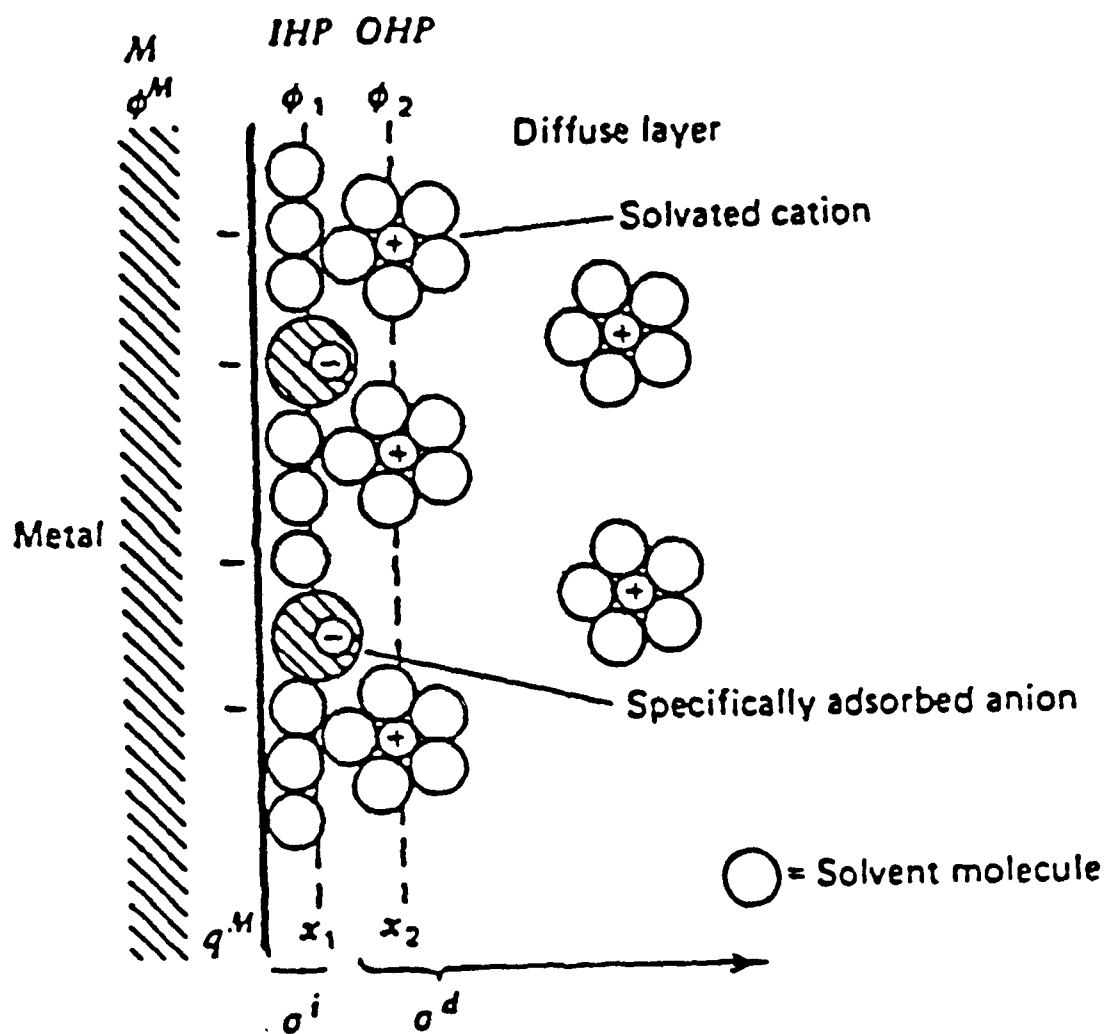


FIGURE 5. Double layer at the surface of a metal in a solution which results from a charge differential across a thin film of non-charged solvent molecules.⁷

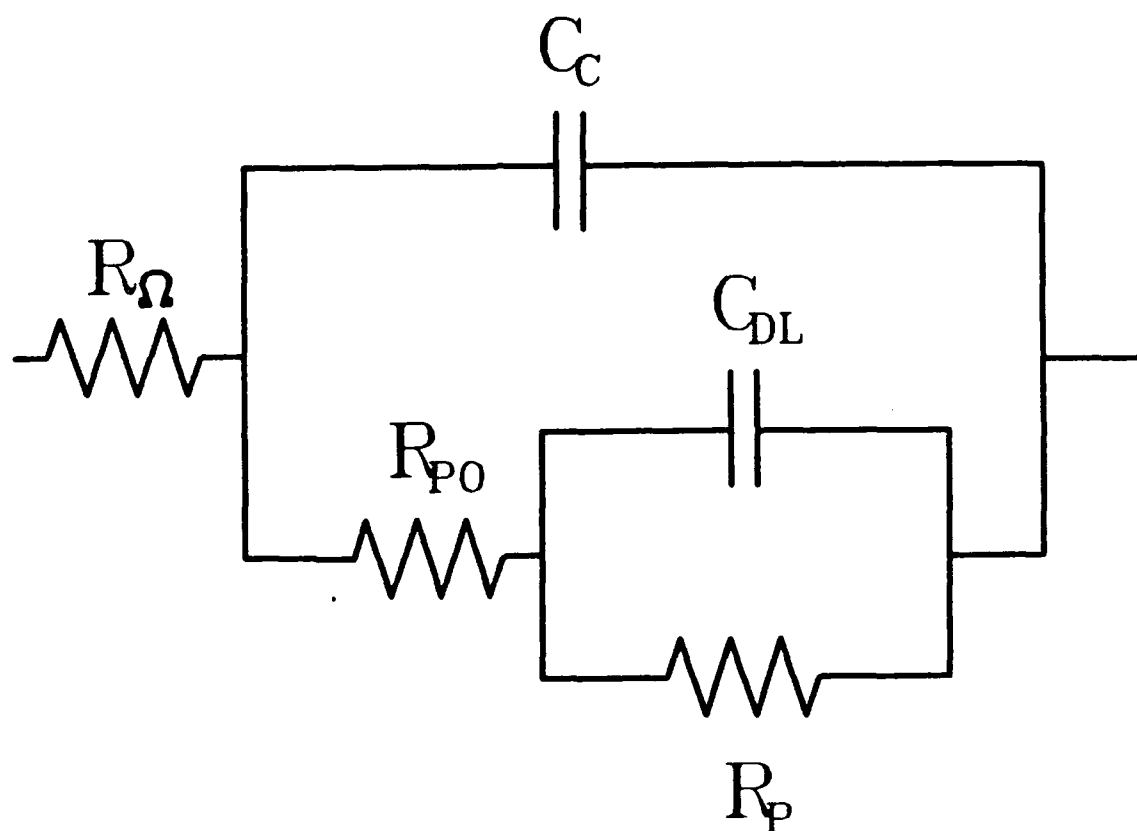


FIGURE 6. Equivalent circuit typically used to model the corrosion behavior of a coated metal.

For these more complicated cases, software exists that will allow the user to input a generic model (without values) and the computer will calculate values for the circuit elements to coincide with the impedance data that was measured. The use of computer software to model EIS data greatly simplifies the task of evaluating coatings, and models can be created that have very close agreement with the measured data. It should be pointed out that the software is designed to fit the data and it is up to the user to ensure that the circuit components have some significance to the corrosion system.

The literature contains other models that may be found to be useful. These range from theoretical models that can be applied to many different systems¹⁰ to complex computer generated circuit models that can be applied to only the case for which they were derived.¹¹ Several of these models will be discussed later in this thesis. For a start, however, it is best to stick to a simple, well established and well defined model such as the Randle's circuit to begin analysis.

C. Energy Dispersive Spectroscopy (EDS)

When electrons strike a target material, x-rays are produced with energy levels characteristic of the element that produced the x-ray. The composition of a material can then be determined by measuring the energies of the x-rays produced and the relative numbers of x-rays at each energy. This technique is of primary interest in verifying the

approximate compositions of the CP-Ti and the Ti-6Al-4V samples.

D. Auger Electron Spectroscopy (AES)

Auger electron spectroscopy is a surface analysis tool that functions similarly to EDS but it measures Auger electrons instead of x-rays. These electrons have a much lower energy than characteristic x-rays. Consequently, only those Auger electrons produced very near the surface are able to escape from the sample to be detected. This technique also allows the detection of lighter elements (such as oxygen) than can be found with EDS. This is useful to this project since it will allow the different surface conditions to be more fully evaluated.

The Auger electron microscope also has a depth profiling capability. In this capacity, a surface analysis is made, then argon ions are used to sputter a very thin layer off the surface of the sample. After sputtering, a compositional analysis is conducted of the newly exposed surface. This process of sputtering and surface analysis is repeated until the surface layer has been penetrated and only the base material remains. At this point, the composition measured after each cycle can be plotted as a function of the number of sputtering cycles to determine how the composition of the surface layer changes across its thickness. A quantitative relationship between the amount of sputtering and the thickness of the surface layer could not be made here. The thickness of one coating relative to another, however, was to

be compared in terms of sputtering time. The relative thicknesses of the oxide coatings were compared to the differences in corrosion rates for the different materials and surface treatments.

CHAPTER II

LITERATURE REVIEW

Surface Treatments

Arguably the most fundamental, yet often overlooked piece of corrosion related literature is the Atlas of Electrochemical Equilibria in Aqueous Solutions by Marcel Pourbaix. This reference contains the potential versus pH (Pourbaix) diagrams for various metals. These diagrams provide the thermodynamics of corrosion in terms of potential and pH.⁵ The chapter on titanium is useful in this study in that it defines the regions of equilibrium for the different oxides of titanium, as well as information on the nature of the different oxides themselves.¹² This information is particularly important when attempting to evaluate the effects of different methods of improving corrosion resistance through oxide enhancement.

Titanium implant materials are routinely subjected to nitric acid passivation¹³ which enhances the natural oxide on the surface. To further protect its surface, titanium can be anodized in a number of different solutions.^{14,15,16} Anodization has been shown to produce a much thicker oxide than the nitric acid passivation and this has been related to better corrosion properties.¹⁵ Furthermore, the applied currents and

potentials during anodization had been shown to produce different color oxide layers on the surface of the metal.¹⁶ These different colors were shown to correspond to different oxide thicknesses and different corrosion properties. Pourbaix, however, attributed the different colors of the oxides to different compositions.¹²

It is suspected that anodization initially produces low valency oxides of titanium which require extended time at potential in order to transform to the more stable TiO_2 .¹⁴ The oxides formed during anodization were also determined to be duplex in nature, with the outer layer being more susceptible to dissolution than the inner layer.¹⁴

Corrosion Measurement Techniques

The most basic types of corrosion tests are exposure tests in which the subject material is exposed to actual use conditions for a period of time and monitored for such things as visible corrosion and weight loss.¹⁷ These techniques are slow to produce results. The speed of analysis is one of the biggest advantages of electrochemical corrosion measurement techniques.

Electrochemical corrosion measurement techniques have been around for some time. The most common are the direct current (DC) techniques such as potentiodynamic polarization. There are countless papers written on this technique and its variations. These tests provide information on corrosion rates, passivation properties, pitting and crevice corrosion.⁵ The various DC techniques have provided a wealth of

information on the corrosion properties of many materials, however they do not give any information as to the kinetics of the corrosion processes that are occurring. Furthermore, DC polarization can often damage the surface that is being tested.¹⁸

A more informative electrochemical technique is that of electrochemical impedance spectroscopy, EIS. Impedance spectroscopy has been around for some time and many of its diverse applications are discussed in a text by Macdonald.¹⁹ The application of these techniques to electrochemistry, however, is just now starting to see widespread use. The lack of popularity of this technique has been primarily due to the need for sophisticated electronic equipment.⁵ Thanks to the recent advances in microelectronics, EIS hardware and software have now become readily accessible to investigators in both industry and academia.⁵

The study of corrosion by EIS offers many advantages over the use of DC techniques. The main advantage, however, is the ability to determine the corrosion mechanisms that are occurring on a surface. This can be done by modeling the impedance data obtained as an equivalent electrical circuit. While some caution against the use of such analogues due to the risk of oversimplification, these equivalent circuits are generally accepted as a link between the observed impedances and the electrochemical processes that caused them.²⁰ The most basic model is the simple RC circuit as shown in Figure 4. It has been found that coated metals exhibit this type of

impedance behavior only when their coatings contain water and ions.¹⁸ Since the water was dispersed throughout the coating, however, there was no corrosion of the base metal or delamination of the coating observed.¹⁸ The general impedance model for a coated metal (Figure 6) applies when the metal under the coating is corroding due to free water accumulating at the coating-metal interface.¹⁸

Another study by Tait²¹ showed that the Bode phase angle plots can be used to identify the frequency of different time constants (or different electrochemical events). The capacitance values determined from the Bode magnitude plots at the same frequencies can then be used to determine what types of processes are occurring. The ranges of capacitive values that correspond to particular processes are dependent on the particular system.

Equivalent circuits often contain diffusion related terms such as a Warburg impedance which is used to model semi-infinite diffusion. Macdonald²⁰ found that when such diffusion processes are significant to the system, they generally begin to dominate the impedance at frequencies below 1 Hz.

With relatively little work in the area of EIS, the researcher may ask how one can be sure that the data itself is correct. Kramers-Kronig transforms have been used to evaluate impedance data for decades. These transforms compare the real and the imaginary impedance data to each other to see if they belong together. The Kramers-Kronig

transforms can identify if data is good but they cannot prove that data is bad.¹⁰ Furthermore, these transforms require that the entire impedance spectra be present, that is, the data must reach its low frequency limit in order to be accurate.²² Recent studies²³ have shown that the impedance data for many systems such as polymer coated materials and anodized aluminum do not reach this limit. It is therefore necessary to evaluate impedance data by another method. One suggestion is to use the Bode phase angle plot to evaluate the fit of equivalent circuits to the data.²³ This is suggested due to the sensitivity of the phase angle to the presence of additional frequency dependent events, also known as time constants.

Equivalent Circuit Models

When modeling a set of impedance data as an equivalent circuit it must be remembered that each component of the model must represent some physical phenomena or the model will have no real significance to the data. The models presented earlier are the most general models that are commonly used. Often times, however, these models do not accurately describe the complex nature of the electrochemical processes that are occurring. Because of this, many other more specialized models have been developed for different circumstances. Of principle interest are those models that deal with metals which have been coated or oxidized.

Juttner and Lorenz²⁴ have presented several impedance models for different types of protective surface layers. The

first type is for a metal with a uniform, protective surface layer. This is modeled as a simple RC circuit with a layer capacitance, C_L , and a layer resistance, R_L , as shown in Figure 7. The series resistance, R_Ω , represents the solution resistance.

If the uniform layer is porous, the circuit becomes more complex as shown in Figure 8. In this case, the same reaction as before is occurring away from the pores. At the pores, however, there is a pore resistance, R_{po} , in series with an RC sub-circuit which represents the double layer capacitance, C_{DL} , and corrosion resistance, R_{corr} , at the surface of the exposed metal.

From these two models, three additional models are derived for the two layer conditions of two non-porous layers, one porous and one non-porous layer, and two porous layers. These models are presented in Figures 9, 10 and 11, respectively.

Another model presented for porous films is the transmission-line equivalent circuit.¹⁰ This circuit models an individual pore as an infinitely long pore through an infinitely conductive solid phase as shown in Figure 12. There is a solution resistance per unit length along the pore and a pore wall/solution impedance per unit length. The problem with this model is the assumption of the infinitely conductive coatings. While this may be fine for metallic coatings, it is not generally valid for organic and oxide coatings.

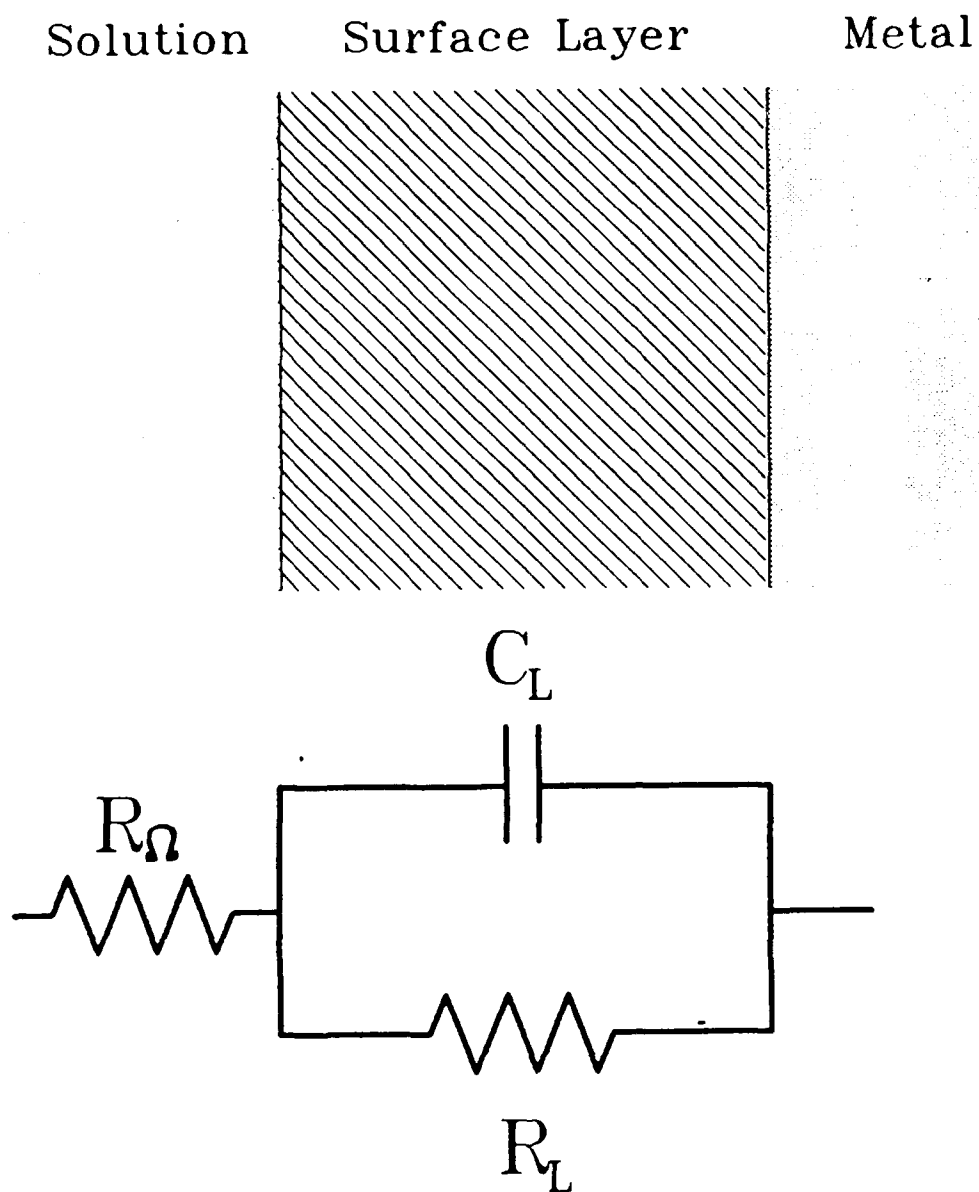


FIGURE 7. Equivalent circuit model for a metal with a single non-porous surface layer.

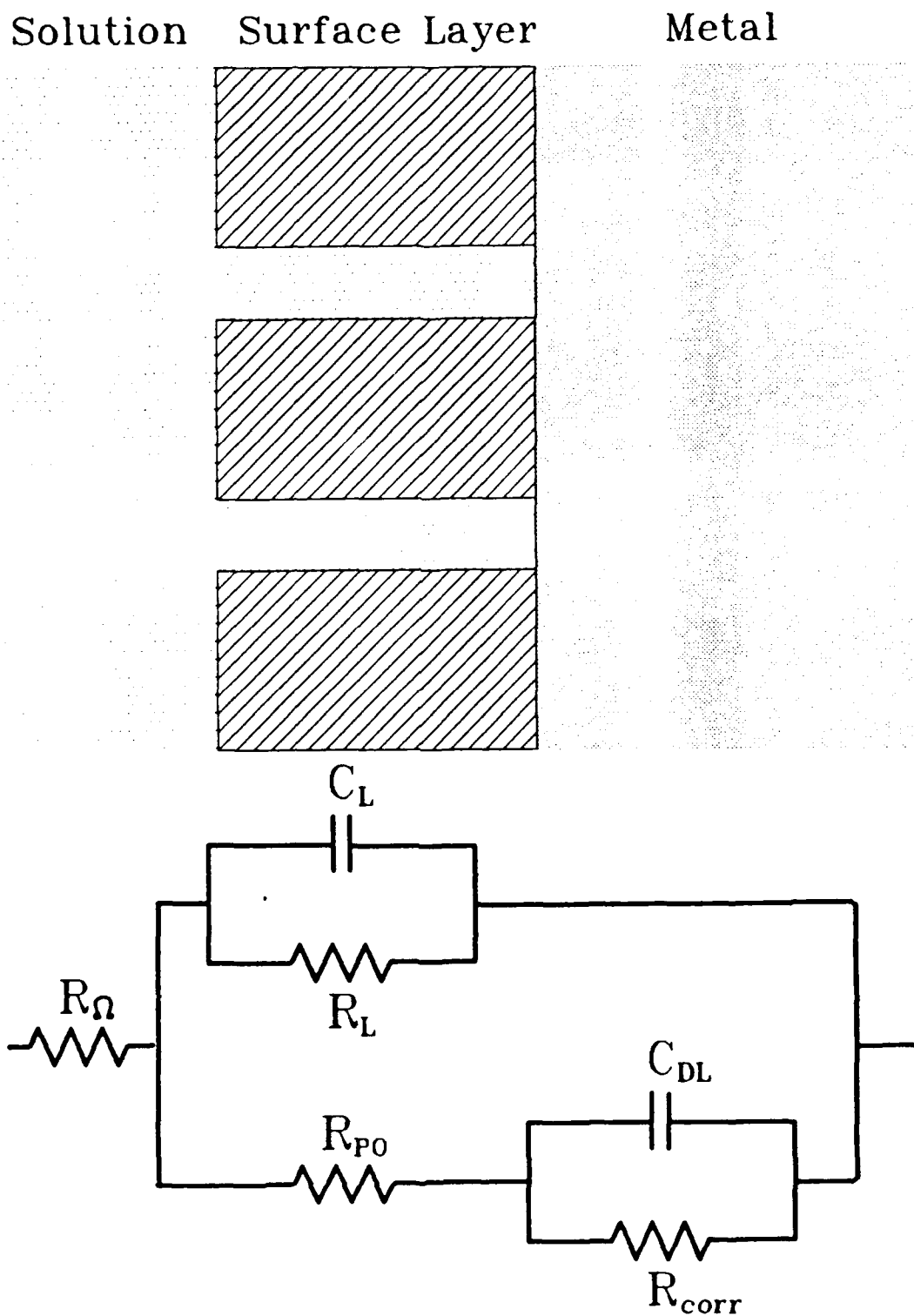


FIGURE 8. Equivalent circuit model for a metal with a single porous surface layer.

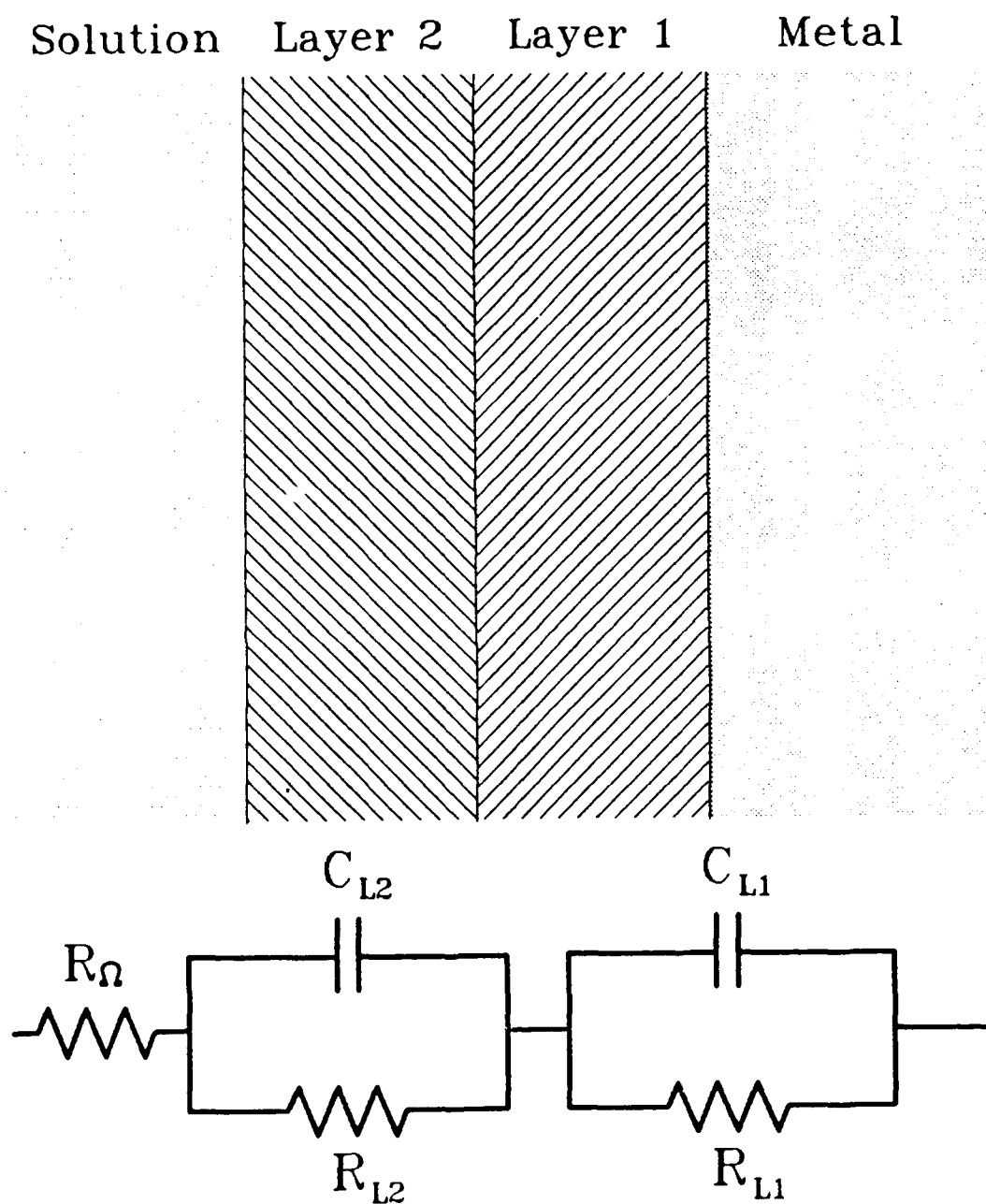


FIGURE 9. Equivalent circuit model for a metal with two non-porous surface layers.

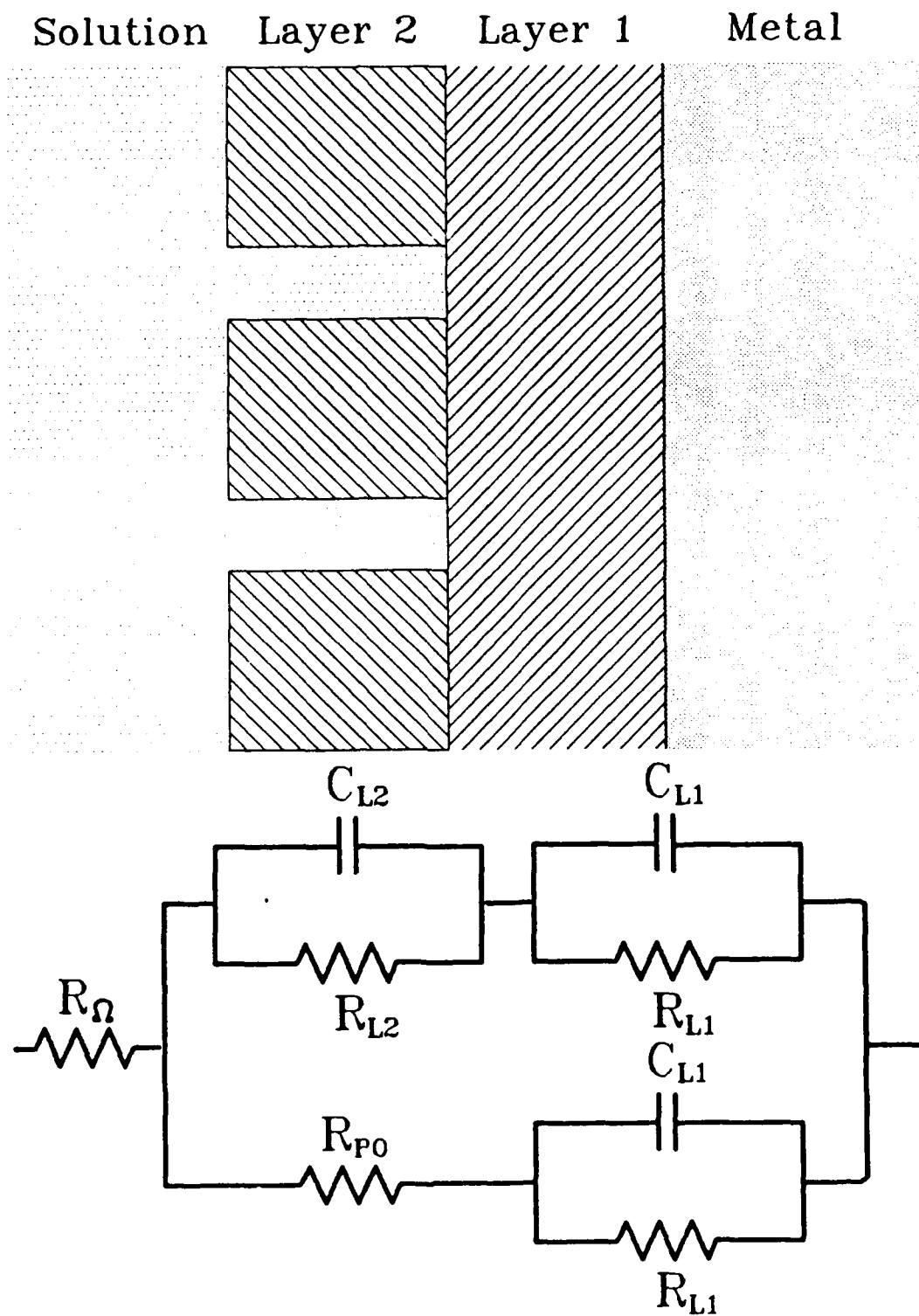


FIGURE 10. Equivalent circuit model for a metal with a porous surface layer on top of a non-porous surface layer.

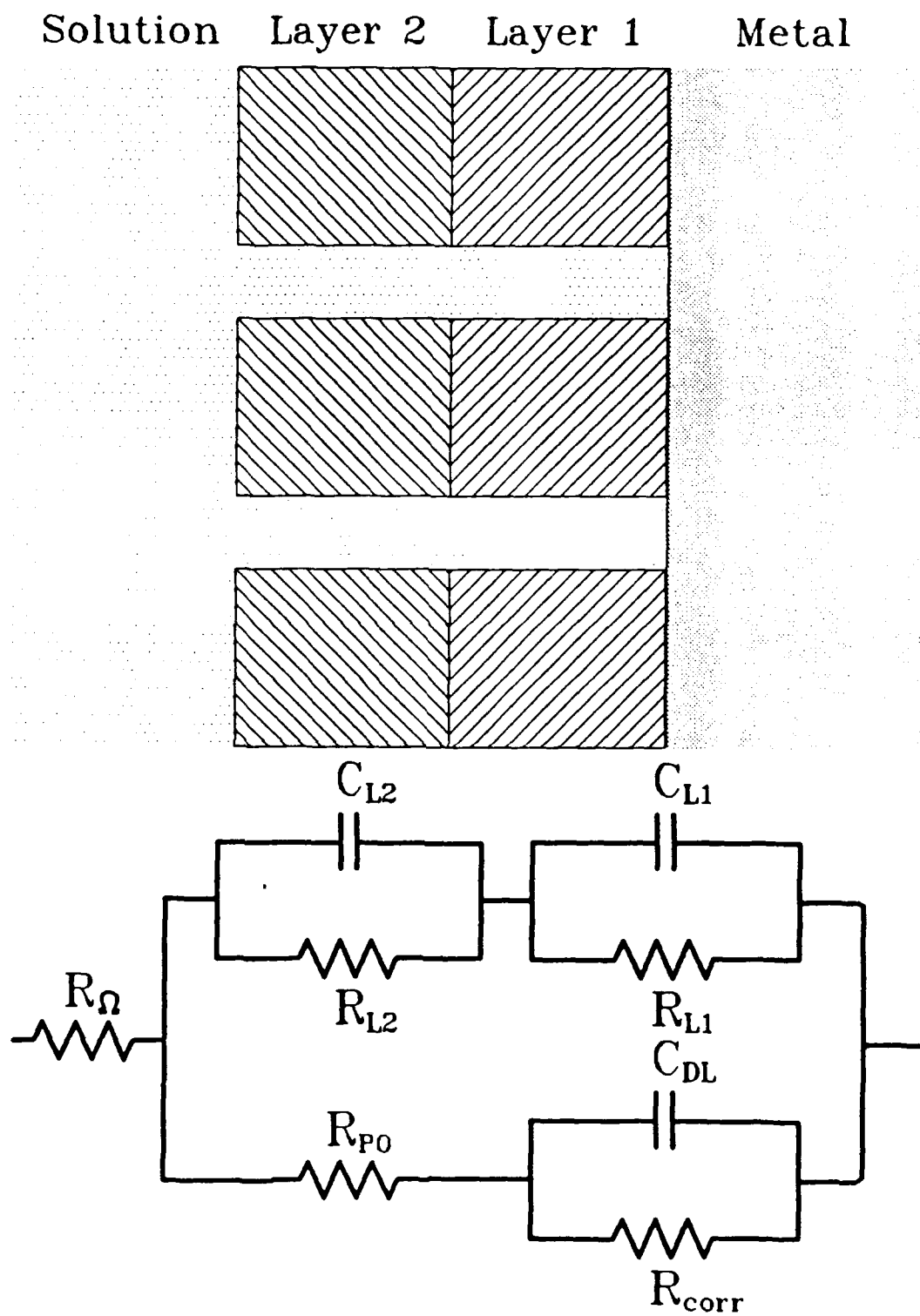


FIGURE 11. Equivalent circuit model for a metal with two porous surface layers.

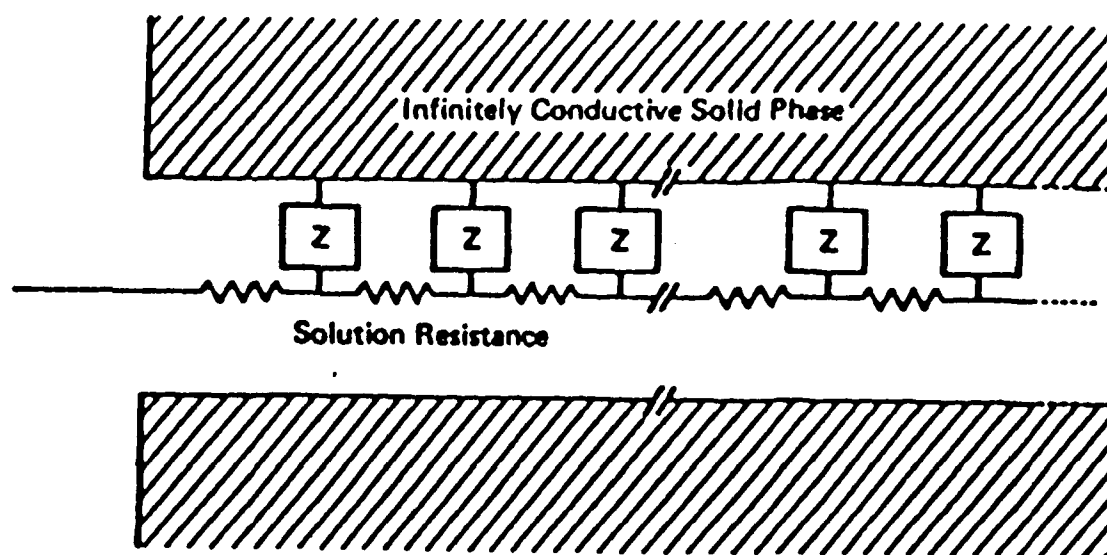


FIGURE 12. Equivalent circuit which models pores in a surface layer as semi-infinite transmission lines where Z is the impedance per unit length between the pore wall and the solution within the pore.¹⁰

Studies on Related Materials

While there have been some DC corrosion studies conducted on passivated and anodized CP-Ti and Ti-6Al-4V as previously mentioned, the amount of literature in this area is far from extensive. This is most likely due to the limited use of these two materials in industry. Consequently, literature dealing with EIS studies of these materials is practically non-existent.

In the past few years, however, there has been a considerable amount of EIS studies conducted on anodized aluminum. What makes these studies useful to this project are the similarities in the electrochemical behavior of aluminum and titanium.

Both aluminum and titanium readily oxidize to form an adherent, protective coating which limits further corrosion. Three models that have been derived by various researchers to fit the EIS data for anodized aluminum are presented in Figure 13 along with a drawing of the surface that they model.²⁵ The problem with relating these models to anodized titanium is that the oxide layer on anodized aluminum is generally porous and is typically sealed by immersion in hot water or dichromate.²⁵

Another widely published model for the EIS behavior of anodized aluminum²⁶ accounts for pitting of the base metal. This brings up one of the main problems in relating data for aluminum to a study of titanium which is the fact that aluminum experiences pitting corrosion in chloride

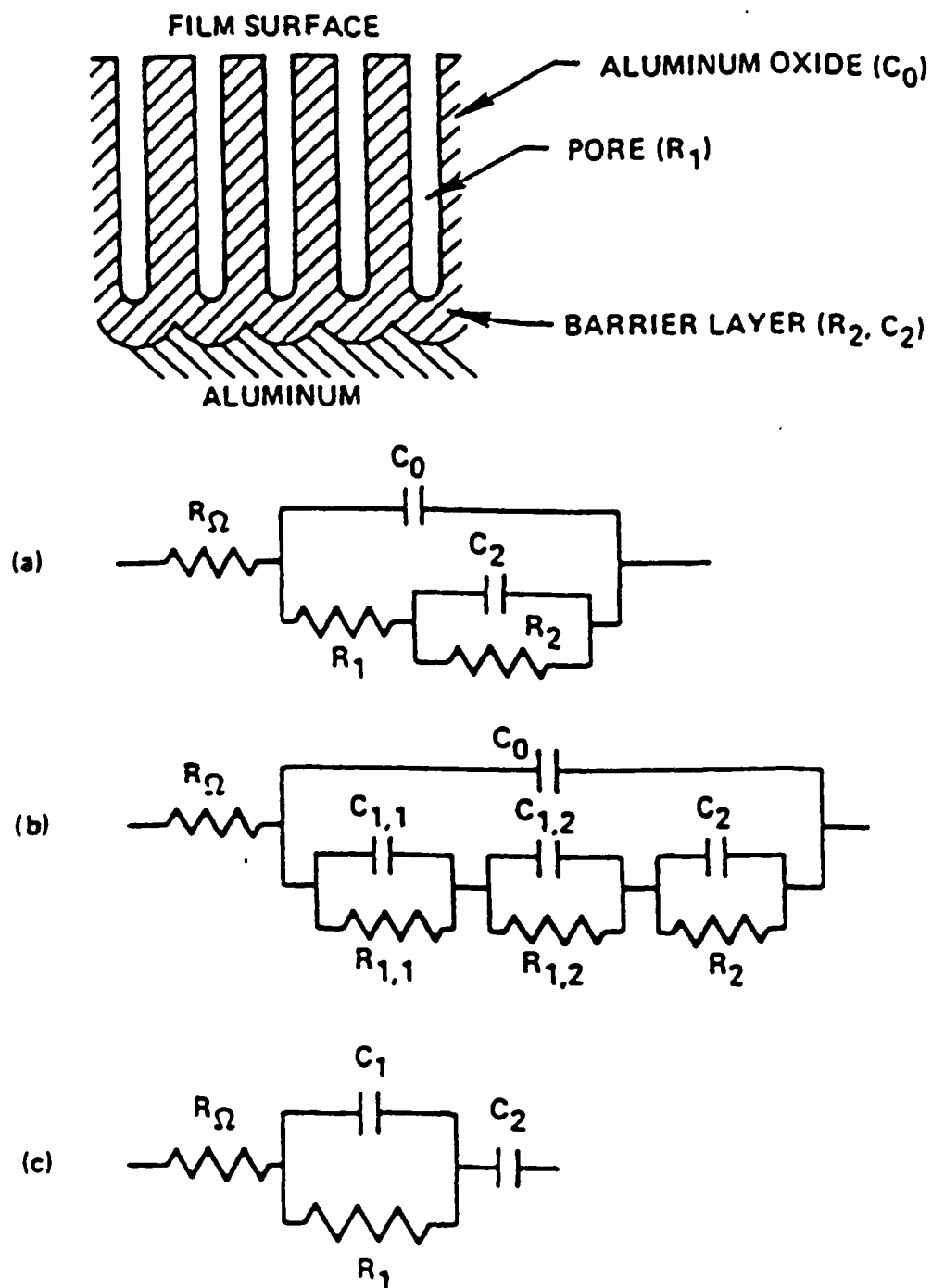


FIGURE 13. Schematic drawing of the surface of anodized aluminum along with several different equivalent circuit models.²³

environments. It is just this fact which drives researchers to use EIS to study anodized aluminum because EIS will reveal pitting corrosion in a much shorter time than the traditional salt spray tests.²⁷

An in vitro corrosion study can not be adequately conducted without the presence of chloride ions. Since these ions cause pitting in aluminum yet have essentially no affect on titanium, the impedance data for anodized aluminum could only be extrapolated to anodized titanium when there was no pitting of the aluminum. The methods of arriving at an equivalent circuit model can be used, but the models themselves cannot be used without justification.

CHAPTER III

EXPERIMENTAL PROCEDURE

Sample Preparation

In order to perform electrochemical measurements on the sample, a clean surface of known area must be in contact with the corrosive solution. At the same time, an electrical lead must be attached to the sample in such a manner that neither the lead nor the lead's attachment to the sample are exposed to the solution. Due to these requirements and to problems encountered with the use of commercially available corrosion sample holders, the samples were mounted so that the mounting medium also acted as the sample holder.

The metal samples were cut from 5/8 inch diameter drawn bar stock of the appropriate composition. The samples were approximately 1/2 inch thick. The samples were attached to aluminum disks approximately 3/8 inches thick, and the same diameter as the samples. This attachment was made using carbon paint which provided an electrically conductive bond between two pieces of metal. The bonded samples were then cold mounted using Leco two part mounting epoxy. The mounting was conducted so that the flat surface of the sample material was exposed on one end, and the aluminum was completely imbedded in the mount. The epoxy mount was chosen

both because it was clear, allowing the aluminum to be seen during subsequent machining, and because it provided a strong bond between the mount and the metal. This second point is important since the samples were ground and polished in the mounts and other mounting media that were tried all pulled away from the sample, forming a crevice between the mount and the sample. This led to crevice corrosion causing inaccurate results. After mounting, each sample was numbered, and this number as well as the type of sample material were engraved into the back of the mount for identification purposes.

To provide the electrical connection necessary for electrochemical studies, the aluminum was drilled and tapped so that a threaded steel rod could be screwed into the aluminum. This was done by first drilling a 7/64 inch hole into the epoxy and through the aluminum. The hole was drilled through the aluminum but not completely through the epoxy mount. This provided a place for chips to fall and allowed more threads to be cut into the aluminum. After drilling, the hole was tapped with a 6-32 tap, stopping often to clean out the chips formed. A 6-32 threaded rod could then be screwed into the aluminum, providing both an electrical contact and a secure attachment to hold the sample. The drilling and tapping were performed dry since cutting fluid could have adversely reacted with the epoxy. Furthermore, any residual fluid in the hole could have resulted in galvanic corrosion between the aluminum disk and the steel rod, thereby resulting in erroneous corrosion

measurements. The electrical contact was verified by testing the electrical resistance between the steel rod and the test surface of the sample using a digital multimeter. If the resistance was more than 0.5 ohms then the sample was not used. Several of the samples that failed this test were salvaged by drilling a small hole from the back side of the mount, through the aluminum to the titanium sample material. Copper wire strands were then forced into the hole, forming the electrical connection between the aluminum and the titanium. The hole was then sealed with solder and this was covered with fresh epoxy.

After the hole was tapped, a 3/8 inch recessed seat was cut into the epoxy around the tapped hole. This seat was cut using a 3/8 inch end mill to provide a flat bottomed hole. After the surface of the sample was prepared for testing as discussed in the following section, the sample and mount were installed in the cell. To do this, a rubber gasket was placed in the recessed hole and a 3/8 inch outside diameter glass tube was placed over the threaded rod into the recessed seat. A nut and washer were placed on the threaded rod at the other end of the glass tube and tightened. This sealed the rod and connection from the solution and provided a rigid mounting for the sample. The finished sample mount can be seen in Figure 14. The glass tube was then inserted into a Swageloc tube fitting to suspend the sample in the corrosion cell.

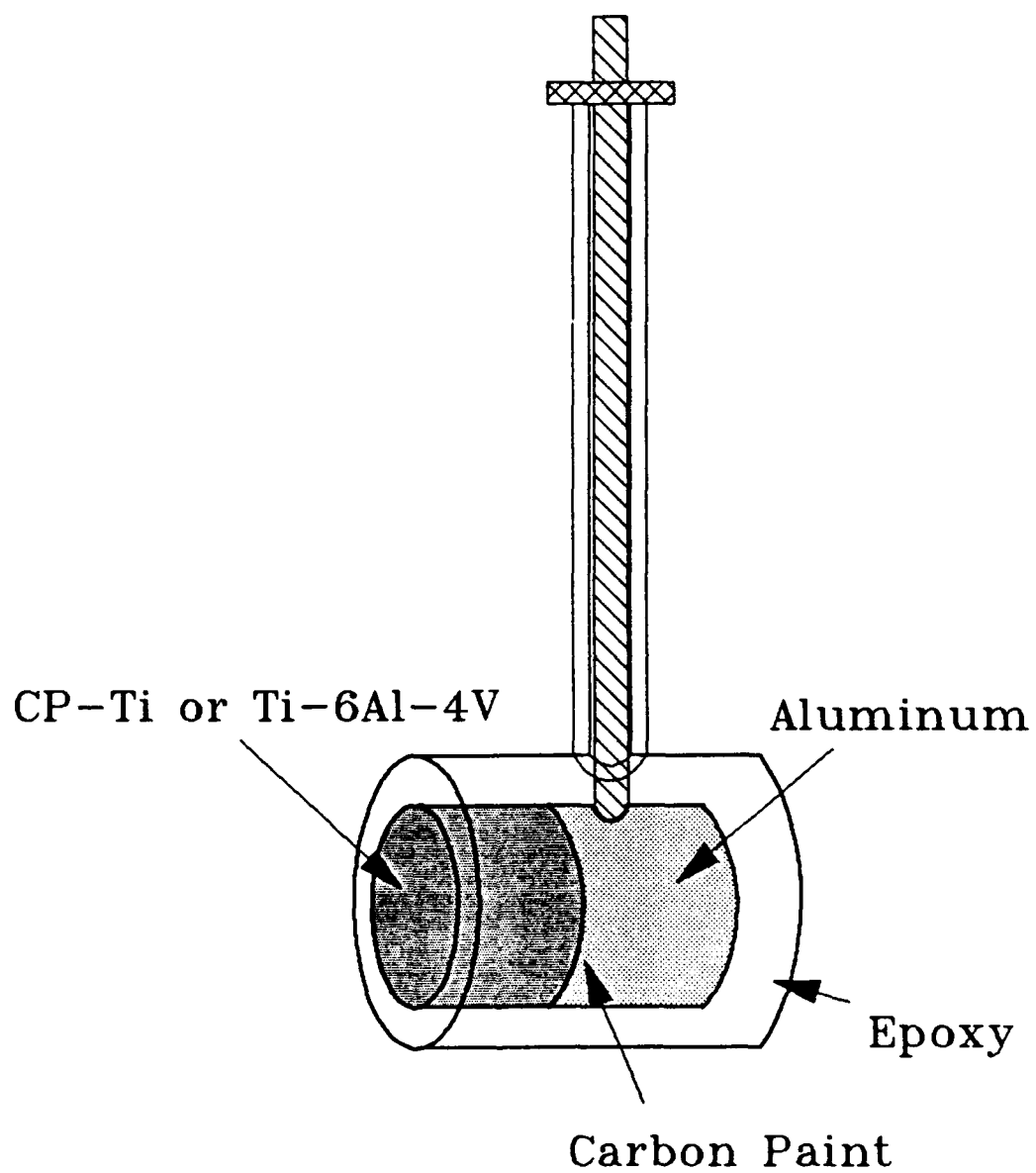


FIGURE 14. Sample mounting technique.

After verifying the electrical continuity of the sample, the test surface was prepared for testing by first grinding to a 600 grit finish using silicon carbide paper. This was followed by polishing with 5 micron and 0.3 micron alumina suspensions. Due to titanium's strong affinity for oxygen, the polishing procedures were conducted immediately prior to degreasing the samples. This was done in an attempt to minimize the amount of oxide on the polished surfaces prior to subsequent surface treatments or in the case of the untreated surfaces, prior to actual corrosion testing.

All samples were degreased by first washing with laboratory soap and rinsing with tap water. This was followed by 10 minutes of ultrasonic cleaning in a 50% ammonia solution. The samples were then rinsed thoroughly in distilled water and air dried.

At this point some of the samples were passivated in accordance with ASTM standard. The procedure consisted of submersing the sample in 40% nitric acid for 30 minutes at 25 °C.¹³ The potential was recorded throughout the passivation treatment using an EG&G Princeton Applied Research Model 278 potentiostat. The passivation treatment was followed by a thorough rinsing in distilled water. This procedure was established to enhance the natural protective oxide layer on the surface of the metal, making it more resistant to corrosion.

Several of the samples were anodized immediately following the degreasing procedure. This was performed by

connecting the sample to a DC power source as the anode and submersing the sample in a corrosive solution with a stainless steel cathode. When current was applied by the power source, the surface of the sample rapidly formed a thick, protective oxide. The corrosive solution used consisted of 110 ml glycerin, 60 ml ethanol, 35 ml water, 10 ml lactic acid, 5 ml phosphoric acid, 5 gm citric acid and 5 gm oxalic acid.¹⁵

Studies have shown that the color of an anodized coating is indicative of the coating's thickness.¹⁶ Experimentation showed that the color of the coating was primarily a function of potential and independent of current. The current did however determine the rate of the process. Therefore, a potential of 75 volts was selected to coincide with previous studies¹⁵ and a current of 20 milliamps was applied so that the reaction was slow enough to allow the operator to be consistent in turning the current off when the proper potential was reached. Since this was a DC circuit, the relation $V=IR$ was used to find the total resistance in the circuit. The solution resistance was negligible, leaving only the resistance of the oxide layer formed on the surface of the sample, which was compared to the resistance values from both the DC and AC measurement techniques.

Solution Preparation

In order to simulate conditions in the body, a 0.9 normal NaCl solution, buffered to a pH of 7.2 to 7.4, heated to 37 °C and saturated with oxygen, was used. For

convenience, the NaCl solution was mixed in 15 liter batches with 9 grams of NaCl per liter of distilled water. Immediately before each test, 2 liters of the solution were placed in the corrosion cell beaker. This solution was buffered to a pH between 7.2 and 7.4, using sodium bicarbonate ($\text{Na}(\text{CO}_3)_2$) to increase the pH and hydrochloric acid (HCl) to decrease the pH as needed. The solution was then heated to 37 °C. After heating, 150 ml of the solution was poured into a 250 ml beaker for the reference electrode. The corrosion cell beaker with the remainder of the solution was then placed into the water bath which was also heated to 37 °C.

The solution in the corrosion cell was saturated with oxygen by diffusing oxygen directly into it. The oxygen was diffused into the solution for 15 minutes before the sample was inserted. The oxygen flow continued throughout the experiment. The oxygen diffusing into the solution also provided a mixing action within the cell.

Cell Setup

The corrosion cell consisted of a 2500 ml beaker to contain the solution as discussed earlier. A teflon cell top was placed on the beaker and the various cell components were inserted as shown in Figure 15. These components included: oxygen diffuser, two platinum counter electrodes, thermistor, thermometer, and a Luggin probe. The reference electrode was a standard calomel electrode which was placed in the 250 ml beaker along with a second Luggin probe. A salt bridge was

drawn between the two Luggin probes. The sample to be tested served as the working electrode and was placed in the cell so that the tip of the Luggin probe was between 2 mm and 5 mm from the surface of the sample. The final step was to connect the leads from the potentiostat and enable the cell.

Water Bath

The water bath maintained the required 37 °C for the corrosion cell. To do this, the water in the bath had to be heated and circulated. Preliminary tests showed that the EIS measurements were adversely affected by external electrical and magnetic fields such as those produced by resistance heaters and magnetic stir plates.

These problems were solved by having a remote reservoir where the water was heated and then pumped into the water bath. A drain on the water bath allowed the water to flow back to the reservoir to be reheated. A thermistor was submerged in the corrosion cell and connected to a controller which in turn was connected to a heater in the reservoir, thereby regulating the temperature remotely from the corrosion cell itself. To further isolate the EIS equipment from the effects of the pump and heater, these two components were plugged into a different electrical circuit than the EIS equipment. This configuration is shown in Figure 16.

The DC measurement techniques are not as sensitive as the EIS technique, and therefore the DC measurements were not affected by the pump or heater.

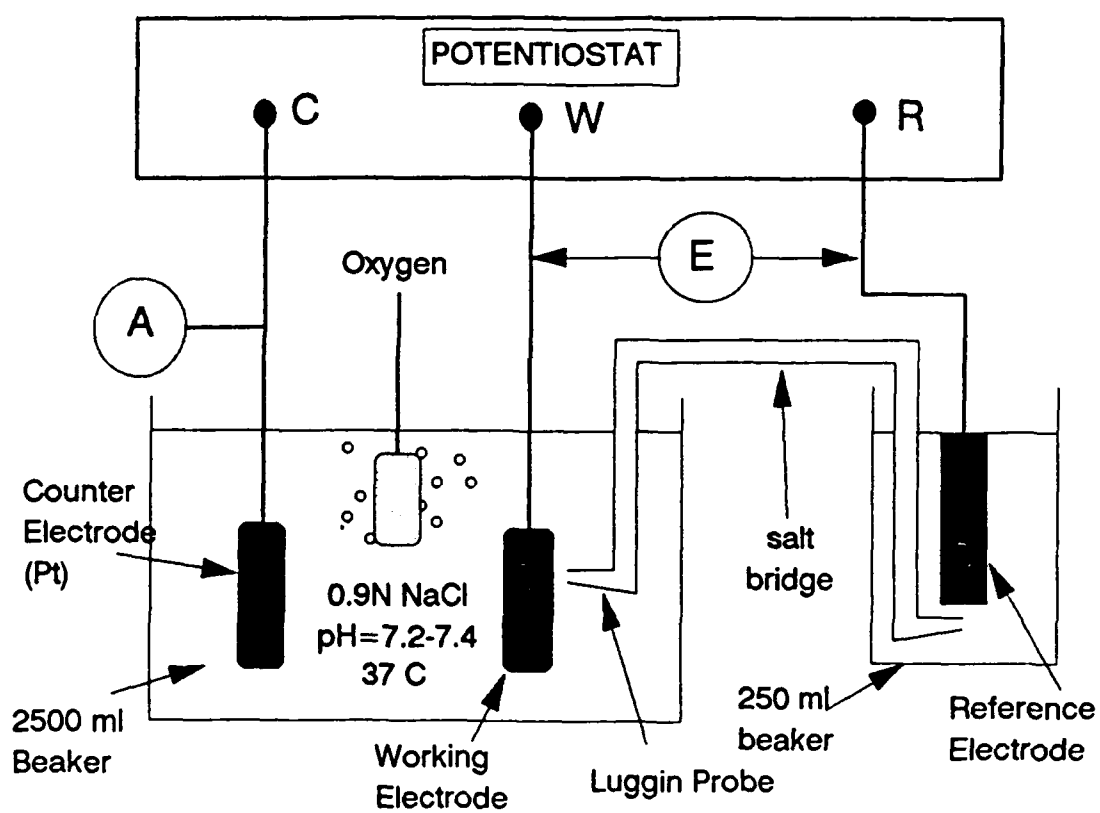


FIGURE 15. Corrosion cell components and electrical connections.

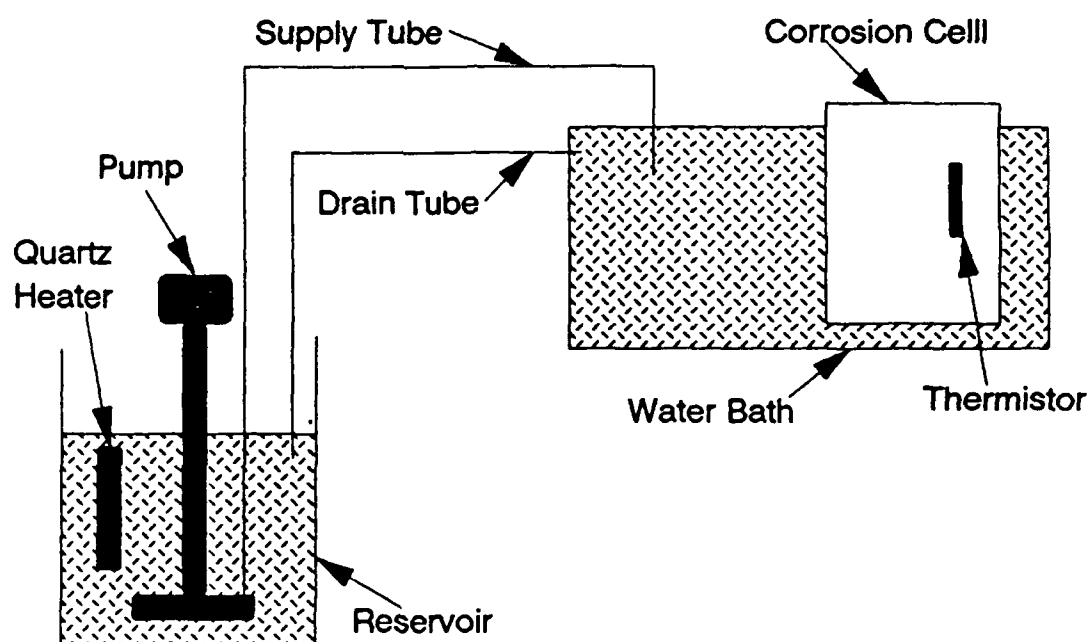


FIGURE 16. Water bath and reservoir used to maintain the desired temperature without affecting the EIS measurements.

Potentiodynamic Polarization

The DC technique of potentiodynamic polarization was performed using the EG&G Princeton Applied Research Model 278 potentiostat and the accompanying software. In this test, the cell was allowed to equilibrate for 1 hour, during which time the potential was monitored. After this, the open circuit potential was measured and taken to be the equilibrium potential. The potentiostat then applied a current to the counter electrode, driving the cell potential away from equilibrium. As the potential moved away from equilibrium, first in the cathodic and then in the anodic directions, the computer recorded the current densities at specific potential differences between the working and reference electrodes. This allowed a potential versus current density curve to be drawn. For this study, the polarization proceeded from 500 mV below to 500 mV above the equilibrium potential at a scan rate of 0.2 mV/sec.

The potentiodynamic polarization technique was validated by performing a standard run. This standard was conducted in accordance with ASTM G5 Standard Practice for Standard Reference Method for Making Potentiostatic and Potentiodynamic Anodic Polarization Measurements.²⁸ One change that was made to the standard procedure is that the corrosion sample used was a 5/8 inch diameter disk of 430 stainless steel mounted in accordance with the mounting procedures presented above instead of the cylindrical sample

called for. This change validated the new sample mounting technique that was used in this project.

Electrochemical Impedance Spectroscopy

Electrochemical impedance spectroscopy was performed using an EG&G Princeton Applied Research Model 278 potentiostat, lock-in amplifier and accompanying software. Again the cell was allowed to equilibrate for 1 hour while monitoring the potential before the actual test began. EIS consists of applying small sinusoidal perturbations (5 to 10 mV) about a DC potential over a range of frequencies. For this study the DC potential used was the open circuit potential of the cell. The frequency range used was from 0.001 to 100,000 Hz. It is important to cover a wide enough frequency range so that the high and low frequency conditions approach the infinite and zero frequency conditions, respectively. Furthermore, the slower the corrosion rate, the lower the frequency needed to obtain the zero frequency condition. At the same time, the time that the experiment takes to run must be considered. For each order of magnitude lower in frequency that is tested, the time that the test takes to run increases by approximately one order of magnitude.

Since this study dealt with corrosion resistant materials in a mild solution, the zero frequency condition was not always reached at 0.001 Hz. Therefore, tests of these conditions were run with a lower frequency limit of 0.0001 Hz and 0.00005 Hz (the lower limit of the

instrumentation). These tests provided little additional information.

Test Matrix

As previously mentioned, this project considered two different sample materials, CP-Ti and Ti-6Al-4V. Each of these materials was tested in the as-polished condition, in the passivated condition, and in the anodized condition. All surfaces were prepared as discussed above.

In the real world, there are no two surfaces that are identical and therefore no two surfaces will have exactly the same corrosion properties. However, by using samples of the same bulk composition and structure, and by taking care to follow the same procedure for each test, it can be assumed that the corrosion data obtained will be normally distributed. In order to obtain reasonably reliable data, three tests were conducted for each material and surface treatment condition as depicted in Table 3 below. This matrix of 18 tests was conducted for both the potentiodynamic polarization and the EIS techniques for a total of 36 tests.

TABLE 3
Test Matrix

Material	Surface Treatment		
	Polished	Passivated	Anodized
CP-Ti	3	3	3
Ti-6Al-4V	3	3	3

Energy Dispersive Spectroscopy

Energy dispersive spectroscopy (EDS) was used to verify the bulk composition of the test materials. The material purchased was to have conformed to ASTM standards. The EDS system available was useful in verifying the presence of aluminum and vanadium in the Ti-6Al-4V samples and the absence of any large constituent in the CP-Ti samples.

In order to obtain the bulk composition, the maximum contributing volume was desirable. This was done by using a tilt angle of zero degrees and the maximum spot size of 500 nm. In order to decrease the amount of absorption of the lower energy x-rays, such as the characteristic aluminum x-rays, a relatively low accelerating voltage of 16 kV was used. All of the EDS measurements were conducted with a beryllium detector window.

Auger Electron Spectroscopy

Auger Electron Spectroscopy (AES) samples were made following the same procedures as for the corrosion samples. Three samples each of the CP-Ti and the Ti-6Al-4V were prepared with one of each of the three surface conditions: polished, passivated and anodized. Care was taken so that after the samples were prepared they would be loaded into the ultra-high vacuum of the Auger Electron Microscope within one hour. This was done to minimize any additional oxide formation on the surface of the sample, particularly on the polished sample.

Once a sample was loaded in the microscope, the instrument's scanning electron microscope (SEM) was used to view the surface to see if any distinct features could be seen.

The second step was to use AES to gather a surface spectra to determine what elements were present on the surface. The surface spectra swept the energies from 50 eV (electron volts) to 1700 eV with a step size of 1.0 eV and a dwell time of 64 ms. The accelerating voltage used was 10 kV. In order to reduce the background, 10 sweeps of the energies were conducted and averaged.

The third step was to conduct a depth profile of the surface in order to determine the thickness of the surface oxide. The exact thickness of the surface was not measured. Although the ion gun voltage was known, the sputtering rate could not be determined quantitatively. However, since all of the samples compared were sputtered with the same filament at the same gun voltage, it can be assumed that the sputter rate was essentially the same for the different samples. To give comparable results, the same ion gun voltage of 3 kV was used for sputtering all of the samples, with a sputtering time of 10 seconds per cycle. The thickness of the oxide layer in terms of sputtering time was determined by continuing the depth profile until virtually no oxygen was detected. The relative thicknesses of the oxides on the different samples could then be compared.

CHAPTER IV

RESULTS

Anodization Treatment

As mentioned earlier, both the CP-Ti and the Ti-6Al-4V samples were anodized by the same process, using a direct current of 25 milliamps until a potential of 75 volts was reached. The potential began near zero. The rate of increase in potential was slow at first but increased throughout the process until the potential reached 75 volts. The solution resistance was negligible. Using the direct current relationship $V=IR$, where V is potential in volts, I is current in amps and R is resistance in ohms, the electrical resistance through the oxide coating was $1.89 \times 10^3 \Omega/\text{cm}^2$. The oxide coatings formed on the surfaces of the two metals were distinctly different. The surfaces of the CP-Ti samples were a light blue in color. The surfaces of the Ti-6Al-4V samples had formed a blue layer during the passivation process, but this changed to yellow before the anodization was complete. The color of the coating was non-uniform on both materials, with different shades across the surface. There seemed to be no pattern in the variations in color on an individual sample.

Potentiodynamic Polarization

The results of the modified potentiostatic standard as discussed in the procedures section are showed in Figure 17 along with the ASTM Standard²⁸ curve. The modified test falls outside of the acceptable standard region between 200 and 800 millivolts. This indicated the occurrence of a limited degree of crevice corrosion

The polished CP-Ti and Ti-6Al-4V both produced potentials that started out in the range of -520 mV to -650 mV, and increased throughout the one hour equilibrium period. The rate at which the potentials increased was rapid at first and slowed as the sample remained in the solution as can be seen in the average potential curves for both CP-Ti and Ti-6Al-4V in Figure 18. All of the polished samples showed this same trend while equilibrating, and they differed only in magnitude.

Unlike the polished samples, the passivated samples showed several different trends during equilibration. These trends were seen with both the CP-Ti and the Ti-6Al-4V samples. These different trends were related to different potential versus time trends during the passivation treatment, which was itself an electrochemical corrosion process. The first trend was characterized by a potential that increased throughout the passivation treatment, and never reached an equilibrium as shown in Figure 19. When placed in the corrosion cell, the potential of a sample that exhibited this first trend would typically drop rapidly and

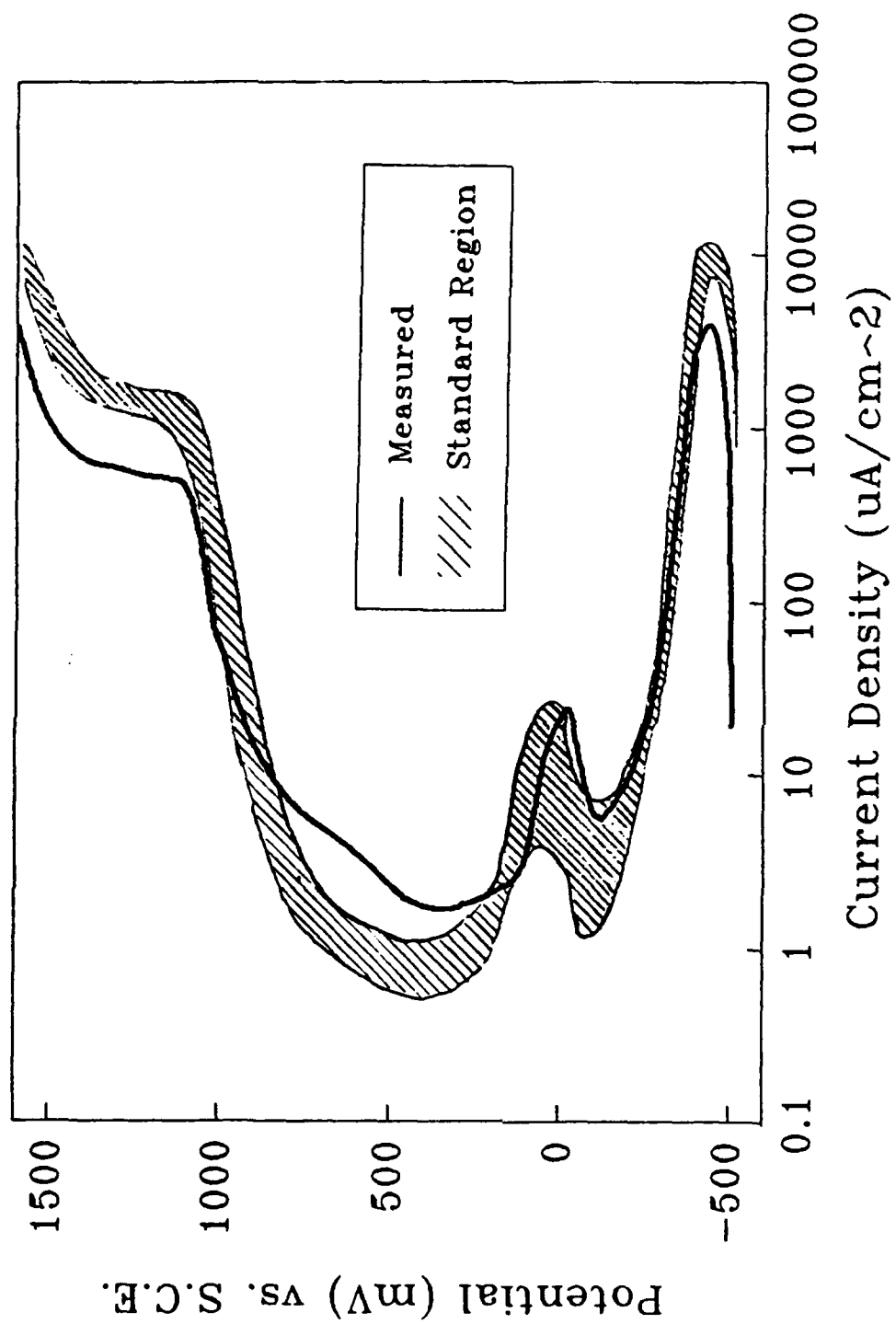


FIGURE 17. Potentiodynamic polarization curve obtained with the modified mounting procedure compared with the ASTM standard curve.²⁸

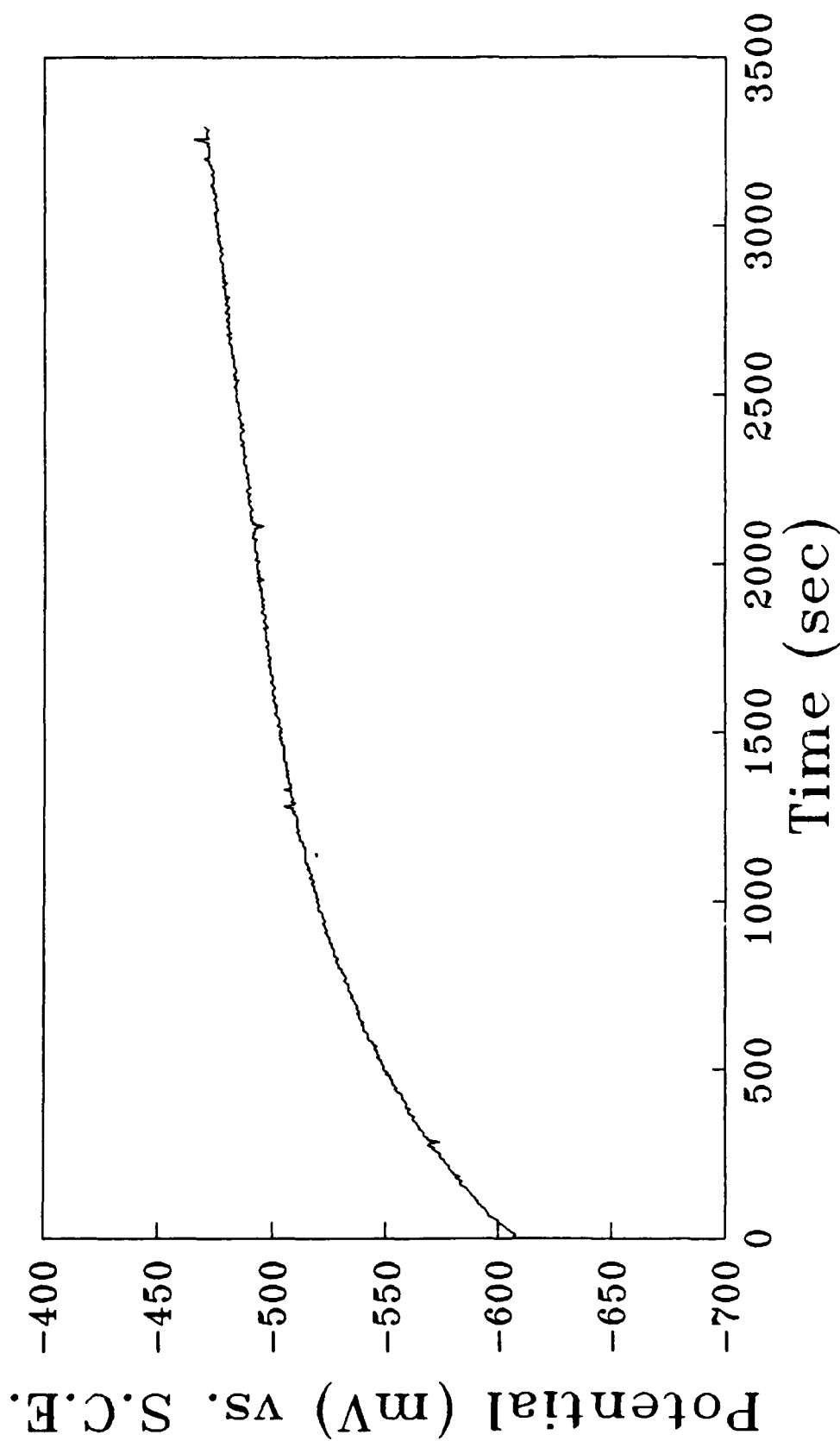


FIGURE 18. Typical potential versus time trend during equilibration for the polished samples.

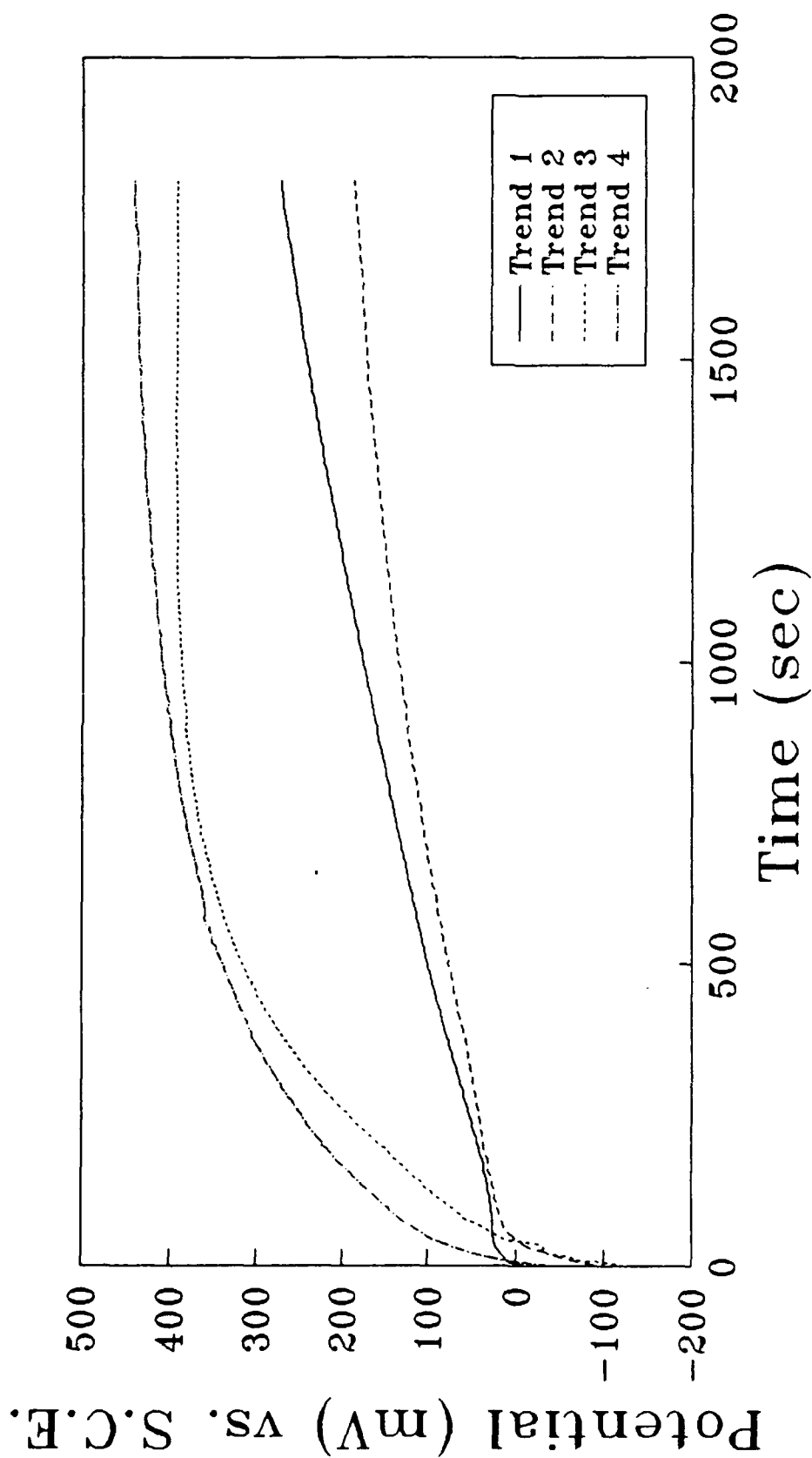


FIGURE 19. Various potential versus time trends during passivation for the passivated samples.

then stabilize at a level that was about equal to that of the polished samples, as shown in Figure 20.

Samples that followed the second trend passivated in the same manner as those of the first trend, as shown in Figure 19. The potential while coming to equilibrium in the corrosion cell, however, increased quite rapidly initially and then began a more gradual descent, never reaching an equilibrium, as seen in Figure 20.

The third trend was characterized by a potential that increased rapidly at first and then reached some equilibrium value, as shown in Figure 19. When this sample was placed into the corrosion cell, the potential dropped fairly rapidly but not as rapidly as the sample that followed the first trend. The potential of this sample also reached an equilibrium value but was slower in doing so, and the equilibrium potential was somewhat higher than that of the former sample, as shown in Figure 20.

The potential during passivation for the fourth trend behaved similar to that of the third trend, as shown in Figure 19. On immersion in the corrosion cell, however, the potential behaved similar to that of the second trend. Since the potential for this trend started higher and declined slowly, the potential at the end of the one hour passivation period was much higher for this trend than for any of the other trends, as can be seen in Figure 20.

The anodized samples also showed different trends while coming to an equilibrium. There were two different trends

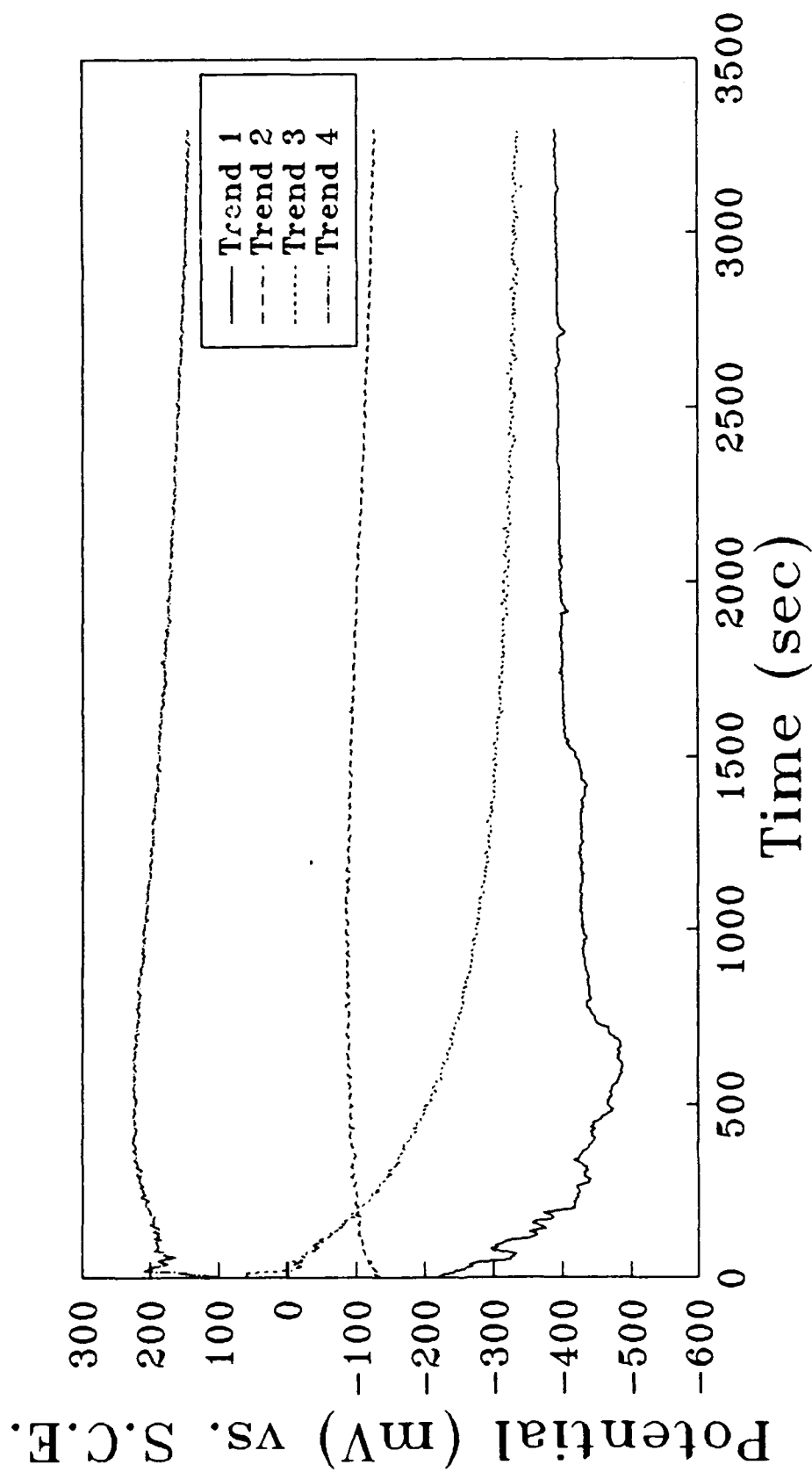


FIGURE 20. Various potential versus time trends during equilibration for the passivated samples.

with both the CP-Ti and the Ti-6Al-4V samples, as depicted in Figure 21. The first trend was for the potential to start at a high value (up to 400 mV), fall rapidly, and then taper off to a stable equilibrium. The second trend was the opposite of the first, starting low and increasing to reach an equilibrium. While these trends were opposite, they both tended toward the same stable equilibrium values somewhere between 50 mV and -50 mV (one sample did not reach an equilibrium).

Since different samples of the same material with the same surface treatment, particularly the passivated samples, had different equilibrium potential values, the potentiodynamic polarization plots were shifted accordingly. The general shape of the curves were the same for the same surface treatment. Therefore, the three individual potentiodynamic tests for each material and surface condition were averaged to obtain one plot to represent each material and surface condition. To obtain the average plots, both the potentials and the current densities were averaged. Figures 22, 23 and 24 show the average curves for both base materials in the polished, passivated and anodized conditions, respectively. Similarly, Figures 25 and 26 give comparisons of the average curves on the basis of surface treatment for the CP Ti and Ti-6Al-4V, respectively.

Electrochemical Impedance Spectroscopy

Three separate tests were conducted for each material and surface condition and the impedance magnitudes and phase

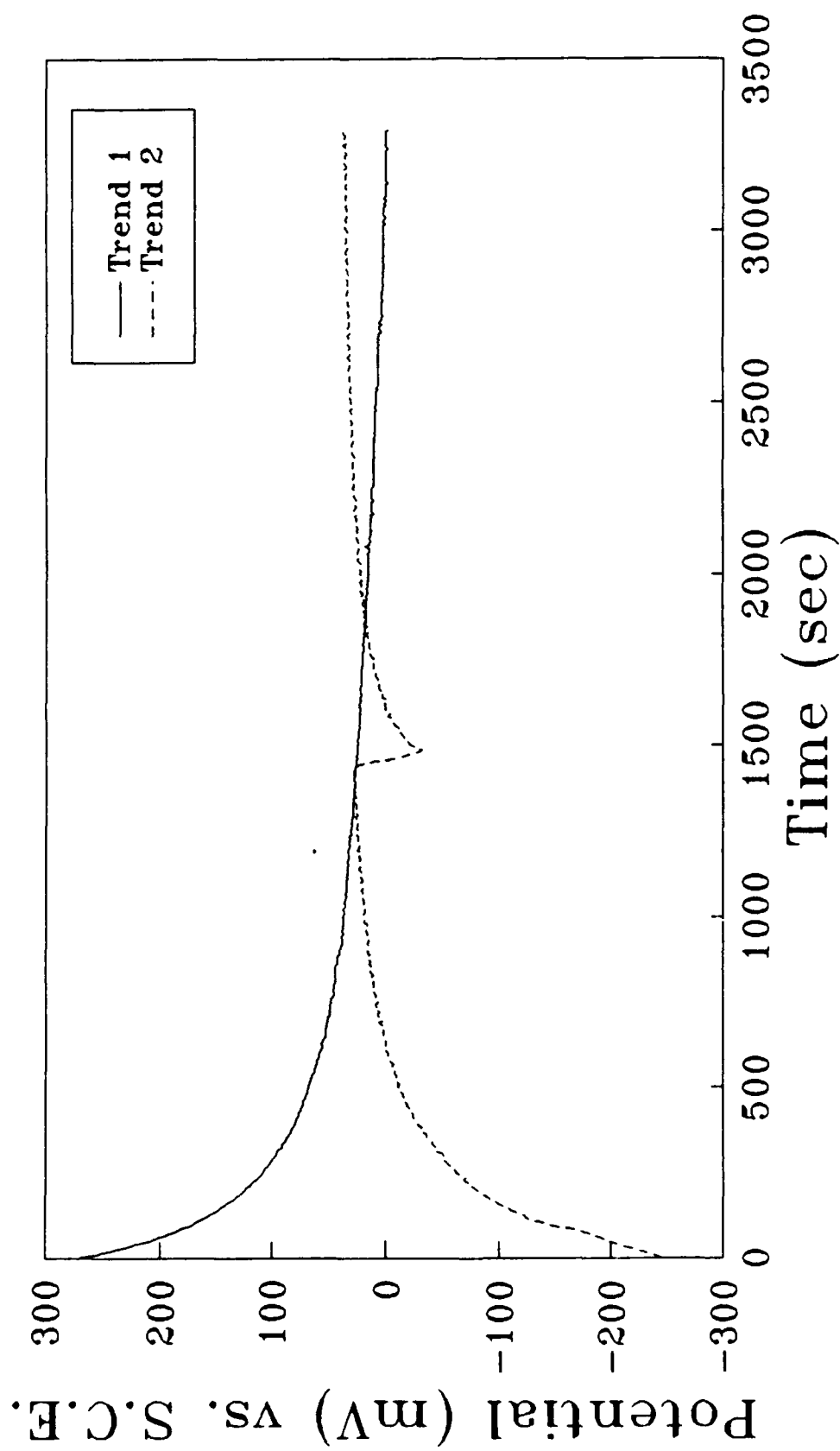


FIGURE 21. Typical potential versus time trends during equilibration for the anodized samples.

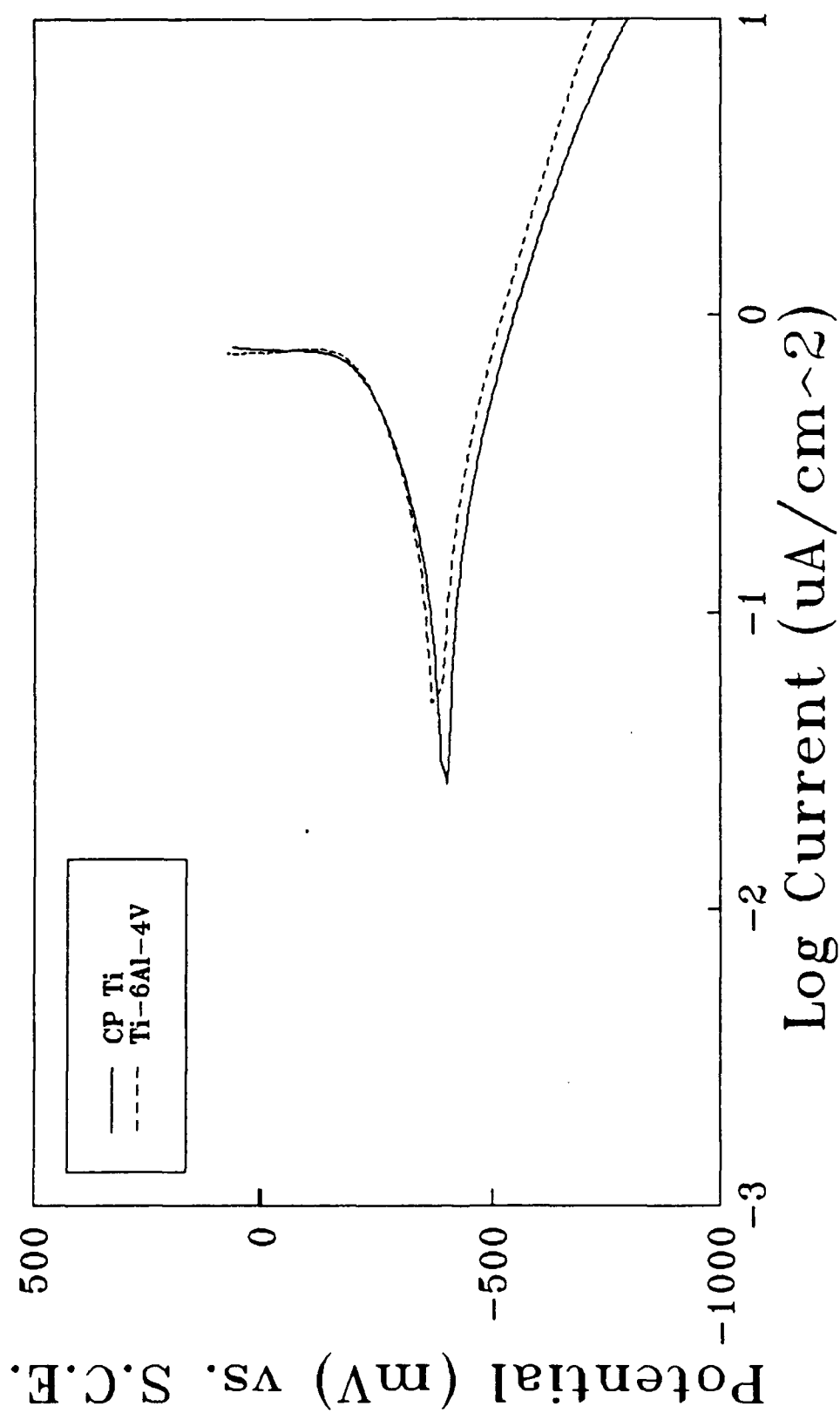


FIGURE 22. Average potentiodynamic polarization curves for the polished CP-Ti and the polished Ti-6Al-4V.

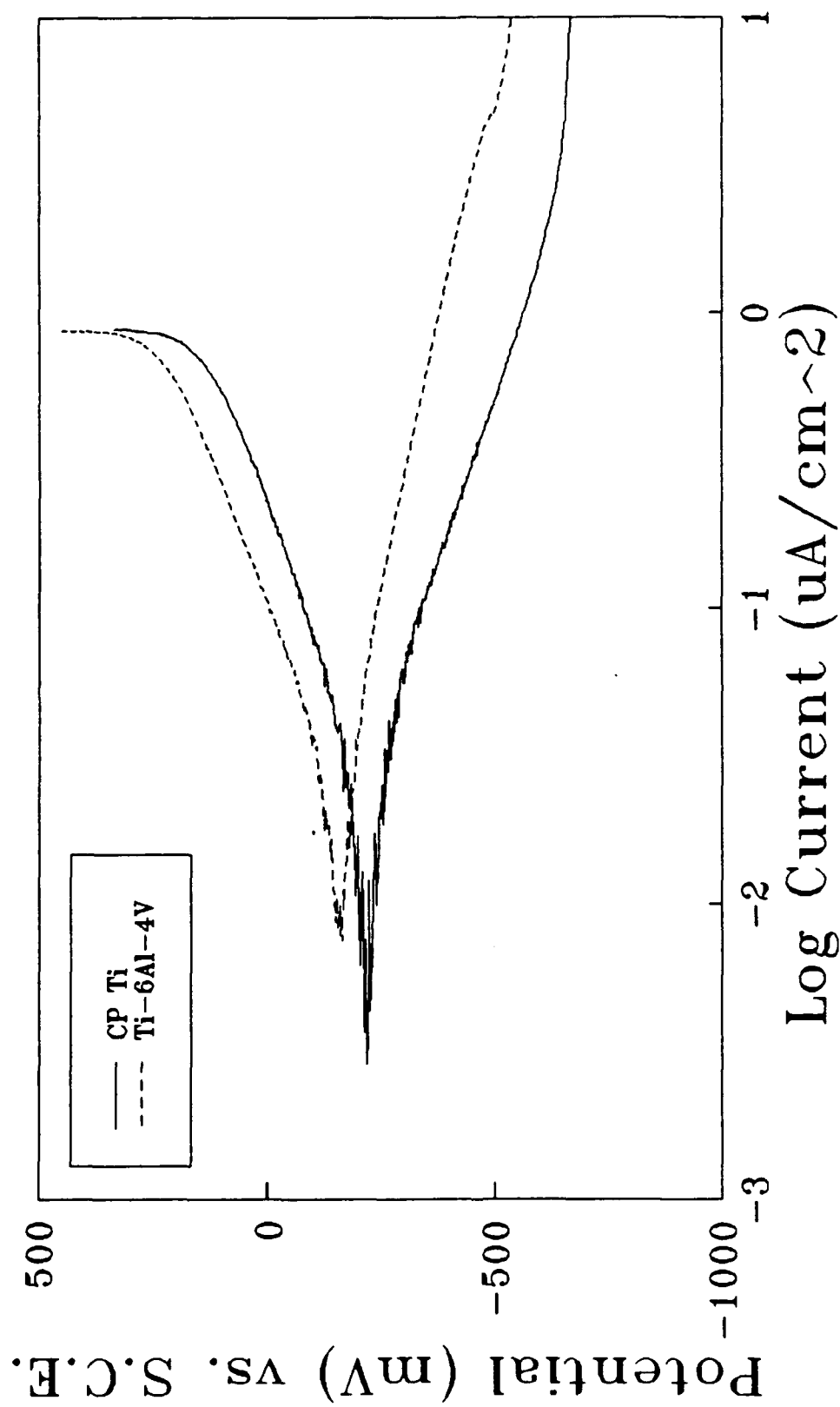


FIGURE 23. Average potentiodynamic polarization curves for the passivated CP-Ti and the passivated Ti-6Al-4V.

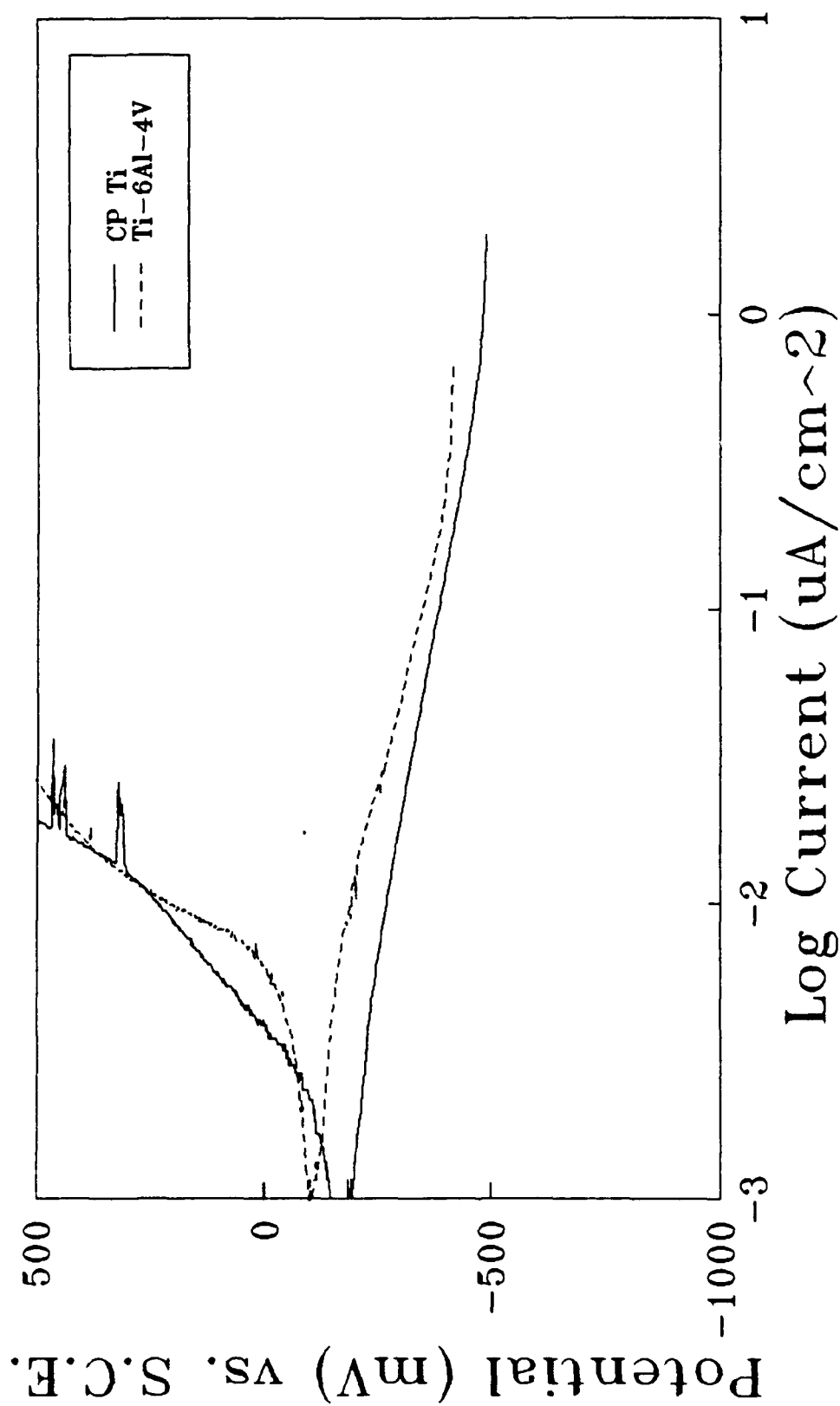


FIGURE 24. Average potentiodynamic polarization curves for the anodized CP-Ti and the anodized Ti-6Al-4V.

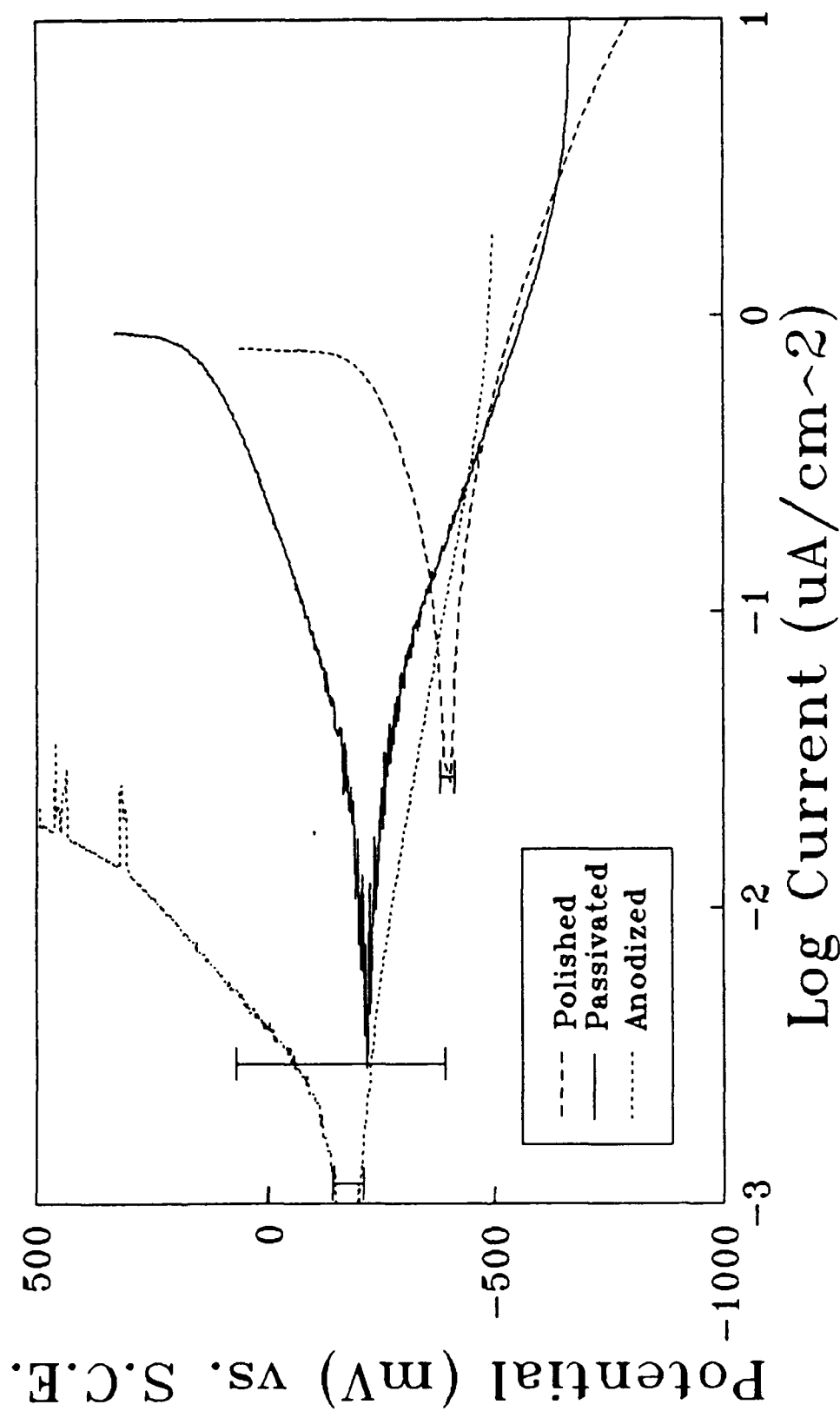


FIGURE 25. Average potentiodynamic polarization curves for the CP-Ti in the polished, passivated and anodized conditions. Error bars are given for the average E_{corr} on each curve.

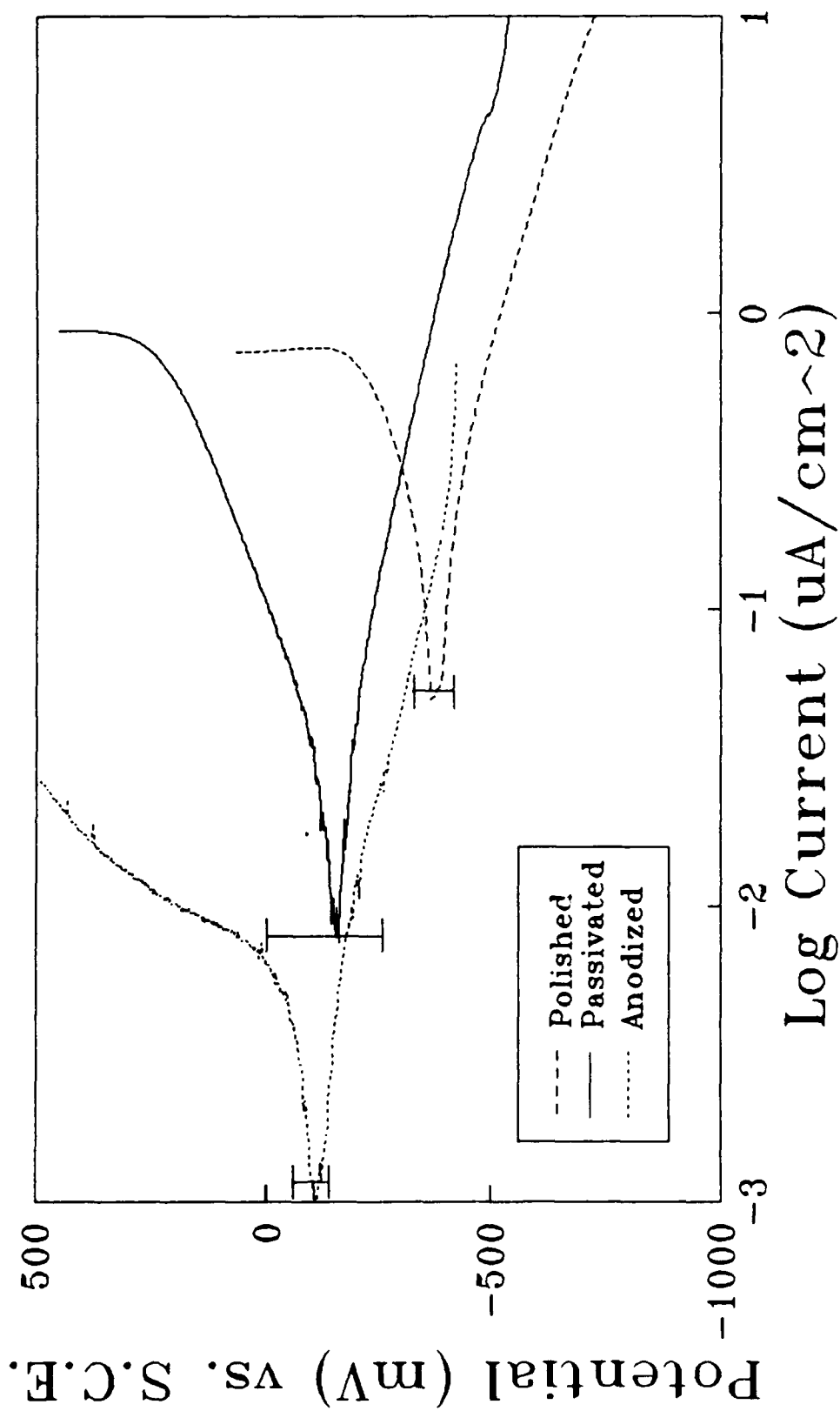


FIGURE 26. Average potentiodynamic polarization curves for the Ti-6Al-4V in the polished, passivated and anodized conditions. Error bars are given for the average E_{corr} on each curve.

angles for each set of tests were averaged. These average values were then used to calculate the corresponding real and imaginary impedance values. There was much less variation in the EIS test data for a given set of conditions than was seen with the potentiodynamic polarization. The average Bode and Nyquist plots for both base materials with polished surfaces are given in Figures 27 and 28, respectively. Likewise, the same plots for the passivated and anodized surfaces are given in Figures 29 through 32.

Figures 27 and 29 show little difference in the behavior of the two metals in either the polished or the passivated condition. Furthermore, the same trend that was seen with the polished condition was also seen with the passivated condition. This same trend was also seen with the anodized CP-Ti in Figure 31. Unlike the other surface conditions, there was a very significant difference between the anodized CP-Ti and the anodized Ti-6Al-4V, as shown in Figure 31. Figures 28, 30 and 32 show that the polished and passivated surfaces, as well as the anodized CP-Ti all have semi-circular Nyquist plots, while the anodized Ti-6Al-4V has a small second curvature near the origin.

Figures 33 and 34 compare the Bode and Nyquist plots for the three different surface conditions on the CP-Ti, while Figures 35 and 36 provide the same information for the Ti-6Al-4V. Figures 33 and 34 show that the EIS data for the CP-Ti samples follows the same trends for all three surface conditions. The magnitude, however, was considerably higher

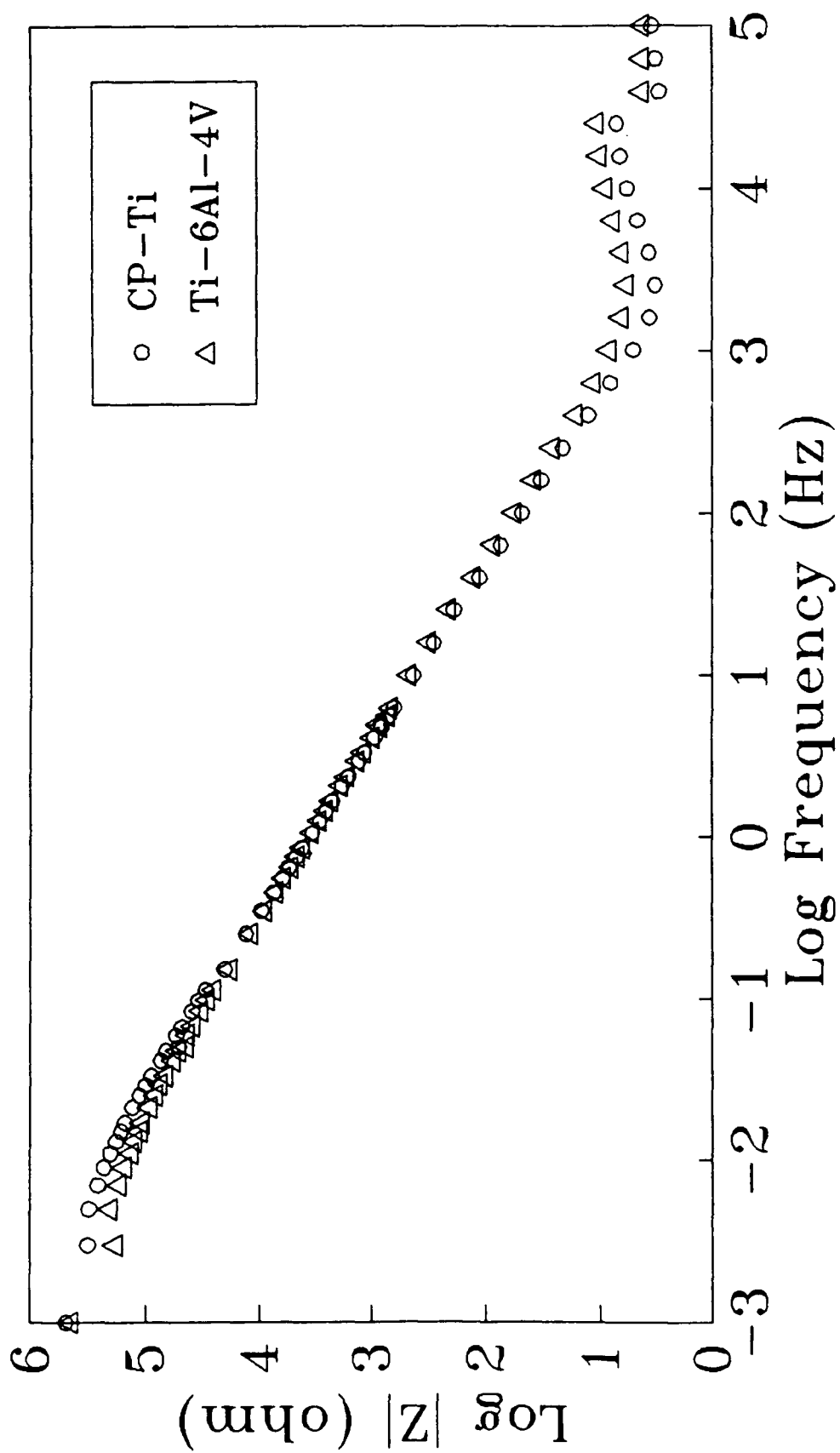


FIGURE 27a. Average Bode magnitude curves for the polished CP-Ti and the polished Ti-6Al-4V.

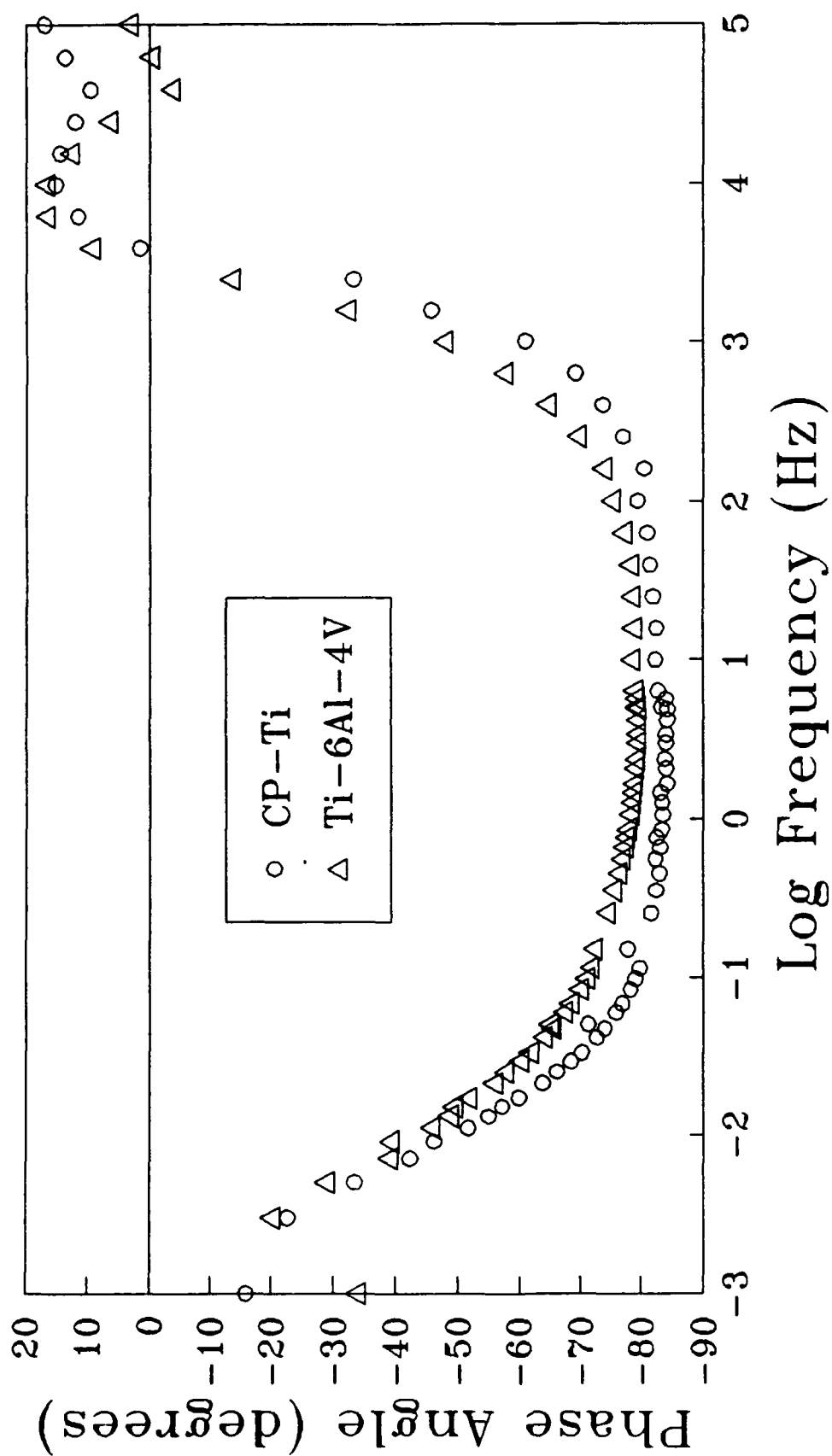


FIGURE 27b. Average Bode phase angle curves for the polished CP-Ti and the polished Ti-6Al-4V.

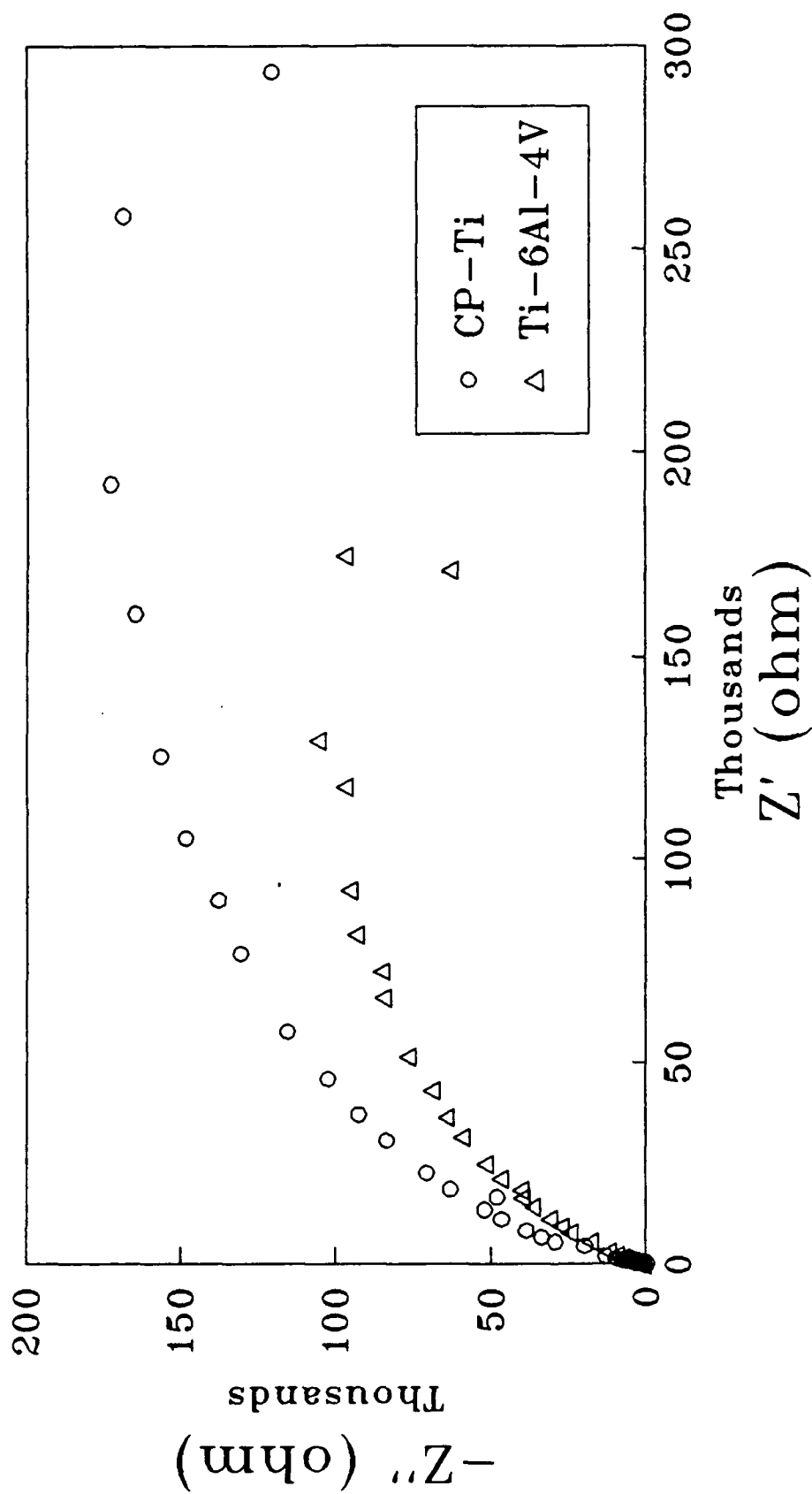


FIGURE 28. Average Nyquist curves for the polished CP-Ti and the polished Ti-6Al-4V.

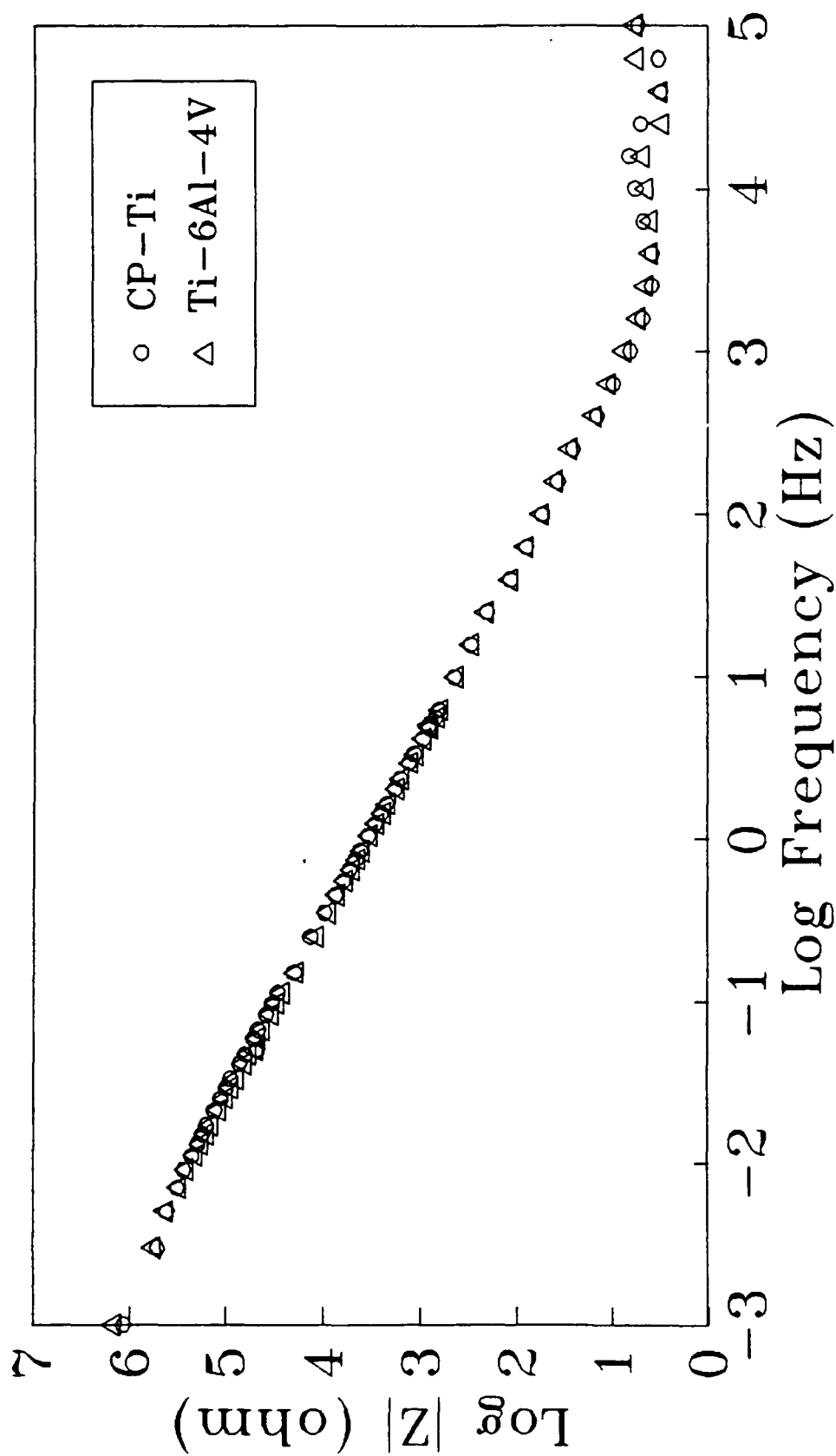


FIGURE 29a. Average Bode magnitude curves for the passivated CP-Ti and the passivated Ti-6Al-4V.

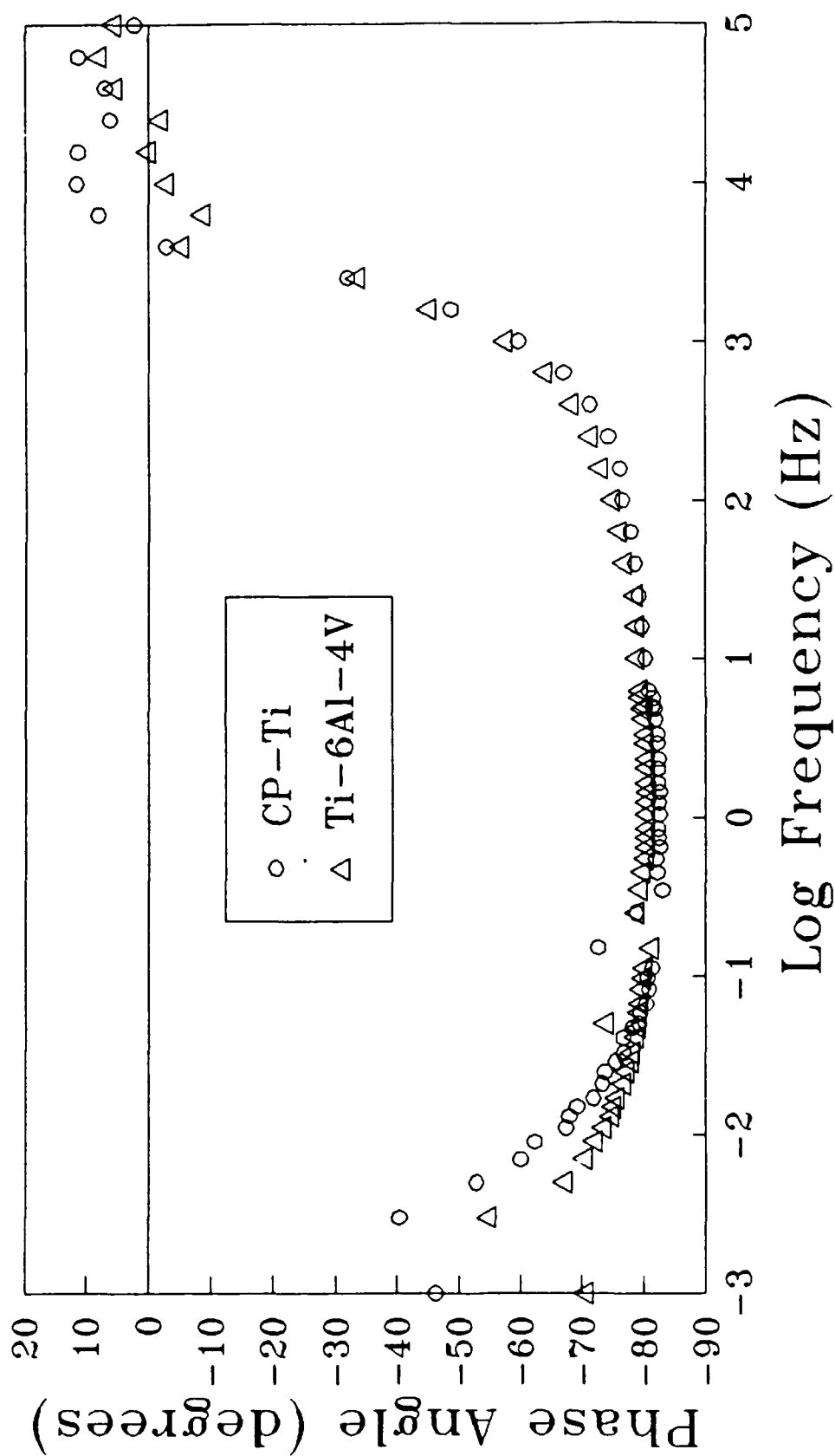


FIGURE 29b. Average Bode phase angle curves for the passivated CP-Ti and the passivated Ti-6Al-4V.

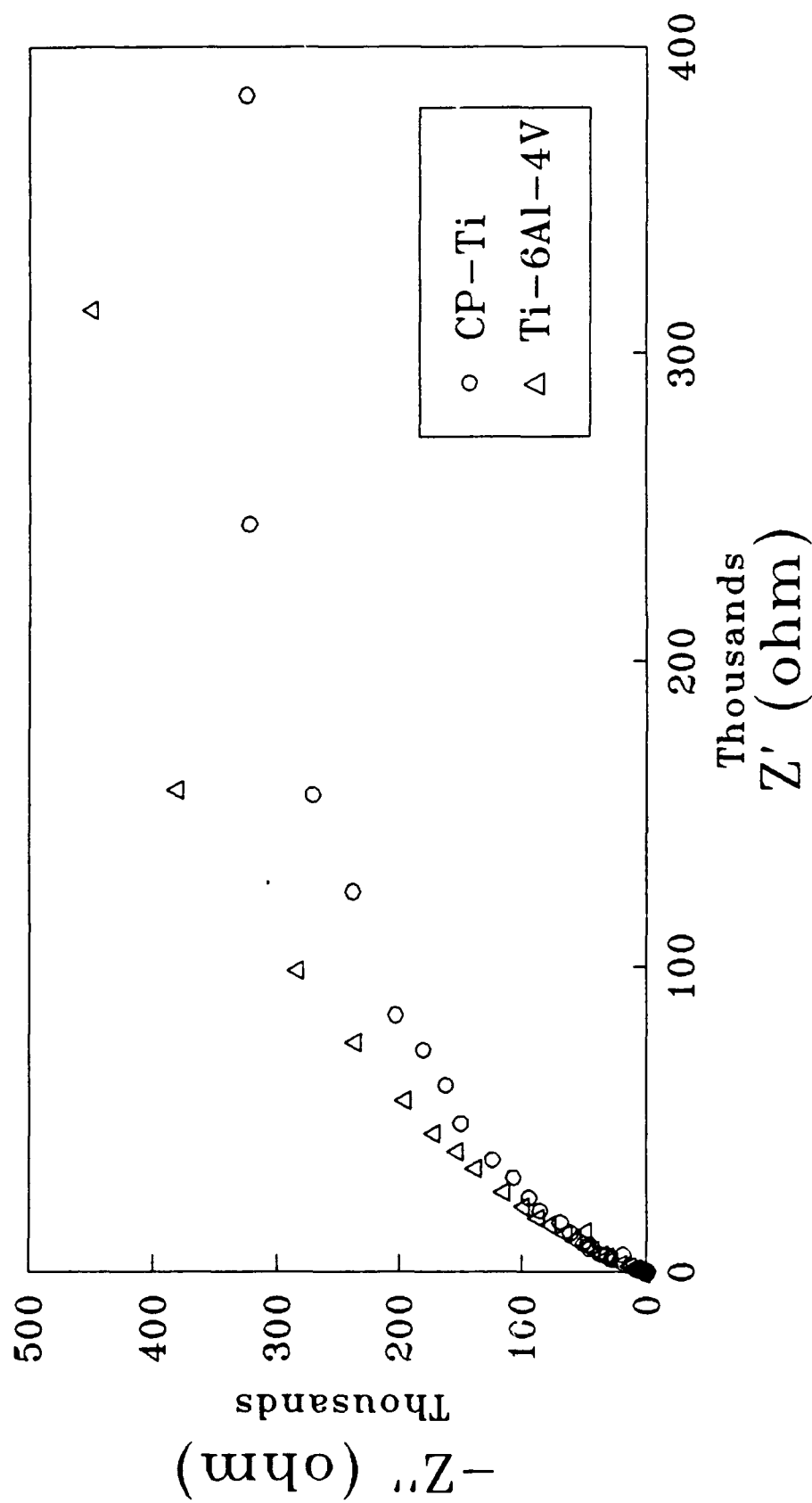


FIGURE 30. Average Nyquist curves for the passivated CP-Ti and the passivated Ti-6Al-4V.

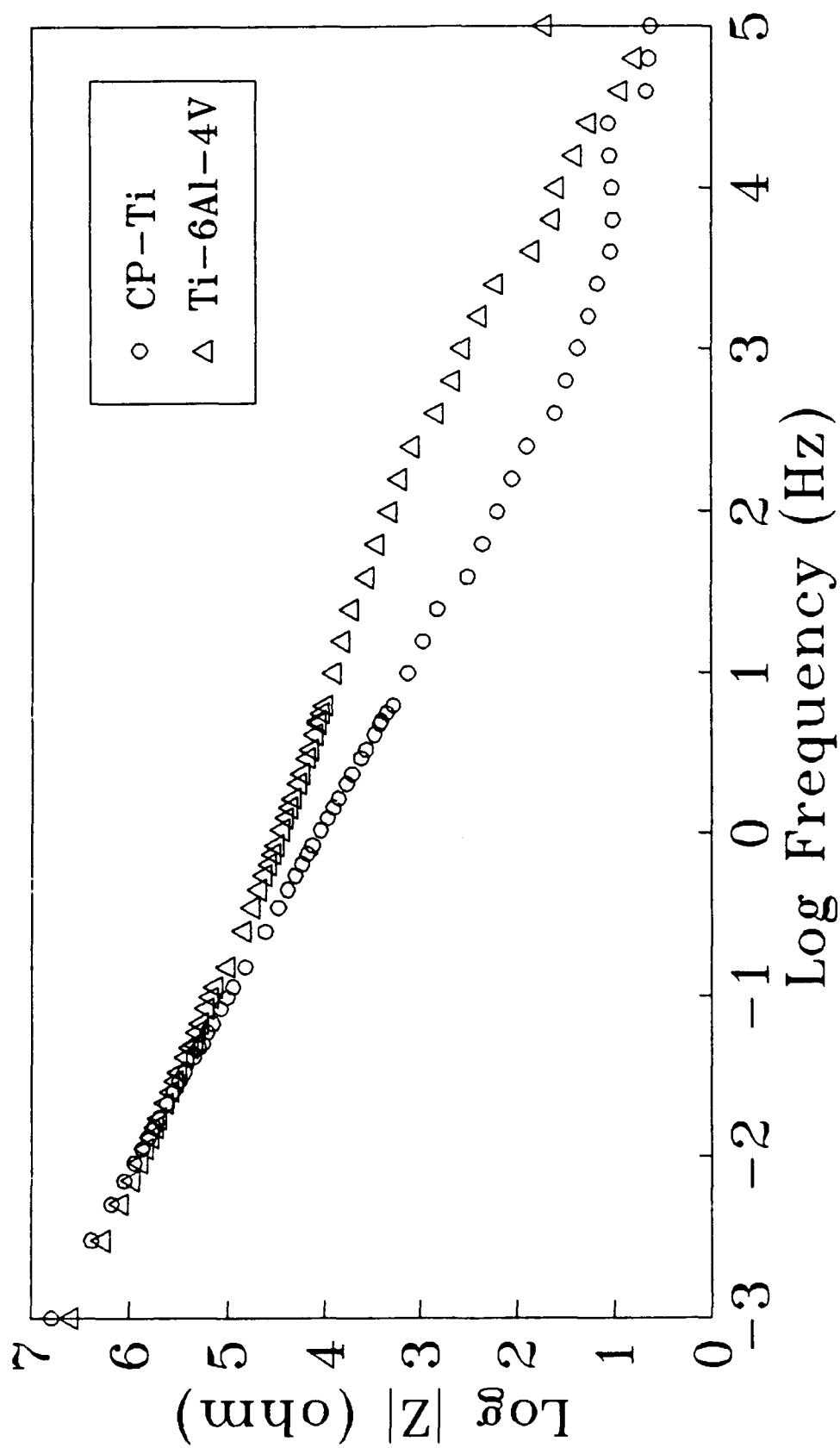


FIGURE 31a. Average Bode magnitude curves for the anodized CP-Ti and the anodized Ti-6Al-4V.

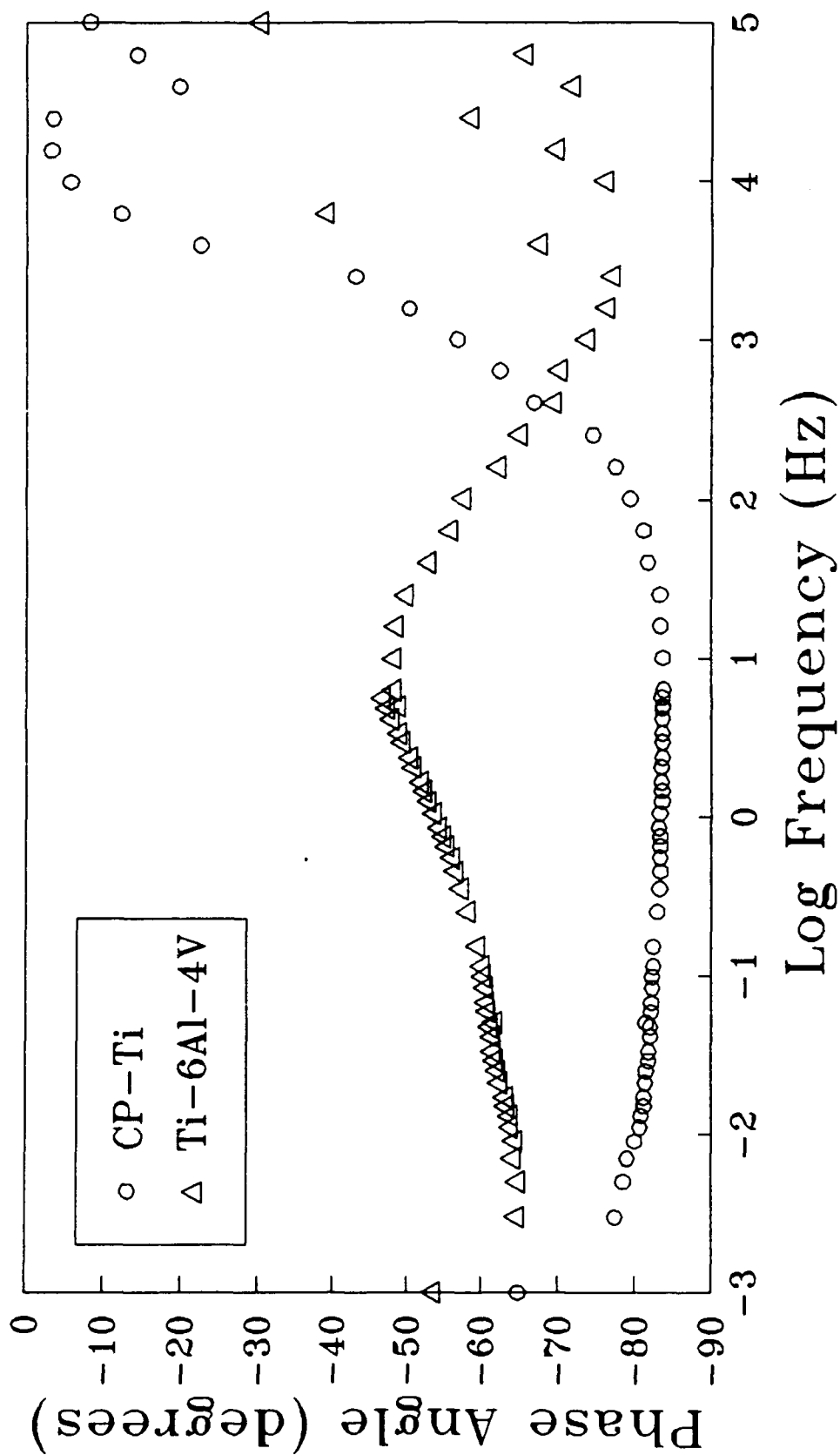


FIGURE 31b. Average Bode phase angle curves for the anodized CP-Ti and the anodized Ti-6Al-4V.

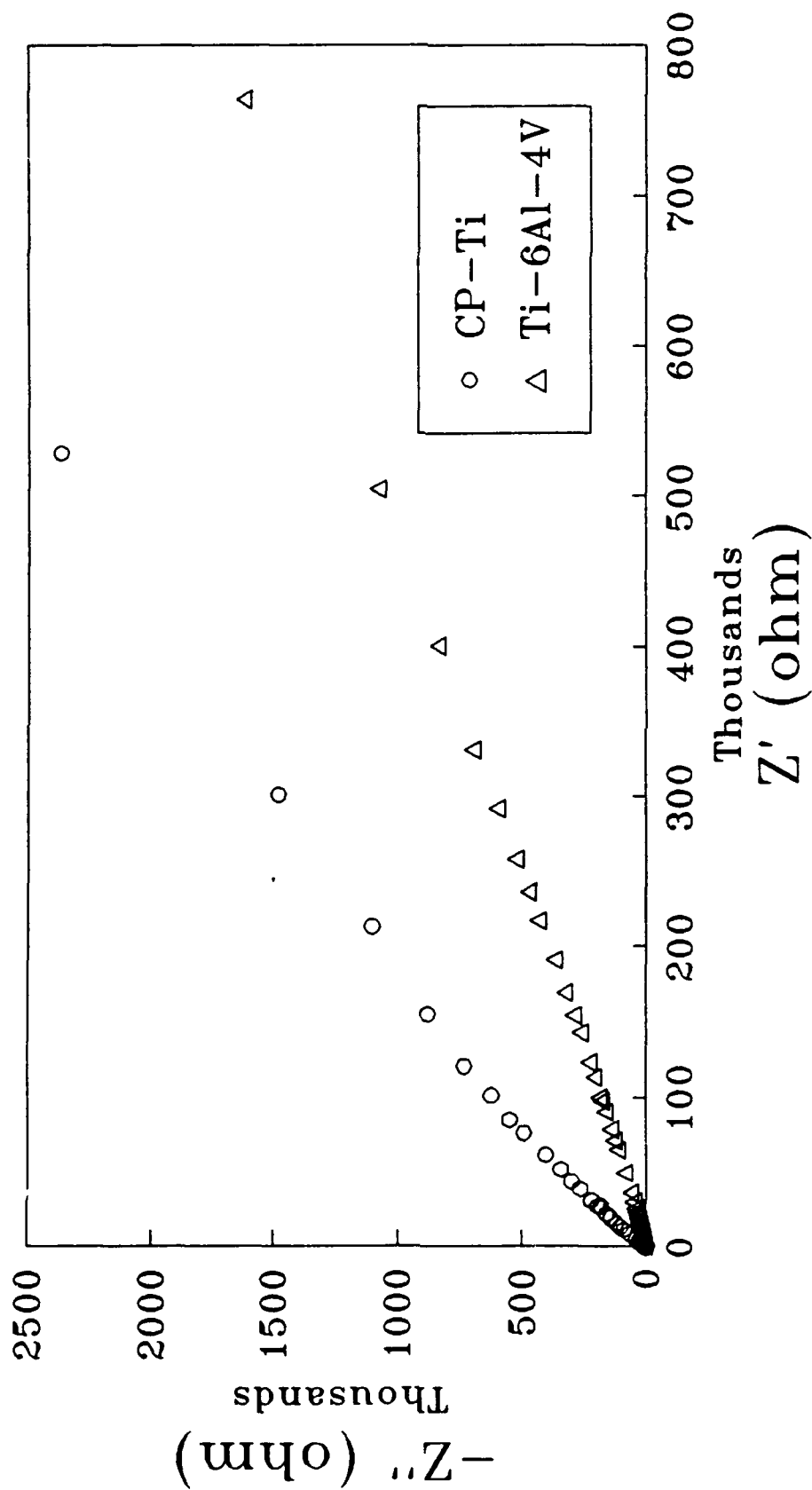


FIGURE 32. Average Nyquist curves for the anodized CP-Ti and the anodized Ti-6Al-4V.

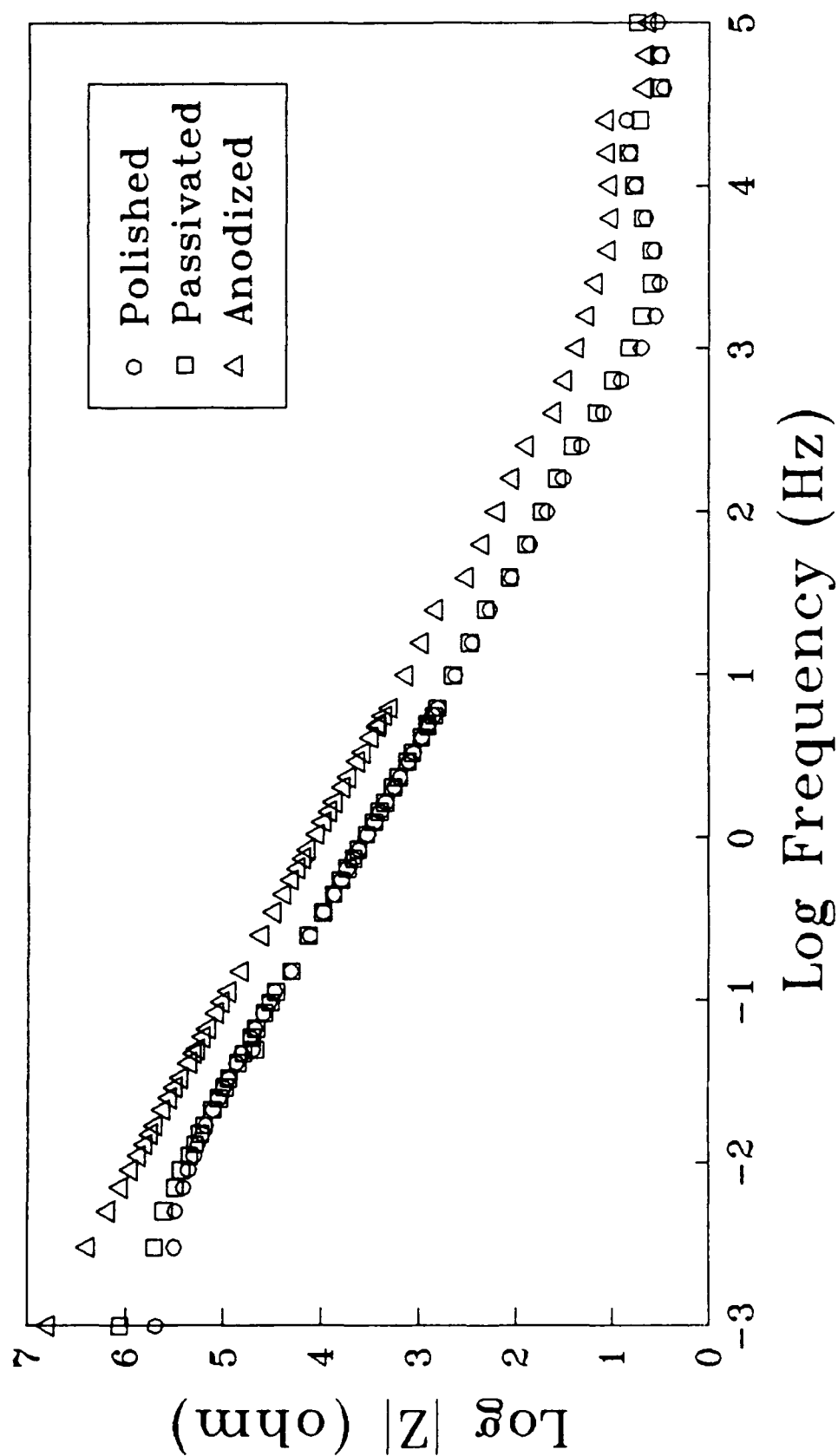


FIGURE 33a. Average Bode magnitude curves for the CP-Ti in the polished, passivated and anodized conditions.

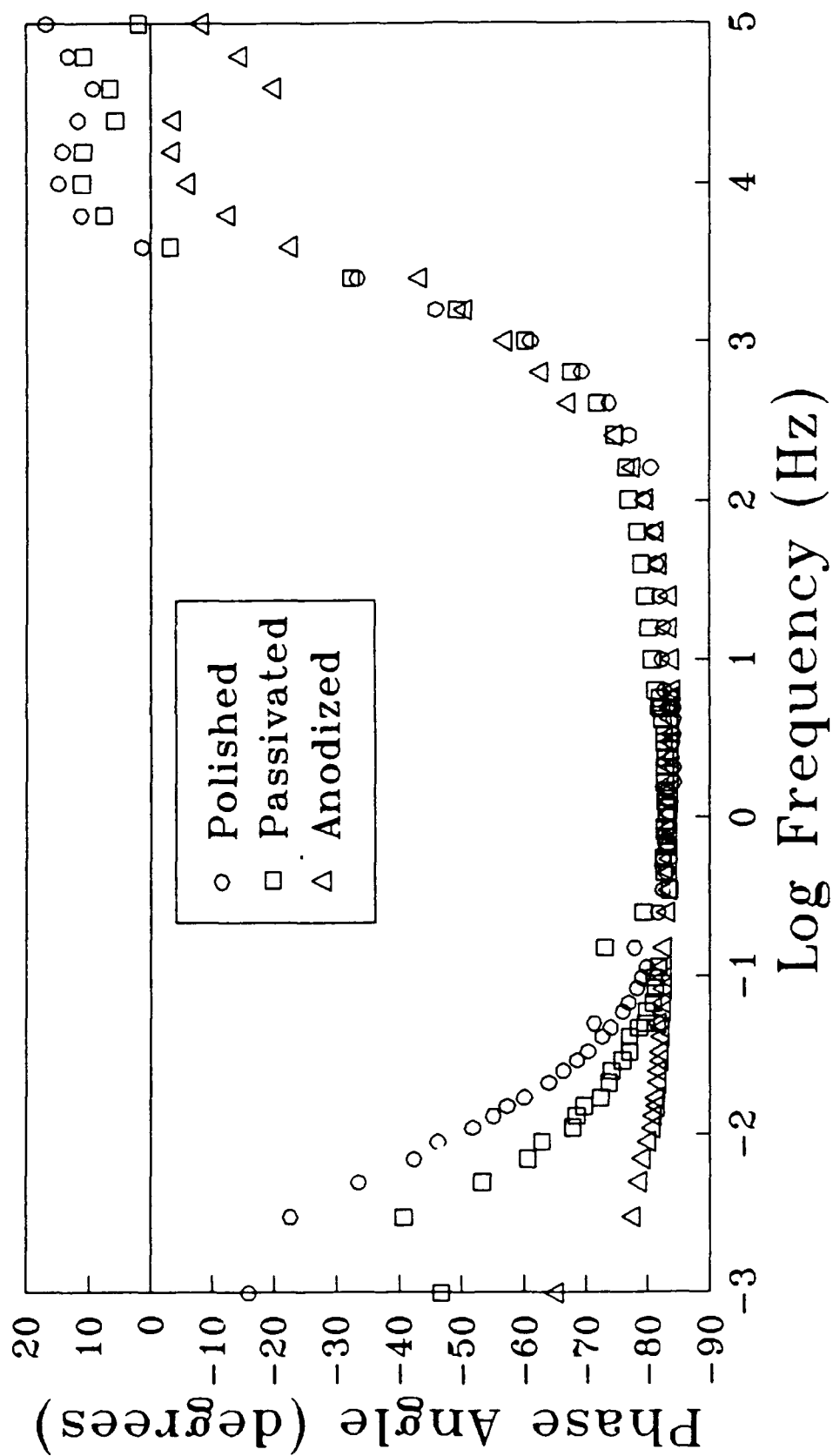


FIGURE 33b. Average Bode phase angle curves for the CP-Ti in the polished, passivated and anodized conditions.

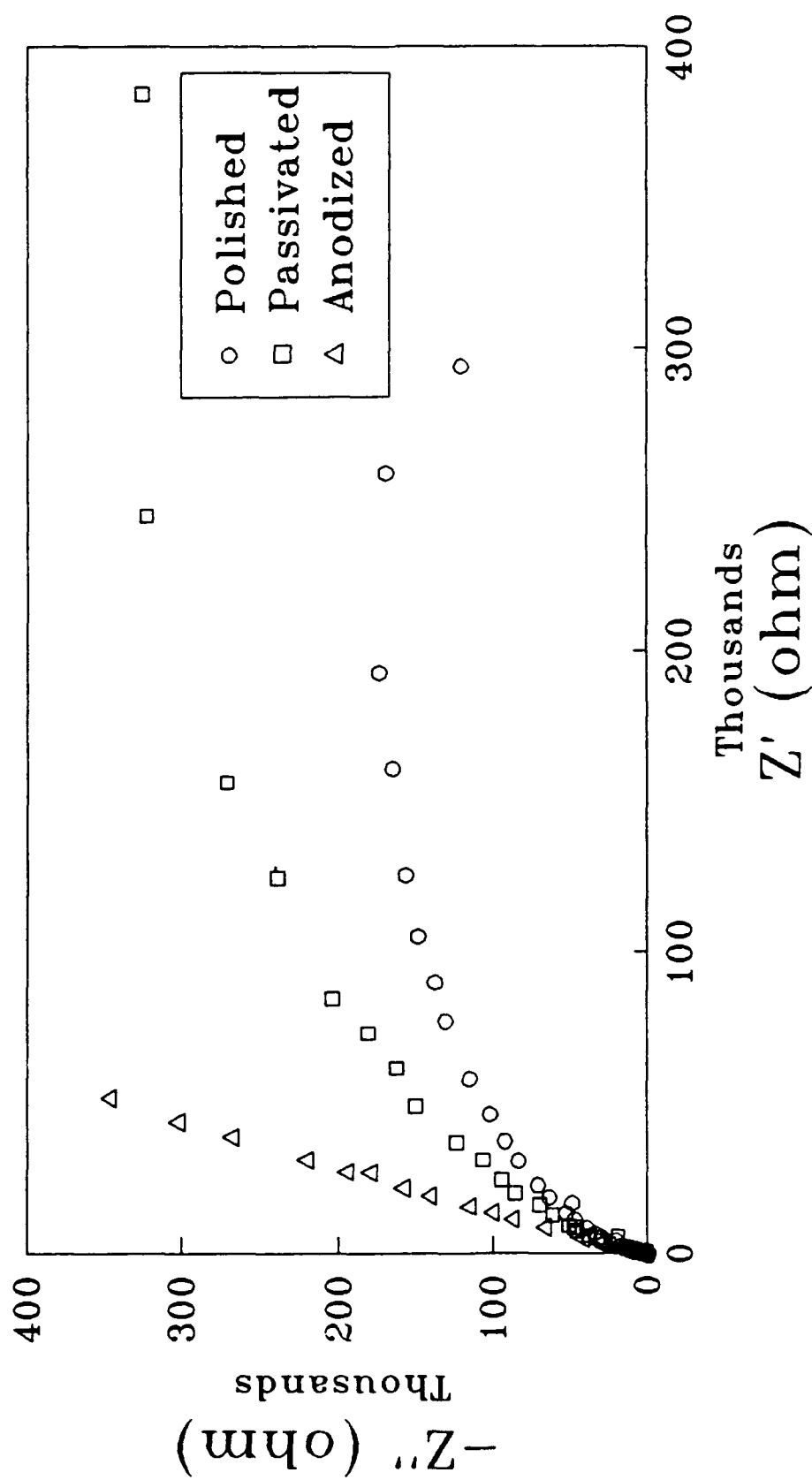


FIGURE 34. Average Nyquist curves for the CP-Ti in the polished, passivated and anodized conditions.

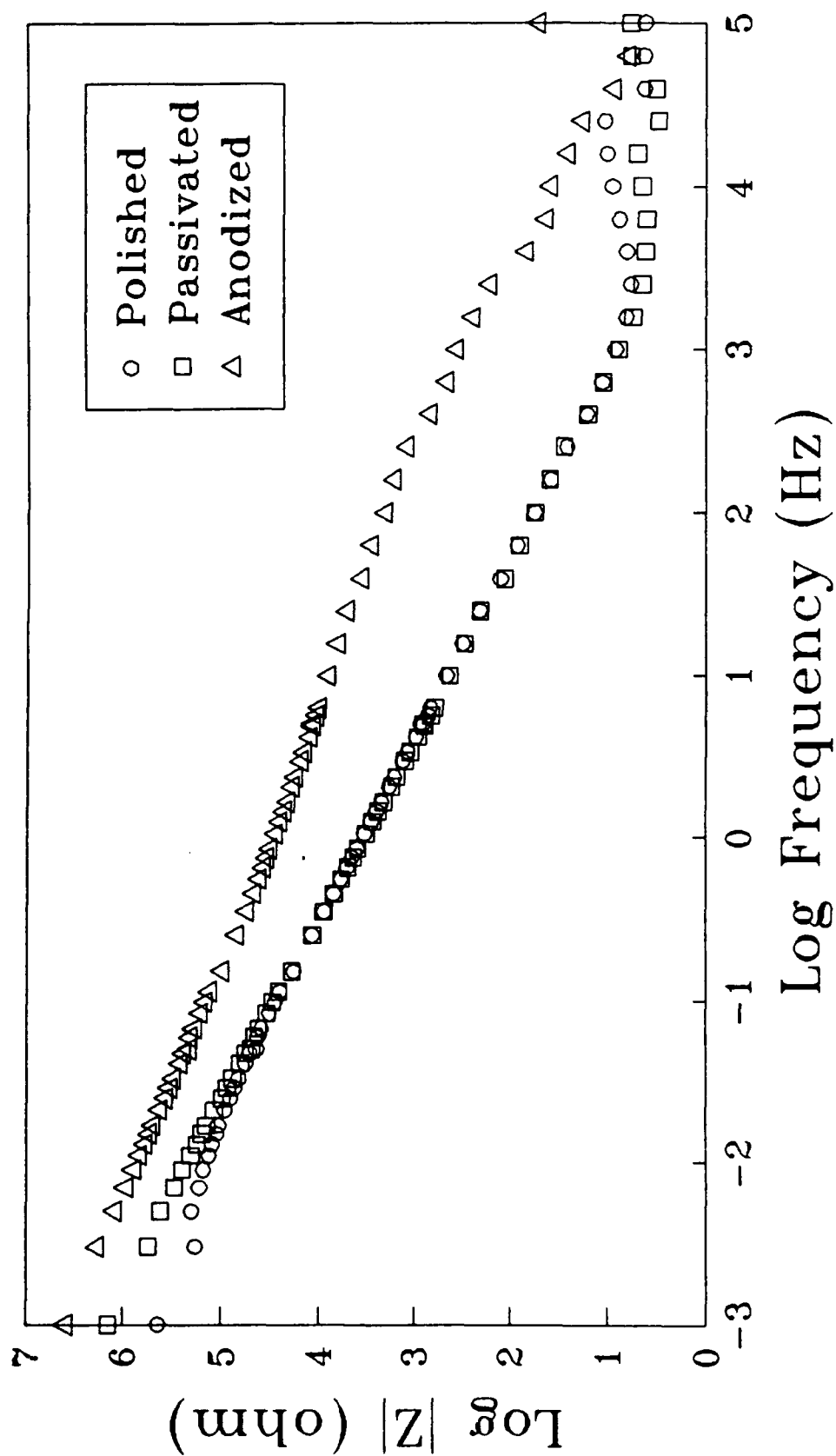


FIGURE 35a. Average Bode magnitude curves for the Ti-6Al-4V in the polished, passivated and anodized conditions.

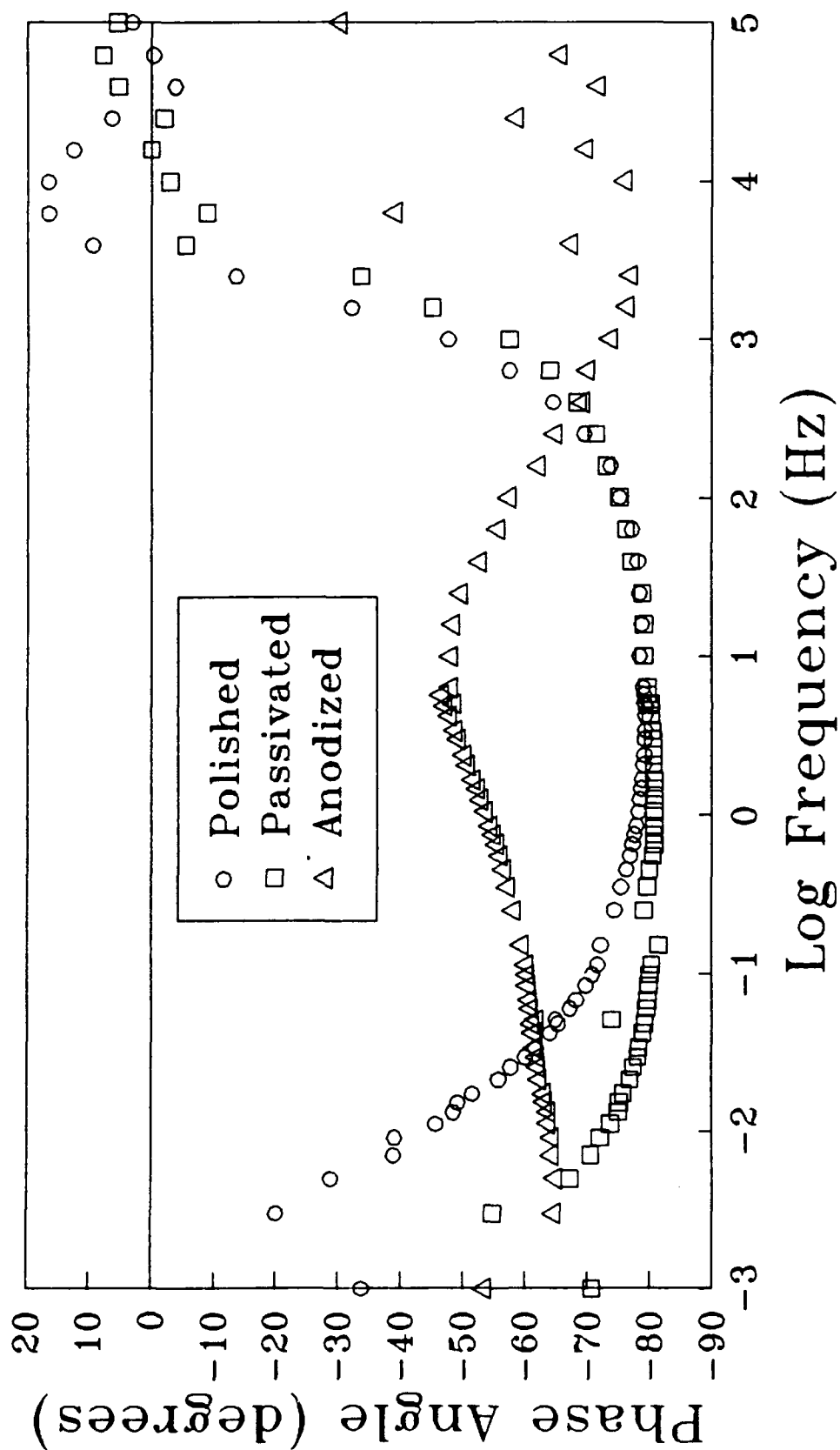


FIGURE 35b. Average Bode phase angle curves for the Ti-6Al-4V in the polished, passivated and anodized conditions.

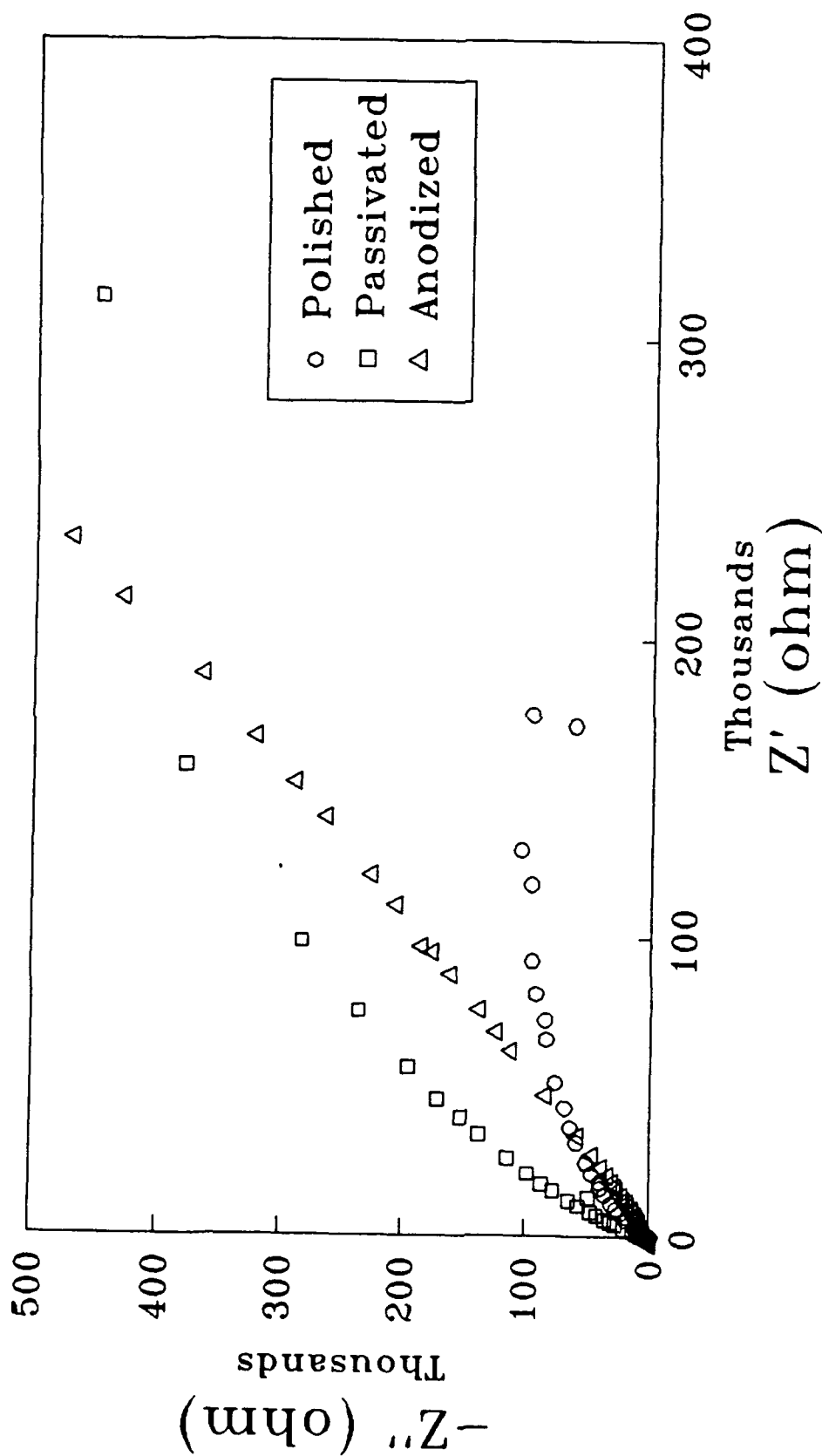


FIGURE 36. Average Nyquist curves for the Ti-6Al-4V in the polished, passivated and anodized conditions.

for the anodized surface than for the other surfaces. Furthermore, the phase shift extends to a lower frequency with the anodized surface than with the passivated surface, which in turn, extends to a lower frequency than with the polished surface.

Figures 35 and 36 show that for the Ti-6Al-4V, the polished and passivated samples behave in the same manner as the CP-Ti samples discussed above. The anodized Ti-6Al-4V sample produced greater impedance magnitudes than either of the other Ti-6Al-4V samples, but it followed a different trend, particularly at the higher frequencies. The phase angle behavior was also significantly different for the anodized Ti-6Al-4V than for the other surface conditions on the same material. These differences also manifest themselves in the different trend and magnitude of the Nyquist plot for the anodized Ti-6Al-4V than for the polished and passivated surfaces of the same material.

Energy Dispersive Spectroscopy

The energy dispersive spectroscopy (EDS) plot for the CP-Ti revealed only titanium as shown in Figure 37. The small peak near 2.75 keV was the escape peak for titanium and does not represent any additional constituent in the material. The larger of the two peaks was the $Ti_{K\alpha}$ peak and the smaller was the $Ti_{K\beta}$ peak.

The EDS plot for the Ti-6Al-4V as shown in Figure 38 revealed not only titanium but also aluminum and vanadium. Both titanium peaks as well as the titanium escape peak were

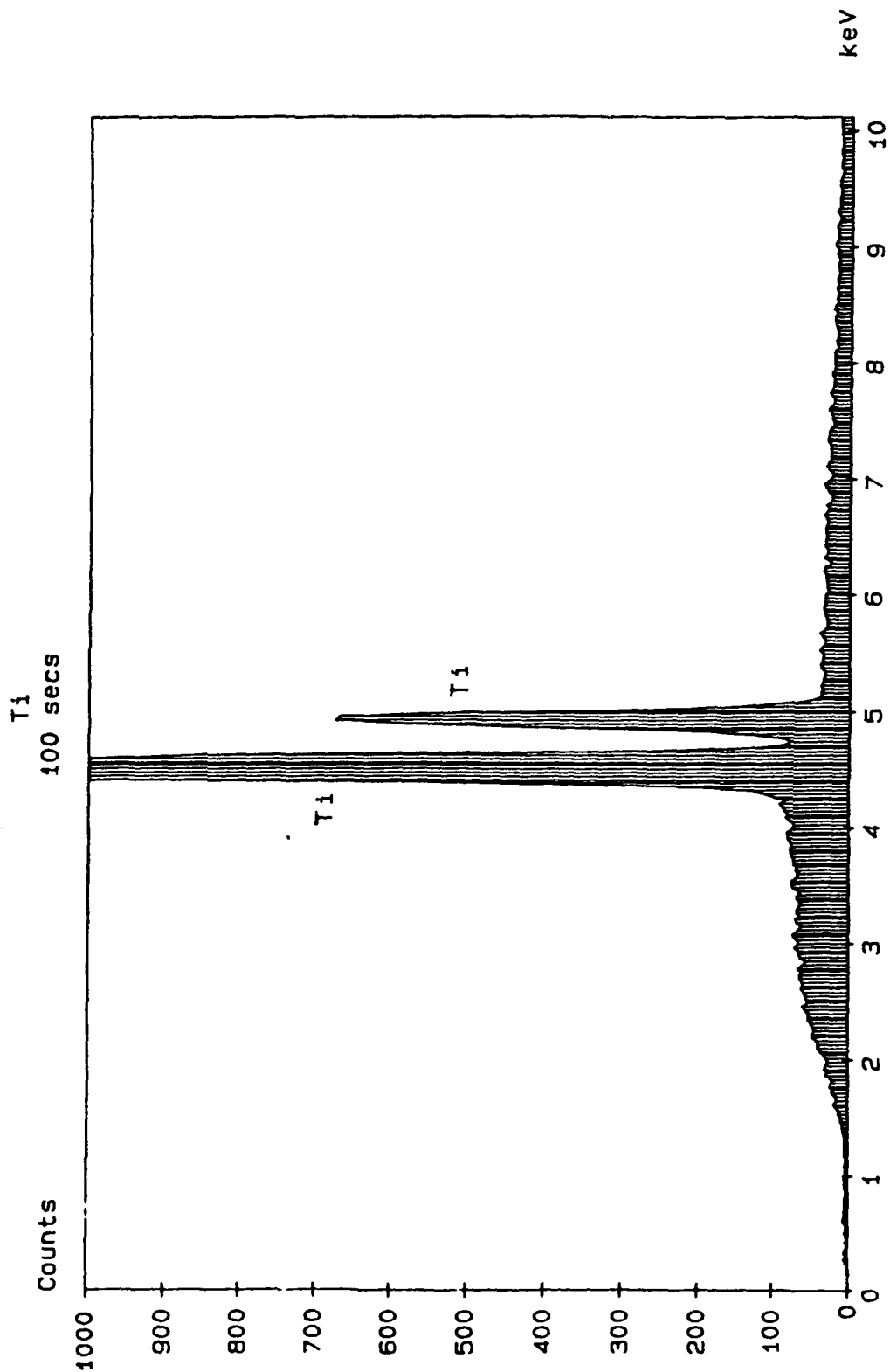


FIGURE 37. Energy dispersive spectroscopy spectrum for the CP-Ti sample showing only the characteristic titanium peaks.

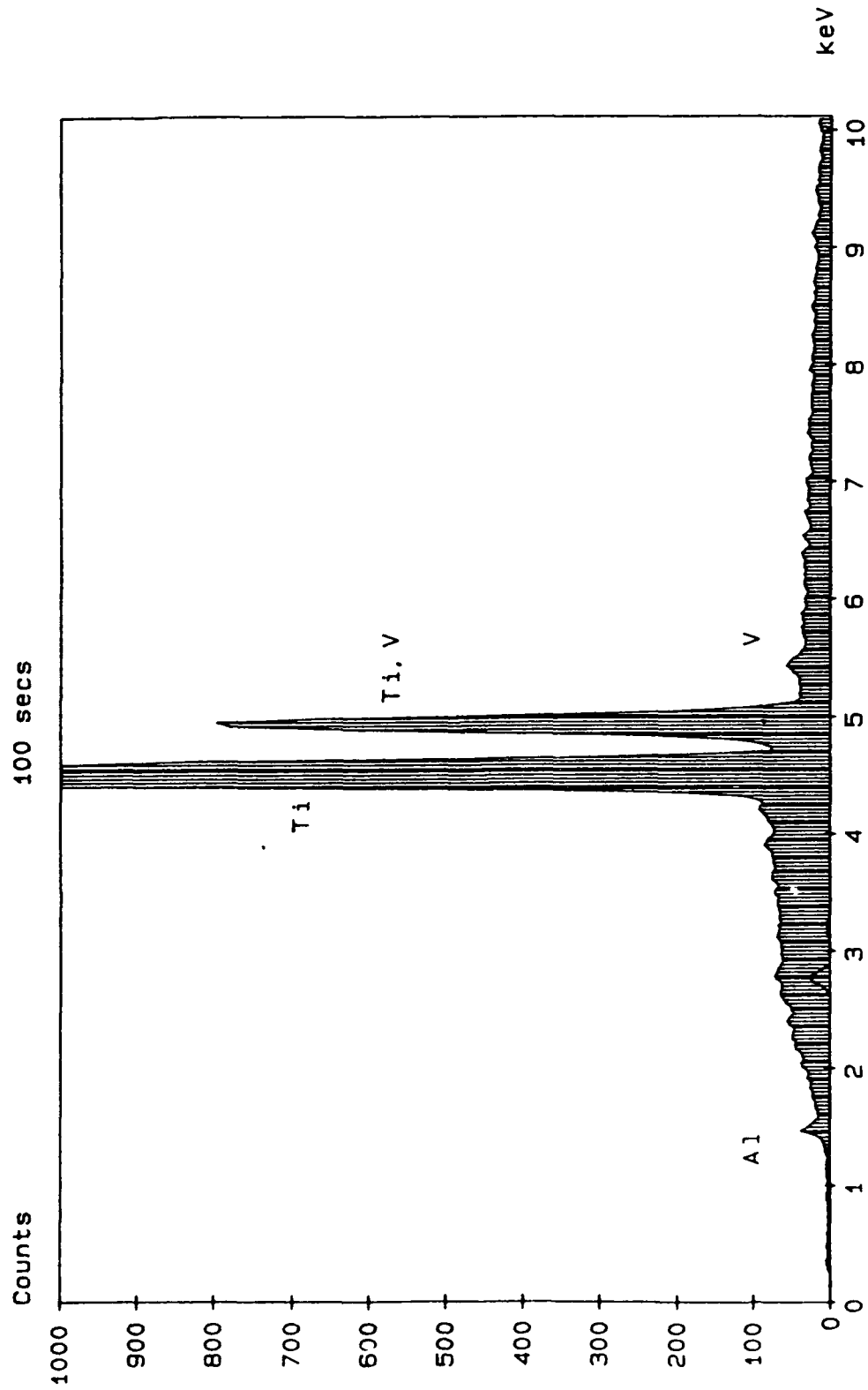


FIGURE 38. Energy dispersive spectroscopy spectrum for the Ti-6Al-4V sample showing the characteristic peaks for titanium, aluminum and vanadium.

again present. The vanadium $V_{K\beta}$ peak was visible while the larger $V_{K\alpha}$ peak was hidden since it overlaps the $Ti_{K\beta}$ peak. The contribution of the $V_{K\alpha}$ peak can be seen in the fact that the $Ti_{K\beta}$ peak was greater for the Ti-6Al-4V sample than for the CP-Ti sample. The aluminum peak was smaller than would be expected for a six percent composition. This can be attributed to absorption of the aluminum x-rays by the sample's matrix and the beryllium detector window. The EDS plot for the Ti-6Al-4V sample was also compared to the EDS plot for a sample of Ti-6Al-V of known composition. These two plots were nearly identical.

Auger Electron Spectroscopy

Upon examination using the instrument's SEM, the surface topography seemed to be similar for all of the samples, with no significant differences between the samples.

The surface analysis of all of the samples revealed the major surface constituent to be oxygen, followed by titanium. Also present were carbon, nitrogen, aluminum in the Ti-6Al-4V samples and phosphorous in the anodized samples. The vanadium could not be readily detected because the vanadium peak falls between the titanium and the oxygen peaks. Consequently, when there were large titanium and oxygen peaks, the vanadium peak was incorporated into them. After the depth profile, the oxygen, carbon and nitrogen were mostly removed and the vanadium peak could be seen, particularly when the Ti-6Al-4V spectrum was expanded and compared with the CP-Ti spectrum, as in Figures 39a and 39b.

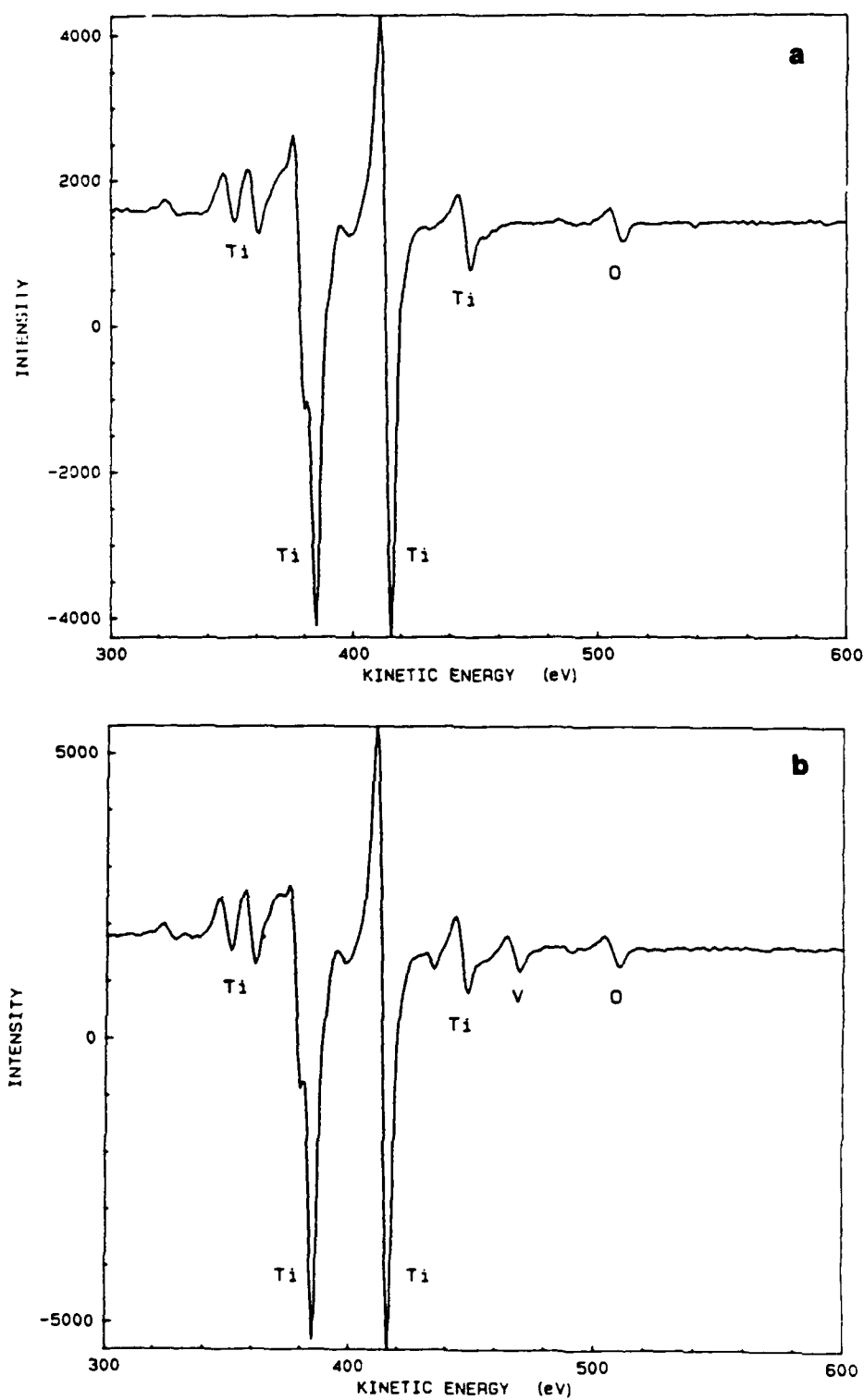


FIGURE 39. Auger electron spectroscopy surface spectra for the CP-Ti (a) and the Ti-6Al-4V (b), revealing the presence of vanadium in the Ti-6Al-4V sample.

The AES depth profiles for each material and surface condition were acquired and are displayed in Figures 40 through 45. This AES depth profile data is not quantitative but merely qualitative. That is, it can be used to determine depths in terms of the number of sputtering cycles but not in terms of actual units of length. In this study this is acceptable since the main concern is not the actual oxide thickness but rather the relative changes in that thickness for different materials and surface treatments. Consequently, all thicknesses reported will be in terms of number of sputtering cycles. The interface between the oxide and the base metal is taken to be that point where the intensities from all of the surface elements have fallen off to a plateau near zero. The oxide thicknesses for each condition are given in Table 4.

Figures 40 and 41 show that the oxide layers on the polished samples were quite thin, and there was not much difference between oxide thickness on the CP-Ti and the Ti-6Al-4V samples. Figure 42 shows that the oxide on the passivated CP-Ti sample was slightly thicker than that on the polished CP-Ti sample. The passivated Ti-6Al-4V sample, however, had a significantly thicker oxide than either the passivated CP-Ti sample or the polished Ti-6Al-4V sample, as can be seen in Figure 43. Figure 44 shows that the oxide layer on the CP-Ti sample was much thicker than that on either of the passivated samples. Finally, Figure 45 shows

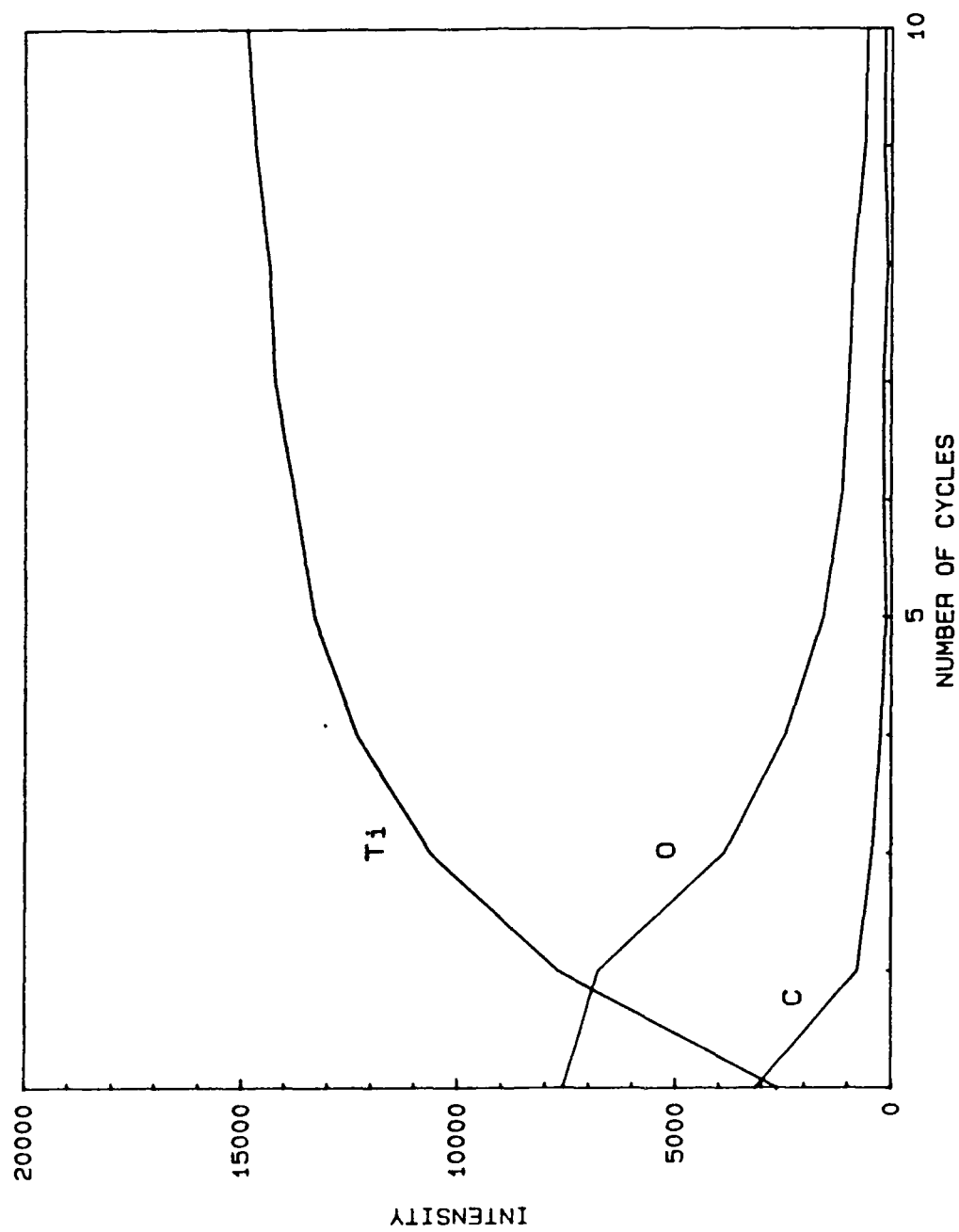


FIGURE 40. AES depth profile for the polished CP-Ti.

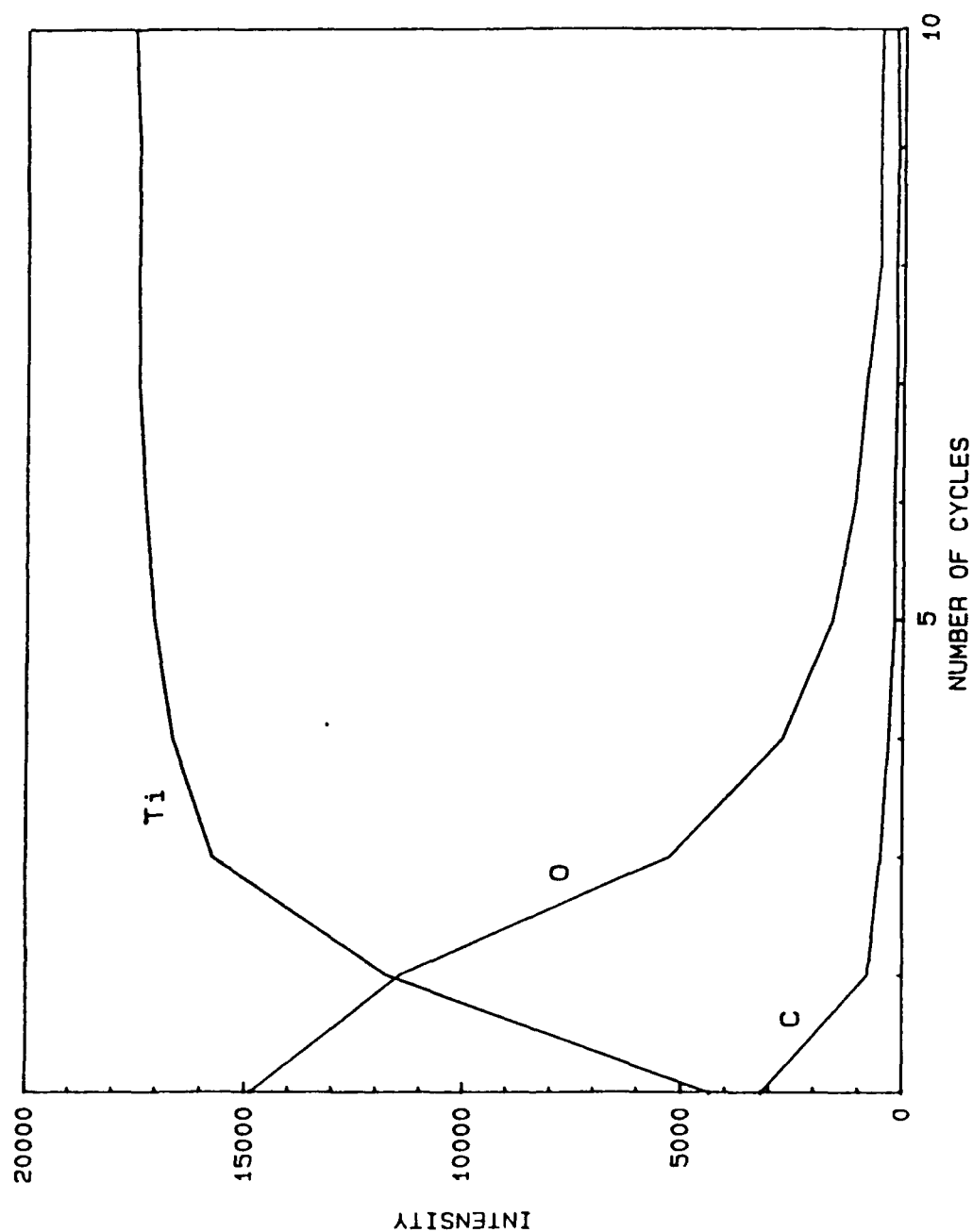


FIGURE 41. AES depth profile for the polished Ti-6Al-4V.

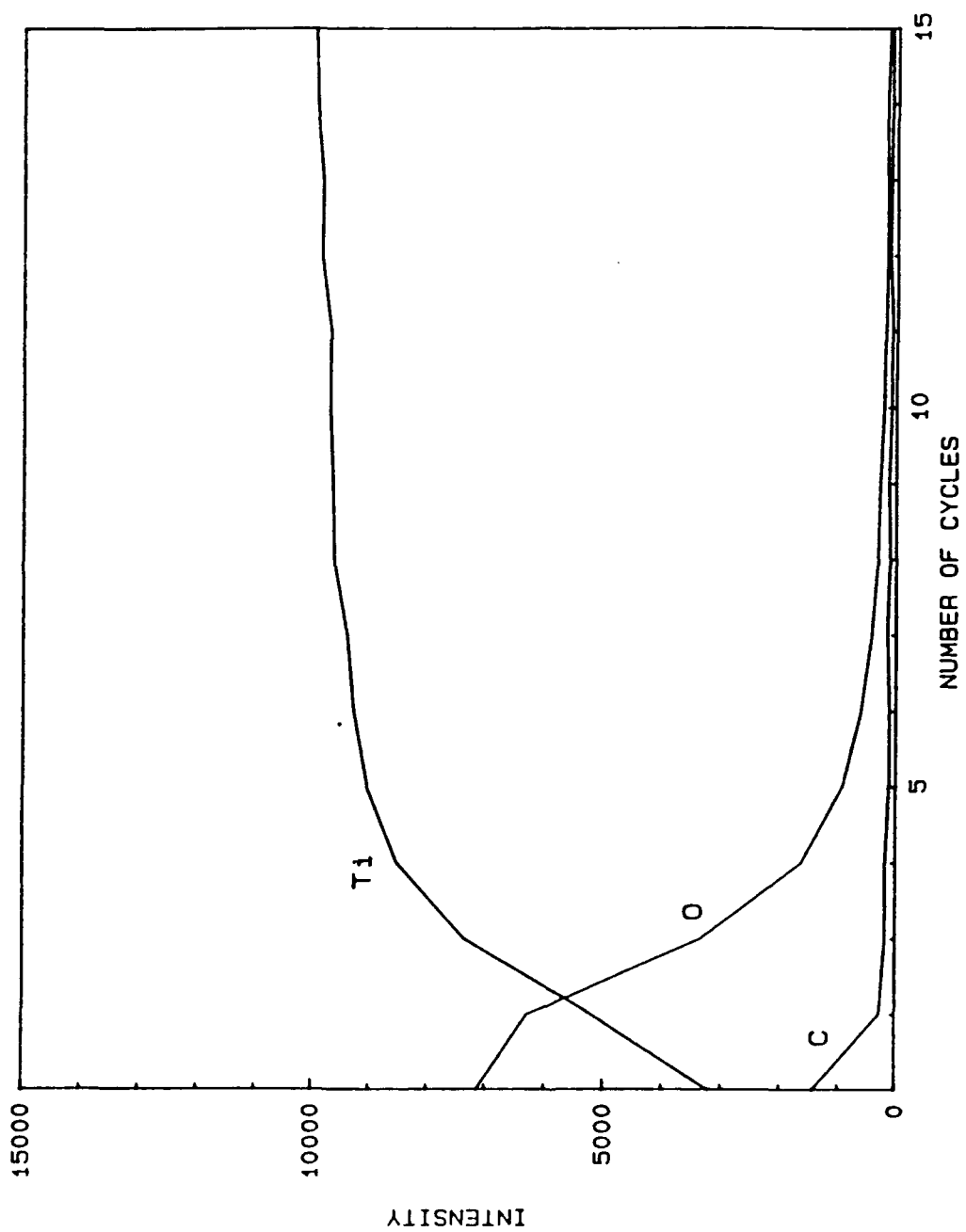


FIGURE 42. AES depth profile for the passivated CP-Ti.

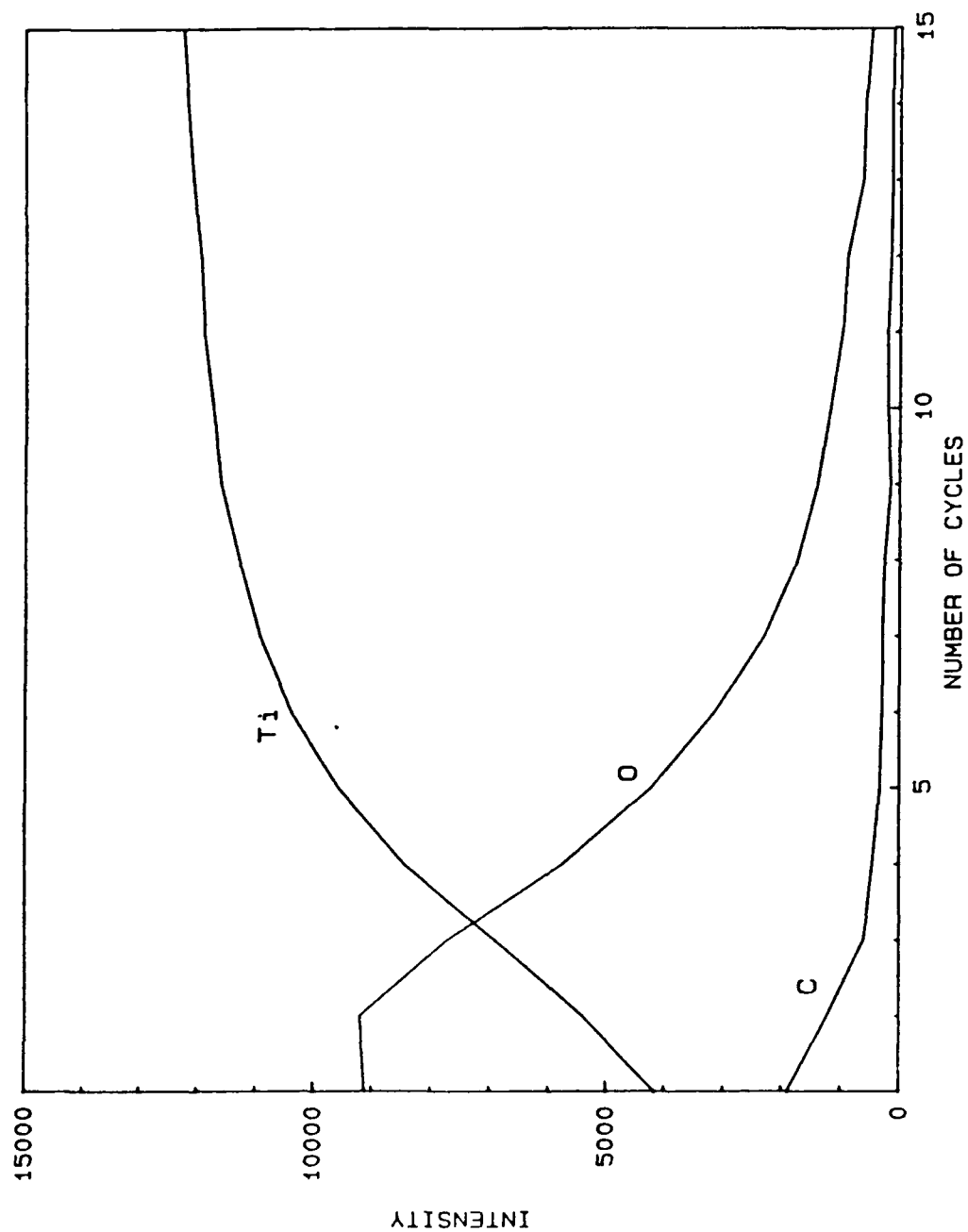


FIGURE 43. AES depth profile for the passivated Ti-6Al-4V.

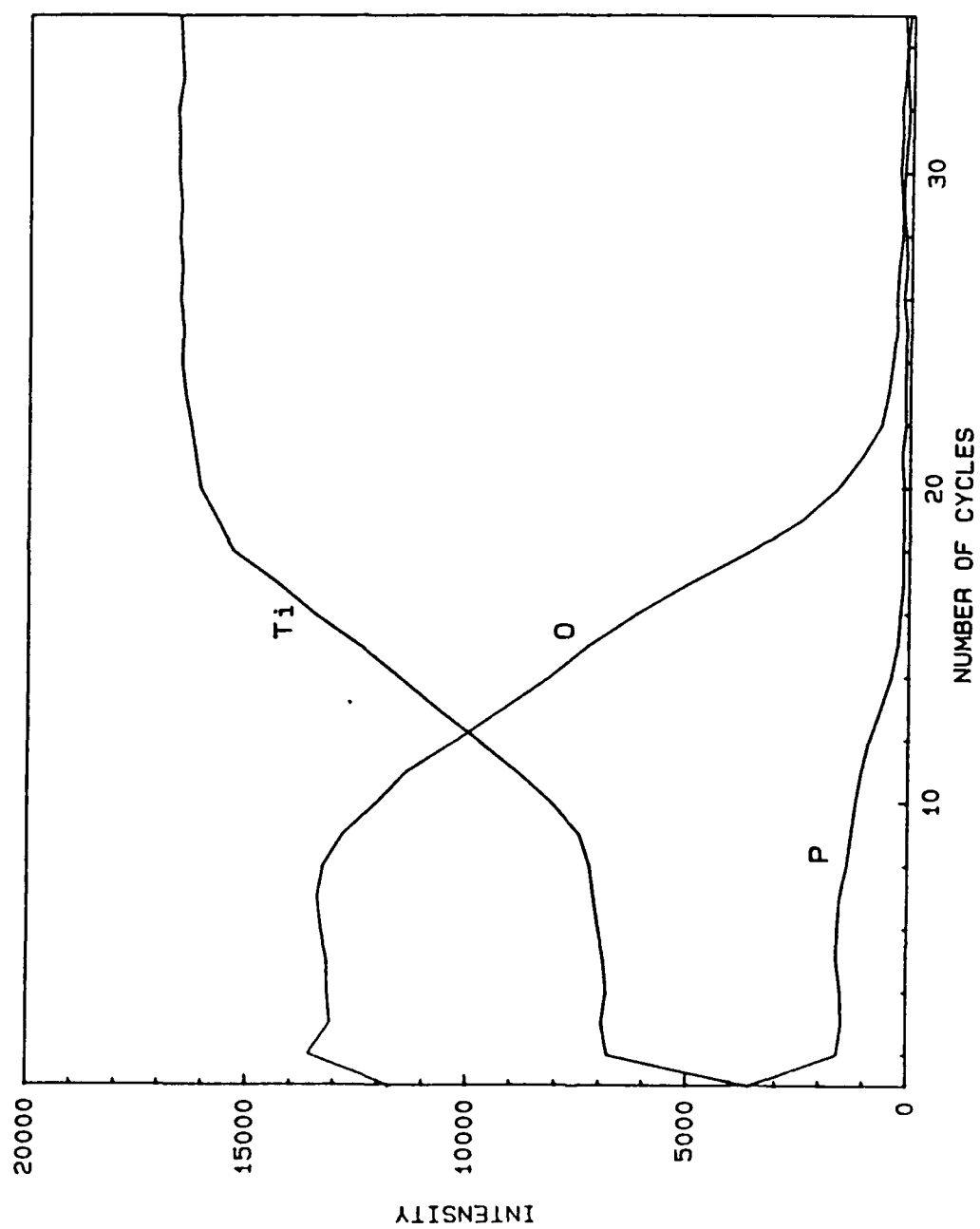


FIGURE 44. AES depth profile for the anodized CP-Ti.

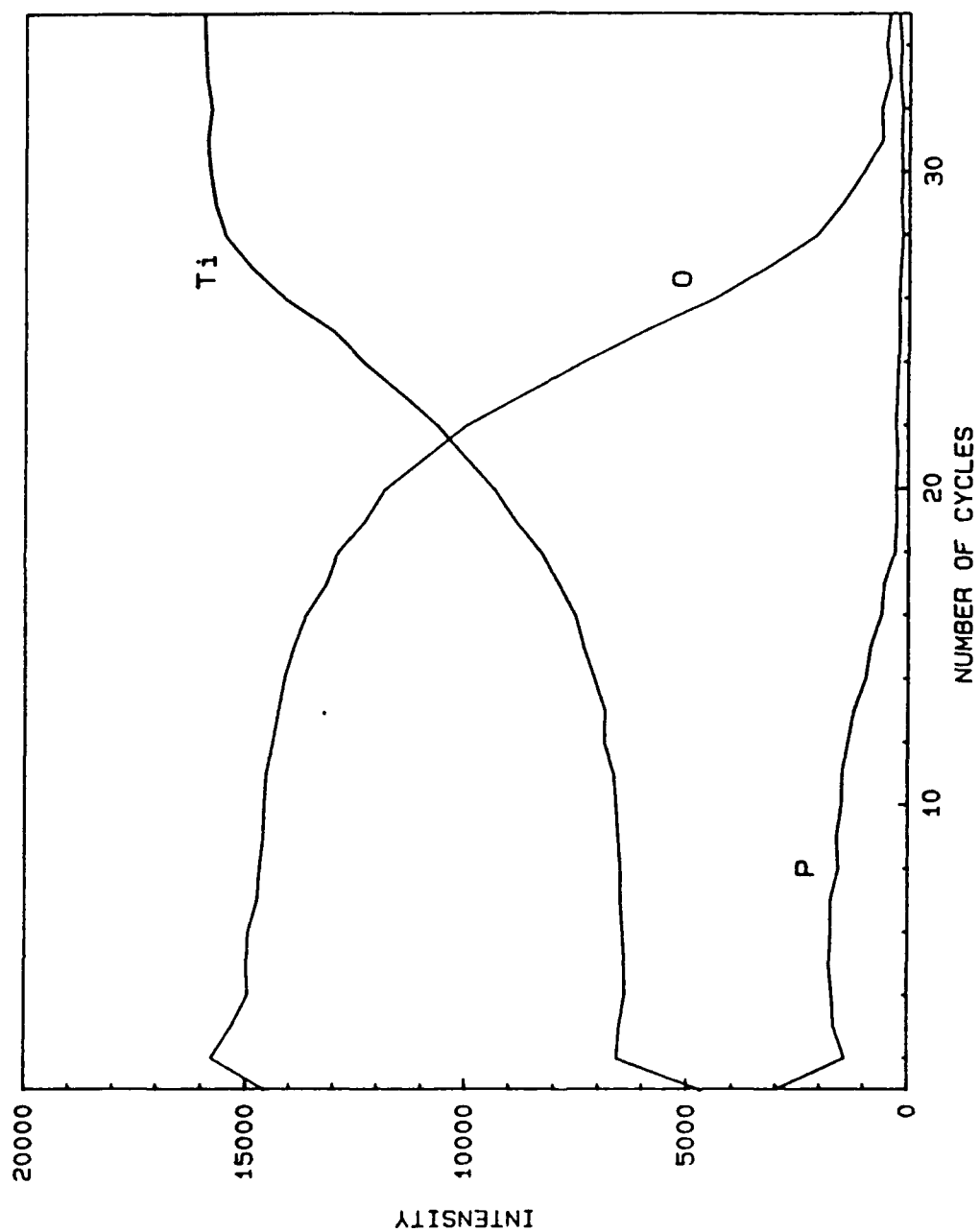


FIGURE 45. AES depth profile for the anodized Ti-6Al-4V.

that the oxide thickness on the Ti-6Al-4V was about 50% thicker than that on the anodized CP-Ti sample.

TABLE 4
Oxide Layer Thicknesses

SURFACE	OXIDE THICKNESS (# OF CYCLES)
<hr/> POLISHED <hr/>	
CP-Ti	9
Ti-6Al-4V	8
<hr/> PASSIVATED <hr/>	
CP-Ti	8
Ti-6Al-4V	13
<hr/> ANODIZED <hr/>	
CP-Ti	22
Ti-6Al-4V	31

CHAPTER V

DISCUSSION

Anodization Treatment

The resistance calculated from the potential and current during anodization is quite different from the resistance obtained from the equilibrium corrosion current and potential. The difference is approximately 5 orders of magnitude. This vast difference stems from the fact that these are two completely different systems. On the one hand is the anodization procedure where relatively large currents and potentials are forced through the sample in a corrosive media. Furthermore, the corrosive media is very viscous, making the reaction diffusion limited so that the surface of the material can not come to an equilibrium with its surroundings. On the other hand is the corrosion cell where a metal with a thick protective oxide is at equilibrium in a mild solution with no external currents or potentials applied. Consequently, a comparison of the resistance values as suggested in the objectives is of little scholarly value.

The different colors on the two different materials, however, are quite interesting. Some research done on Ti-6Al-4V anodized in phosphoric acid suggests that the color of the oxide is indicative of its thickness.¹⁶ Cigada et al. found

that the yellow oxide had a thickness of 200 Å while the blue oxide had a thickness of 800 Å.¹⁶ These results do not coincide with the findings in this study since the AFS depth profile data (Figures 44 and 45) clearly shows the yellow oxide on the Ti-6Al-4V to be much thicker than the blue oxide on the CP-Ti. Furthermore, during anodization, the Ti-6Al-4V formed a blue oxide which changed to yellow before the anodization process was complete. This also suggests that the yellow oxide is thicker than the blue oxide.

Schmets et al. determined that the colors of the oxides of titanium are characteristic of the oxide's composition.²⁹ The blue oxide was reported to be either TiO_3 which is thermodynamically unstable, or anhydrous TiO_2 , which is very stable, while the yellow oxide was reported to be hydrated titanium peroxide, $\text{TiO}_3 \cdot 2\text{H}_2\text{O}$.²⁹ Furthermore, hydrated $\text{TiO}_2 \cdot \text{H}_2\text{O}$ reportedly has a white color²⁹ which could account for some of the variation in the color observed in the blue oxide. This suggests that the oxides on the two different materials are different not only in thickness but also in composition with TiO_2 forming on the CP-Ti and $\text{TiO}_3 \cdot 2\text{H}_2\text{O}$ forming on the Ti-6Al-4V.

Pourbaix diagrams can be used to provide insight into the formation and stability of the different oxides of a pure metal. It should be noted that these diagrams are for pure metals in aqueous solutions at 25 °C. In the case of the Ti-6Al-4V, therefore, the diagrams do not necessarily hold true.

Since titanium constitutes the bulk of this alloy, it will be assumed that this alloy behaves similarly to pure titanium.

The Pourbaix diagrams given in Figures 46a and 46b suggest that the oxidation which occurred on the polished and passivated samples falls into the TiO_2 region. This is the oxide that naturally forms on titanium and protects the metal in aqueous solutions.²⁹ Furthermore, since the potential was initially near zero and increased slowly during anodization process, it is evident from the Pourbaix diagrams that the anodized samples first formed TiO_2 or $\text{TiO}_2 \cdot \text{H}_2\text{O}$ and then, as the potential increased, $\text{TiO}_3 \cdot 2\text{H}_2\text{O}$.

Thus, it is apparent that both metals initially formed TiO_2 but that both metals should have then formed $\text{TiO}_3 \cdot 2\text{H}_2\text{O}$. The lack of formation of $\text{TiO}_3 \cdot 2\text{H}_2\text{O}$ on the CP-Ti may be a result of a lack of time for the reaction to occur. The speed of reaction during anodization was slowed due to diffusion limitations resulting from the high viscosity of the anodization solution. This high viscosity resulted from the presence of a high percentage of glycerine. Furthermore, the CP-Ti seems to oxidize slower than the Ti-6Al-4V in all cases. This is evident in the fact that even though both materials have the same oxide thickness in the polished condition, the Ti-6Al-4V has a substantially thicker oxide in both the passivated and the anodized conditions, as shown by the AES depth profiles. The faster oxidation rate of the Ti-6Al-4V is possibly due to the addition of alloying elements, its two phase structure or other microstructural properties.

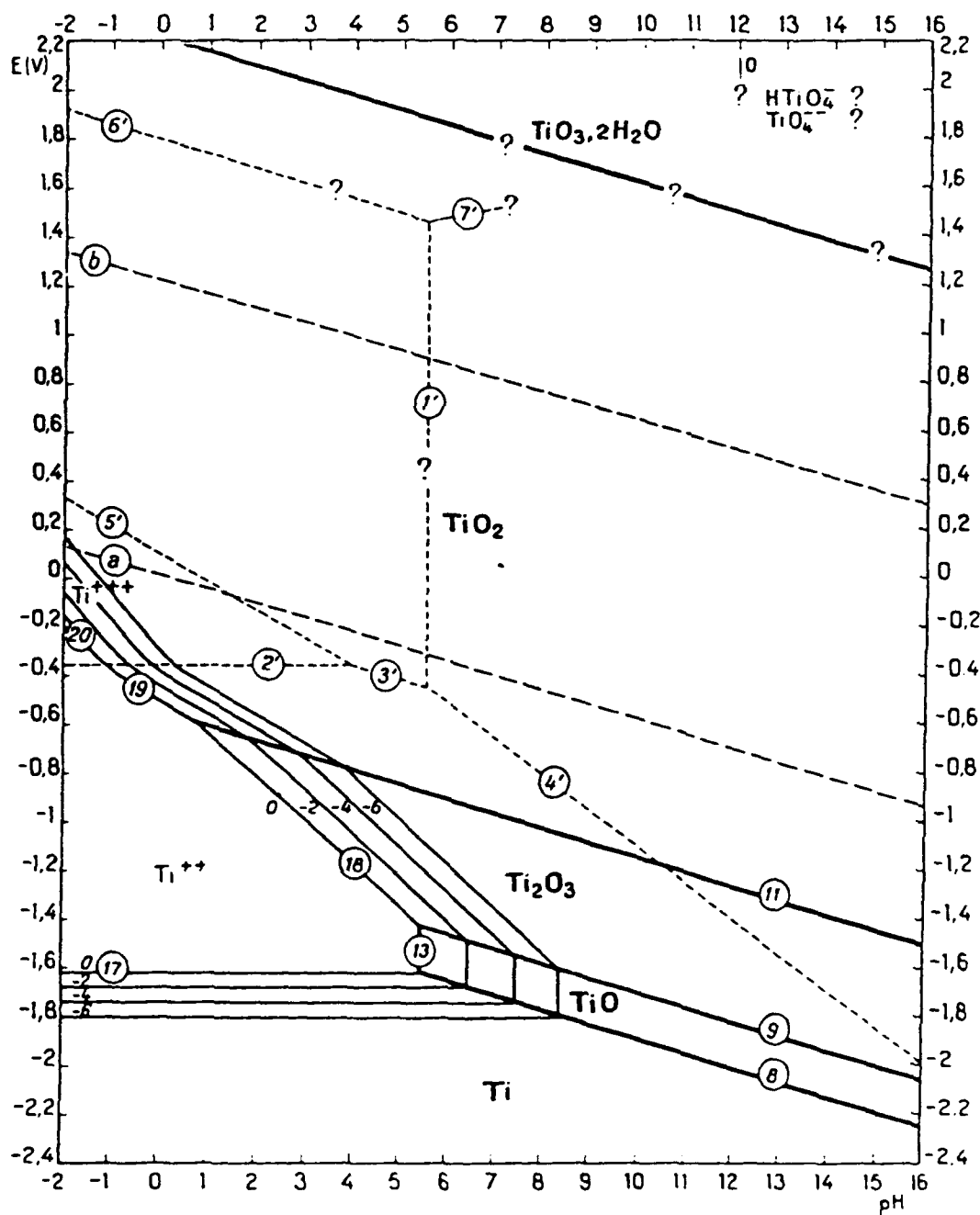


FIGURE 46a. Potential - pH equilibrium diagram for titanium in water at 25 °C, considering Ti_2O_3 and TiO_2 as the derivatives of tri- and tetravalent titanium.²⁹

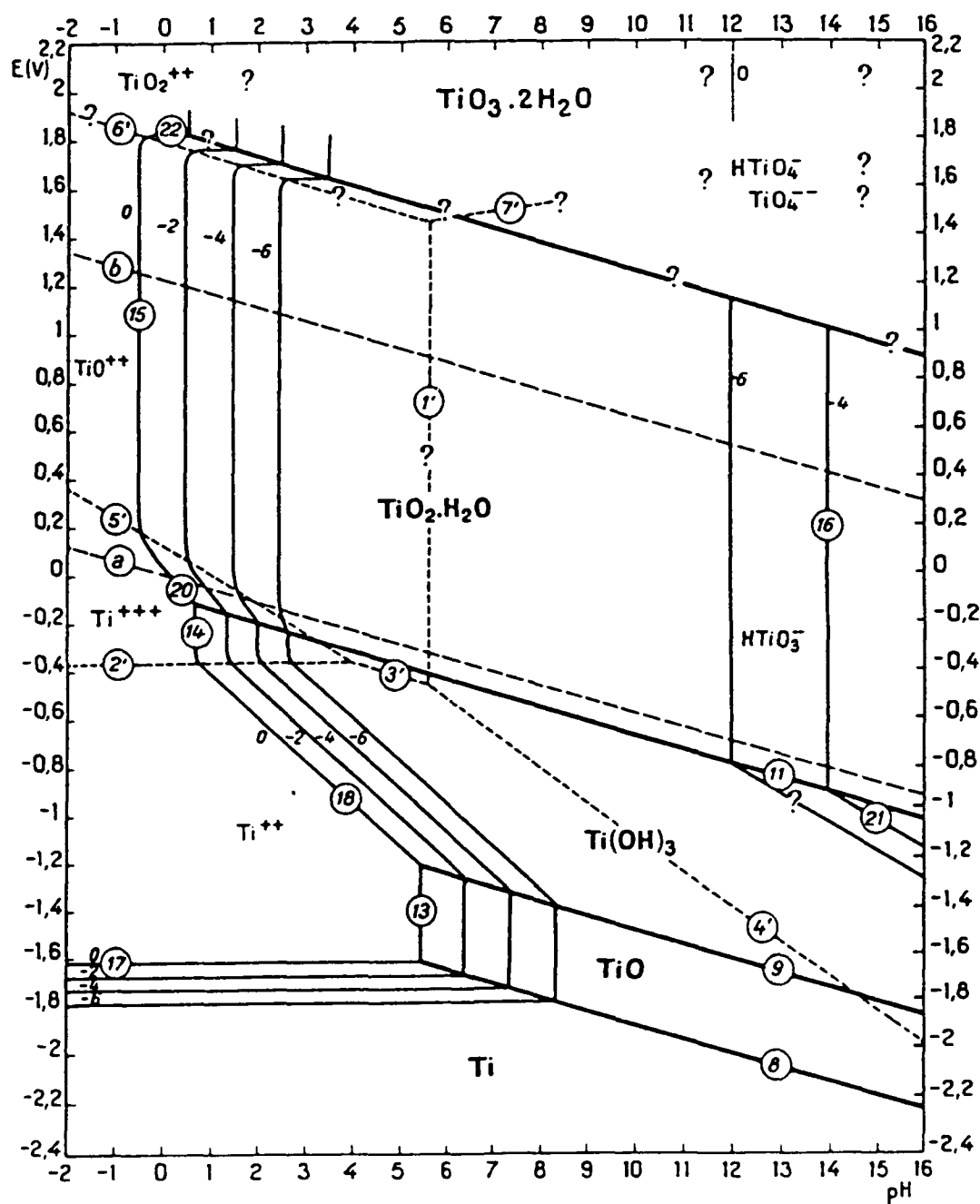


FIGURE 46b. Potential - pH equilibrium diagram for titanium in water at 25 °C, considering $Ti(OH)_3$ and $TiO_2 \cdot H_2O$ as the derivatives of tri- and tetravalent titanium.²⁹

A more rapid oxidation rate for the Ti-6Al-4V explains why this material formed $\text{TiO}_3 \cdot 2\text{H}_2\text{O}$ as well as TiO_2 , while the CP-Ti formed primarily TiO_2 . This was further supported by additional tests which have shown that at the same current and potential settings used in this study, but with a lower viscosity and pH, the CP-Ti also formed a yellow oxide.

The idea that the anodized CP-Ti has the same type of oxide as the polished and passivated samples is further supported by the fact that the anodized CP-Ti showed the same EIS trends as the polished and passivated conditions of both metals. The anodized Ti-6Al-4V, however, showed EIS trends different from all of the other conditions tested. This supports the idea that its oxide is substantially different from those on all of the other samples.

Potentiodynamic Polarization

The potentiodynamic standard test was conducted in accordance with ASTM G5 except the new mounting procedure was used instead of the normal cylindrical sample. This test showed a slight crevice corrosion tendency with the 430 stainless steel specimen. While ferrous alloys are particularly susceptible to crevice corrosion, titanium and its alloys are essentially immune. Ferrous alloys in chloride solutions experience accelerated corrosion in crevices due to a reaction with chloride ions in the absence of oxygen. With titanium and its alloys, this absence of oxygen causes the material in a crevice to be essentially non-reactive. Although the standard showed a slight amount of crevice

corrosion, the mounting method and the test procedure were considered to be acceptable for the materials used in this study.

With the procedure validated, the individual potentiodynamic polarization plots that were presented in the Results section were used to measure corrosion current densities. Since all of the samples had formed a passivating oxide film on the surface, the anodic portion of the curve could not be used in extrapolating the corrosion current densities. Therefore, the corrosion current densities were found by extrapolating only the linear portion of the cathodic curve to the point where it intersected the equilibrium potential line. The average equilibrium corrosion potentials (E_{corr}) and the average corrosion current densities (i_{corr}) as well as the standard deviation for both values are given in Table 5. The polarization resistance (R_p) for each test was calculated using EG&G Princeton Applied Research Model 342 Softcorr Corrosion Measurement Software. The average values and standard deviation of R_p for each condition are also given in Table 5. Since the samples passivated, the software was unable to determine i_{corr} for many of the tests. Furthermore, since the corrosion current densities were very low, some of the values measured were too small for the software calculation program. This was evident in the anodized cases as an i_{corr} of zero which was calculated. Consequently, the computer aided analysis for i_{corr} was considered to be unreliable for these purposes and was not used.

TABLE 5
Potentiodynamic Polarization Values

SURFACE	E_{corr}	I_{corr}	R_p	
	(mV vs S.C.E.)	($\mu\text{A}/\text{cm}^2$)	(k Ω)	
	(Avg/Std Dev)	(Avg/Std Dev)	Avg	Log
POLISHED				
CP-Ti	-397/12.5	0.17/0.057	284	5.45
Ti-6Al-4V	-387/40.3	0.20/0.069	288	5.46
PASSIVATED				
CP-Ti	-220/206	0.03/0.0051	1,336	6.13
Ti-6Al-4V	-170/120	0.032/0.020	1,361	6.13
ANODIZED				
Cp-Ti	-187/33.0	0.0013/0.00026	18,941	7.28
Ti-6Al-4V	-110/35.6	0.0034/0.0019	11,182	7.05

From the corrosion data in Table 5 and the polarization plots in Figures 22 to 26 it can be seen that the equilibrium potentials, current densities and polarization resistances are more a function of the surface preparation than of the base material. Figure 22 shows that there is very little difference in the behavior of the two metals in the polished condition. This is reasonable since the compositions of the two materials are similar, with the Ti-6Al-4V having only about 10 weight percent of its composition made up of aluminum and vanadium. Furthermore, the AES depth profiles of these two conditions (Figures 40 and 41) reveal nearly identical oxide coating thicknesses and compositions.

The polished condition had the lowest relative standard deviation of E_{corr} . This is partially because the polished surfaces all followed the same trend in terms of the potential

during the equilibrium period (Figure 18). Additionally, since the surfaces were polished just before testing, and did not receive any additional surface treatments, there was little time for variations in oxide formation to occur before the test.

The same trends that were seen for the polished surfaces can be seen for the passivated surfaces. Although the E_{corr} is somewhat more positive for the Ti-6Al-4V, the E_{corr} for both materials is higher for the passivated case than for the polished case. This can be seen in Figures 23, 25 and 26, and Table 5. These potentials are, however, slightly lower than the equilibrium potentials that were measured at the start of the test. As a result, the curves are slightly skewed.

The instrumentation scans a range of 500 mV below to 500 mV above the equilibrium potential so the equilibrium potential should be the median potential scanned. The reason for the skewing of the passivated curves, and to a greater extent the anodized curves, is that the scan rate used for the potentiodynamic polarization was not slow enough to approximate the DC or zero frequency condition. The slower the corrosion rate of a metal, the slower the response time. Consequently, if the scan rate is too high, the sample cannot approach an equilibrium and is continually lagging the instrumentation. With a scan rate of 0.2 mV/sec covering a range of 1000 mV the frequency would be 0.0001 Hz. This cannot be directly related to the EIS data, however, since the potential range is so greatly different. Without this effect,

the equilibrium potentials for the passivated curves would be slightly higher. In an attempt to correct this discrepancy, potentiodynamic polarization curves were generated for the anodized samples using a slower scan rate. These tests showed no significant improvement and it was determined that the scan rate would have to be decreased by at least an order of magnitude to correct the problem for the anodized samples. The increase in time that such tests would require made them unfeasible.

The corrosion current densities, i_{corr} , of the two metals in the passivated condition are nearly identical. With both metals, however, the i_{corr} in the passivated condition is approximately one sixth of that in the polished condition.

The polarization resistances, R_p , for the two different passivated materials are also very similar. This R_p for the passivated materials, however, is approximately five times that for the polished materials.

These trends in the i_{corr} and R_p indicate that there is little difference in the corrosion resistance of CP-Ti and Ti-6Al-4V when they have had the same surface preparation. These trends in i_{corr} and R_p also indicate that the corrosion resistance of both materials is about five or six times that of the same materials in the polished condition. This additional corrosion resistance is most likely related to the thickness of the protective oxide layer.

The AES depth profiles of the passivated surface conditions (Figures 40 and 41) reveal a somewhat thicker oxide

layer on the Ti-6Al-4V sample than on the CP-Ti sample. The CP-Ti shows no difference in thickness of oxide after passivation. The Ti-6Al-4V, however, does have a thicker oxide coating in the passivated condition.

Between the two passivated samples, the passivated CP-Ti appears to have a more abrupt transition between the coating and the base metal which is characterized by steeper titanium and oxygen lines on the AES depth profile plot (Figures 40 and 41). The reliability of the AES data for the passivated samples is questionable, however, due to the apparent instability of the oxide surface produced in the passivation procedure. It is suspected that some of the oxide layer may have been removed during the extra cleaning of the samples before they could be placed in the ultra-high vacuum of the Auger electron microscope.

The stability of the passivated surfaces comes into question due to the fact that the passivated surfaces have the largest relative standard deviations in E_{corr} (Table 5). This is supported by the different trends during passivation and equilibration, as shown in Figures 19 and 20. These figures show that the effects of the passivation process are somewhat inconsistent. Some of the samples passivated quickly, coming to an equilibrium within the passivation period, while some of the samples continued to passivate throughout the passivation period. While coming to equilibrium, the potentials of some of the samples remained high while potentials of other samples decreased to varying degrees. Those samples whose potentials

remained high most likely had formed a stable oxide during passivation. The decreases in potentials during equilibration were most likely due to the breakdown of the oxide layers on the surfaces of the specimens.

The potentiodynamic polarization curves for the anodized surfaces (Figure 24) show trends similar to those for the polished and passivated surfaces. As in the passivated condition, the E_{corr} for the anodized Ti-6Al-4V is slightly higher than that for the CP-Ti in the anodized condition. Both materials, however, have higher E_{corr} 's in the anodized condition than in either the polished or passivated condition. These potentials are lower than they should be due to the curves being skewed similarly to the passivated curves discussed above, but to a greater extent.

The more noticeable shift with the anodized surfaces is a result of the lower corrosion rate for the anodized condition. This lower corrosion rate requires a corresponding lower potentiodynamic polarization scan rate in order to approximate the zero frequency, or direct current, condition. Tests were conducted in which the scan rate was decreased and this did tend to correct the problem. From the results of these and the EIS tests, it was estimated that in order to achieve a low enough frequency to approximate the zero frequency, the time of each test would be increased by more than an order of magnitude. This was not done due to time, safety and reliability concerns involved in conducting an electrochemical experiment for that extent of time.

The relative standard deviation of the E_{corr} for the anodized samples is fairly low. This is due to the potential trends during equilibration, as shown in Figure 21. From this figure it can be seen that although there was a wide range of starting potentials, by the end of the equilibration, all of the potentials had approached nearly the same values. The E_{corr} as obtained from these equilibrium curves is approximately 0 mV. More important for this study is the i_{corr} which is not affected by the skewing of the curve since only the potential values are compressed.

The i_{corr} for the anodized condition is significantly lower than that for the passivated or polished conditions, as can be seen in Figures 25 and 26, and in Table 5. The anodized corrosion current densities are about an order of magnitude lower than those for even the passivated condition. Similarly, the R_p for the anodized condition is significantly higher than that for the passivated or polished conditions, as reported in Table 5. This indicates that the anodized samples have a significantly lower corrosion rate than either the passivated or polished samples as was expected.

This trend for a lower i_{corr} and a higher R_p in the anodized condition when compared to the polished or passivated conditions corresponds to the thicker oxide found on the anodized samples with AES.

In the anodized condition, unlike the polished or passivated conditions, there is an appreciable difference between the CP-Ti and the Ti-6Al-4V in terms of the values of

i_{corr} and R_p . Table 5 shows this. The i_{corr} for the anodized CP-Ti is only about one half of that for the anodized Ti-6Al-4V while the R_p for the anodized Ti-6Al-4V is only about two thirds of that for the anodized CP-Ti.

This trend does not agree with the AES depth profile data since Figure 44 and 45 show a much thicker oxide layer on the Ti-6Al-4V sample than on the CP-Ti sample. Consequently, the corrosion rate must be affected by something other than just the thickness of the oxide. The composition and structure of the oxide may also affect the corrosion rate.

Electrochemical Impedance Spectroscopy

The average EIS plots, presented in Figures 27 through 35, show that all of the different conditions tested, except for the anodized Ti-6Al-4V, follow the same trend. Surprisingly, this trend shows only one time constant, or one rate determining process occurring at the surface of the corroding specimen. This is the same trend that would generally be expected for a bare surface and is normally modeled by the Randle's circuit (Figure 4). This is unusual since all of the cases tested had, to some extent, formed a protective oxide layer which is evident from the AES depth profile data (Figures 40 to 45). The EIS data for the anodized Ti-6Al-4V, on the other hand, shows trends that are quite different from all of the other cases. For this reason, the results for all of the cases except for the anodized Ti-6Al-4V will be discussed first as a group, followed by the results for the anodized Ti-6Al-4V.

Those cases that show the same trends do not all have the same magnitudes. It is quite obvious from the EIS data plots (Figures 27 to 36) that the values differ along the same lines as for the potentiodynamic polarization plots. That is, the magnitude of the data is primarily a function of surface condition. Again, there is little difference between the data for the CP-Ti and the Ti-6Al-4V when both materials had the same surface treatment.

As mentioned earlier, these cases all fit the pattern of a bare corroding surface. One characteristic of this is the smooth, semi-circular Nyquist plot. A smooth Nyquist plot signifies that there is only one time constant. A second time constant would be evident from the Nyquist plot by the presence of a second semi-circular trend. The Nyquist plot, however, can be misleading and is typically difficult to interpret since it uses linear scaling which compresses the data near the origin. Furthermore, frequency data is not explicitly stated on the Nyquist plot. For these and other reasons, some researchers have suggested that the Bode plot should be used as the standard for EIS testing.²³

The suggestion to use the Bode plot as a standard plot is based first on the fact that the Bode plot represents all experimental data, and second on the fact that the phase angle is very sensitive to additional time constants.²³ Consequently, the Bode plots will be used primarily from here on in this report.

The Bode magnitude plot is useful in determining the infinite and zero frequency conditions since at these conditions the curve reaches a plateau. This is because at significantly high or low frequencies, the impedance of any imaginary, or capacitive, components approaches zero or infinity, respectively. At this point the real, or resistive elements, which are independent of frequency, can be easily determined.

At the intermediate frequencies, between the high and low frequency plateaus, the curve is dominated by the frequency dependant capacitive elements. For systems with a single time constant, this region is linear with a slope of -1 on a log-log scale, and shifts vertically with a change in the capacitive elements. Additional time constants will result in changes in the slope of this line.

Additional time constants can be easily identified with the Bode phase angle plot. For a single time constant system, the phase angle will approach zero as the system approaches both the infinite and zero conditions. At the intermediate frequencies, the phase angle will approach -90 degrees due to the phase shift associated with capacitive elements. Any additional time constants would be evident by the presence of any local maxima in the intermediate frequency region.

The phase angle plot is also useful in identifying the frequencies at which the impedance data makes a transition from being primarily resistive to primarily capacitive in nature, and vice versa. This is done by realizing that the

resistive elements have only real impedance components and are, therefore, a function of the cosine of the phase angle. Likewise, the capacitive elements have only imaginary impedance components and are, therefore, a function of the sine of the phase angle. Thus, as the phase angle increases above -30 degrees, the resistive component rapidly gains prominence, and as the phase angle decreases below -60 degrees, the impedance behavior is increasingly dominated by the capacitive component. Consequently, the plateaus at the high and low frequency of the Bode magnitude plot occur at approximately the same frequency at which the Bode phase angle plot reaches -30 degrees. This knowledge is particularly useful in cases where the low frequency plateau occurs outside of the frequency range tested. For example, there is no low frequency plateau present on the Bode magnitude plot for the passivated surfaces (Figure 29). Extrapolating the Bode phase angle curve for the passivated CP-Ti to an angle of -30 degrees gives a corresponding log frequency of approximately -2.7 Hz. The same frequency on the Bode magnitude plot gives an impedance value of about $\log 5.8 \Omega$.

There are two further characteristics of the Bode plots that warrant mention here. The first is the inductance at high frequencies which is evident as a positive phase shift on the Bode phase angle plot. This inductance is instrumentation induced and does not have a significant effect on the corrosion tests.⁷ Consequently, any points at frequencies

higher than that where the phase angle reaches zero are not considered in the analysis.

The second characteristic that is of some concern is the apparent inaccuracy of the lowest frequency point of each test. In every EIS test conducted, the lowest frequency point tested, regardless of the actual frequency, did not agree with the trend of the rest of the data. This suggests that this problem is another instrumentation effect. Because of this, the lowest frequency point will not be considered in the data analysis.

As mentioned earlier, all of the cases tested except for the anodized Ti-6Al-4V had only one time constant evident in their Bode plots, making them appear as if they were bare rather than oxidized surfaces. This can not be the case, however, since the AES depth profile tests showed distinct oxide layers on all of the samples. Since the samples are indeed oxidized, a model for a coated metal would be expected.

The model given in Figure 6 is the most general model that is routinely applied to coated metal samples. In this model, the sub-circuit made up of the double layer capacitance, C_{DL} , and the polarization resistance, R_p , represents the actual reaction at the metal's surface. This double layer capacitance, as previously mentioned, results from a charge differential across a thin film of solution on the surface of the metal. Since the solution used in this study was conductive and was continuously circulated, the double layer capacitance is negligible when compared to the

magnitude of the other circuit elements. As C_{DL} approaches zero, the impedance across this element in the circuit model approaches infinity, thereby justifying its removal from the model.

This leaves only R_p in series with R_{po} . Since two resistors in series are additive, the EIS data will appear as if there is only one resistor, with no distinction between R_p and R_{po} . Therefore, the R_{po} will be dropped from the model and the diffusion components of the oxide layer will be absorbed into the R_p term.

This leaves the three component model shown in Figure 47 which is similar in appearance and behavior to the Randle's circuit. The difference is that the capacitance in this new model is the coating capacitance, C_c , and not the double layer capacitance, C_{DL} . This is important in describing the impedance behavior of the different conditions since the coating capacitance should change with the thickness and integrity of the oxide layer.

Computer software developed by Boukamp³⁰ was used to fit this model to the experimental data. The modeling routine first models the impedance data by fitting a semi-circle to the Nyquist plot. The output of this routine are R_o , R_p and a constant phase element, CPE, which is given as an admittance term and an exponent, n . The CPE is a general diffusion related element which is frequently encountered but never given a general physical interpretation with regards to corrosion. The CPE is defined as a pure circuit element for

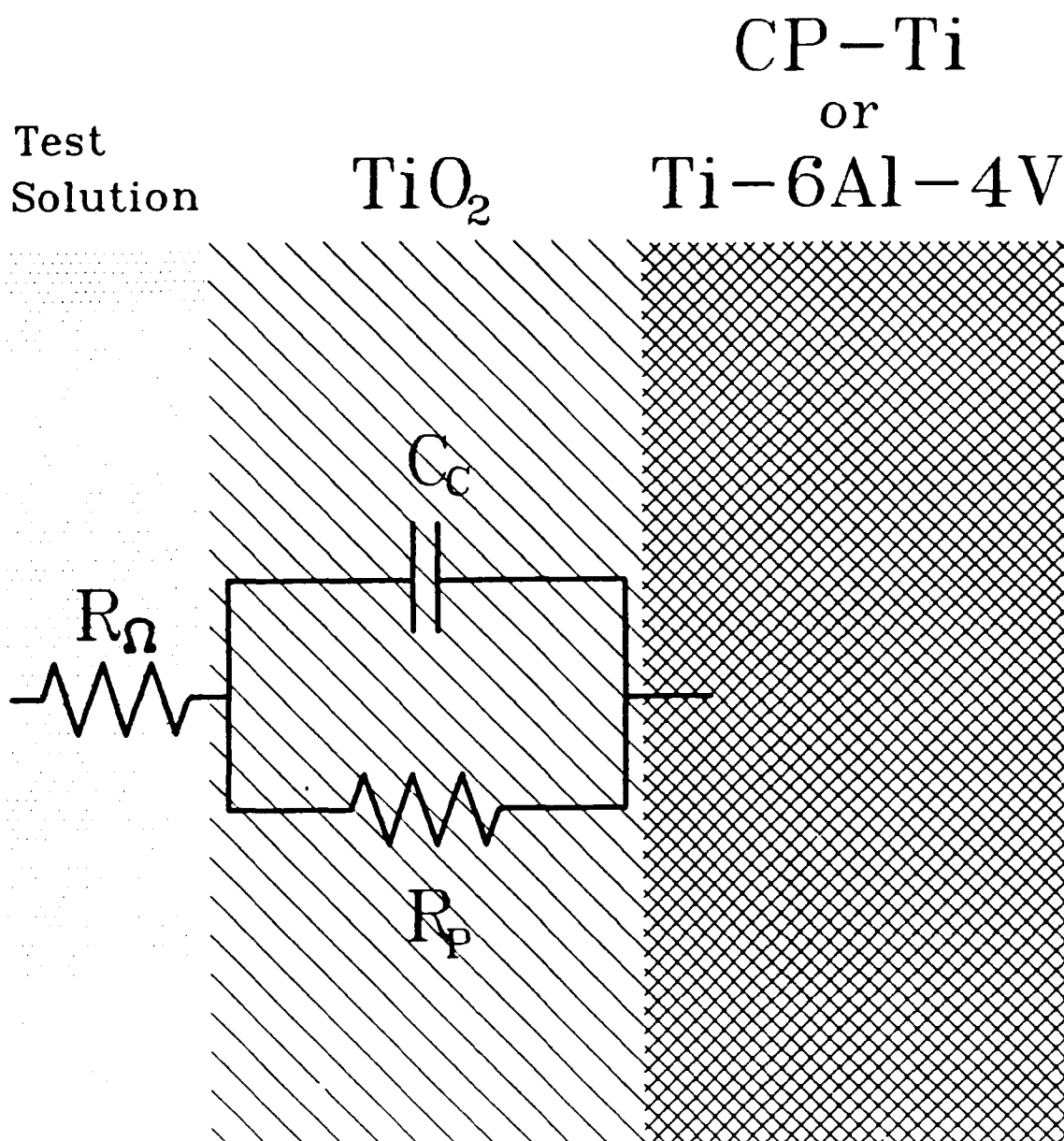


FIGURE 47. Equivalent circuit used to model the polished and the passivated CP-Ti and Ti-6Al-4V and the anodized Ti-6Al-4V as having a single layer of non-porous TiO_2 .

four cases: when $n=0$, the CPE is a resistance; when $n=1$, the CPE is a capacitance; when $n=0.5$, the CPE is a Warburg (an infinite diffusion term); and when $n=-1$, the CPE is an inductance.³⁰ Since for the five cases discussed thus far, the n value ranged from 0.85 to 0.92, the CPE's for these cases were considered to be capacitors.

Some authors have suggested leaving the model in terms of a CPE in order to obtain a better fit to the data.³¹ The problem with this practice is that the model does not have a physical significance due to the undefined CPE. It is better, therefore, to accept a lesser fit that has real physical significance, and then realize that there is also some other small factor that has not been accounted for yet.

The values for R_o , C_c , and R_p for the polished and passivated samples of both CP-Ti and Ti-6Al-4V and for the anodized CP-Ti are given in Table 6. The value of Chi-squared is also given for each condition. This value is a measure of the statistical accuracy of the fit of the model to the data, with a value of zero being a perfect fit. The fit of these models to the actual impedance data can be found in Figures 48 to 52.

The values for R_o are all small and are only significant in that they can be isolated from the rest of the surface reaction. These can be verified by comparing them to the magnitude of the high frequency plateaus on the Bode magnitude plots in Figures 48 through 52.

TABLE 6
Circuit Element Values for EIS Circuit Model

SURFACE	n	R_o (Ω)	C_c (F) $\times 10^{-5}$	R_p (Ω) $\times 10^5$	R_p Log	Chi ²
<u>POLISHED</u>						
CP-Ti	0.91	3.45	4.55	3.21	5.51	0.054
Ti-6Al-4V	0.85	4.21	4.96	1.62	5.21	0.11
<u>PASSIVATED</u>						
CP-Ti	0.92	5.62	4.72	5.82	5.76	0.097
Ti-6Al-4V	0.89	5.88	5.27	7.68	5.89	0.13
<u>ANODIZED</u>						
CP-Ti	0.92	4.08	1.55	87.4	6.94	0.10

The C_c for the passivated condition is only slightly higher than for the polished condition of the same material. Similarly, the C_c for the Ti-6Al-4V is only slightly higher than for the CP-Ti with the same surface treatment. The similarity in the capacitive nature of these different conditions is evident in the overlap of the capacitive regions in Figures 27, 29, 33, and 35. The C_c for the anodized CP-Ti is somewhat lower than for the other conditions which is evident in the upward shift of its curve, as seen in Figure 33. These trends correlate well with the oxide thicknesses revealed by the AES depth profiles given in Figures 40 to 44. These show that the polished and passivated surfaces have similar oxide thicknesses but the anodized CP-Ti sample has a much thicker oxide. This suggests a connection between the oxide thickness and the coating capacitance, as would be expected.

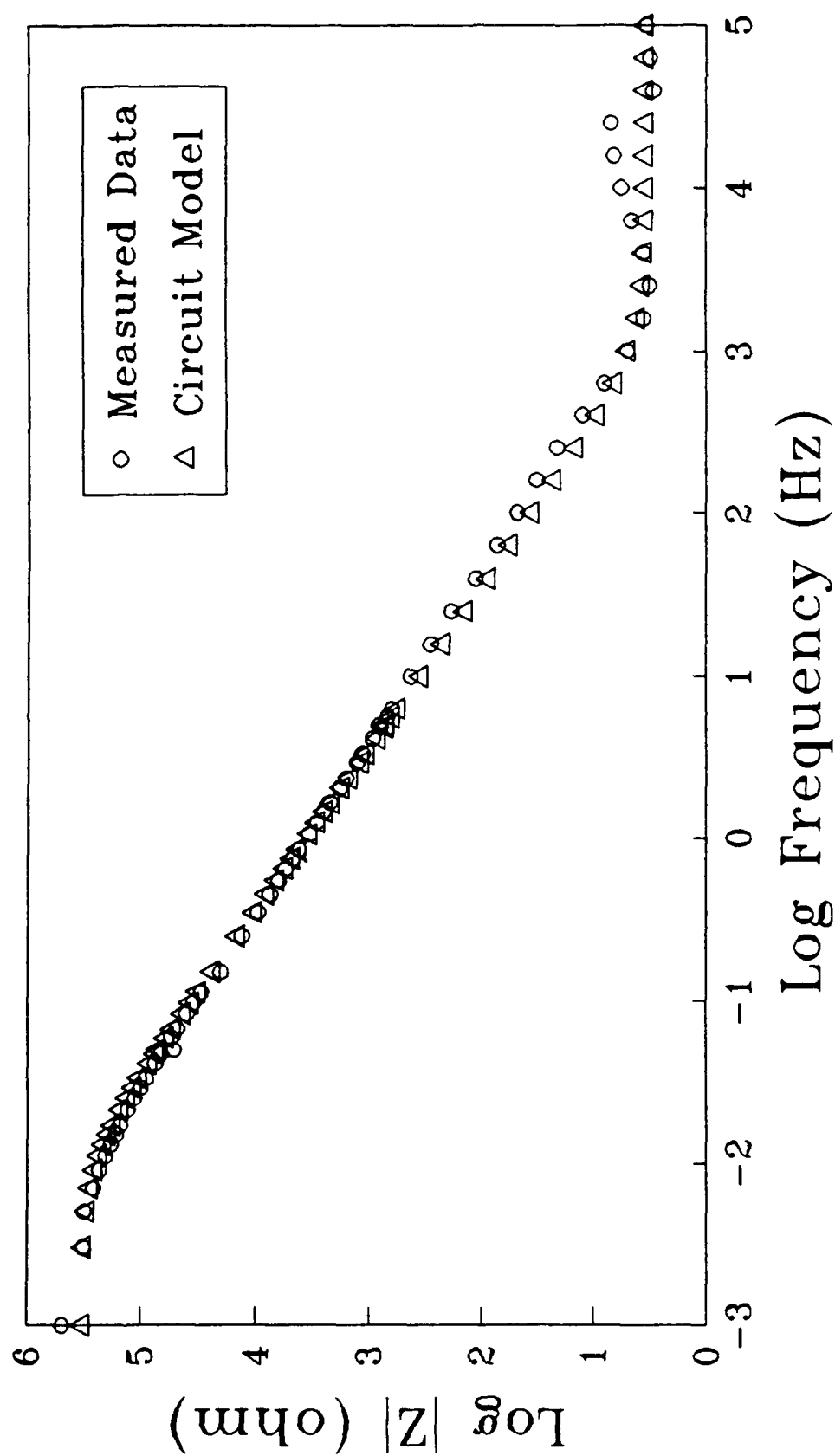


FIGURE 48a. Bode magnitude plot comparing the average measured values to the calculated equivalent circuit values for polished CP-Ti.

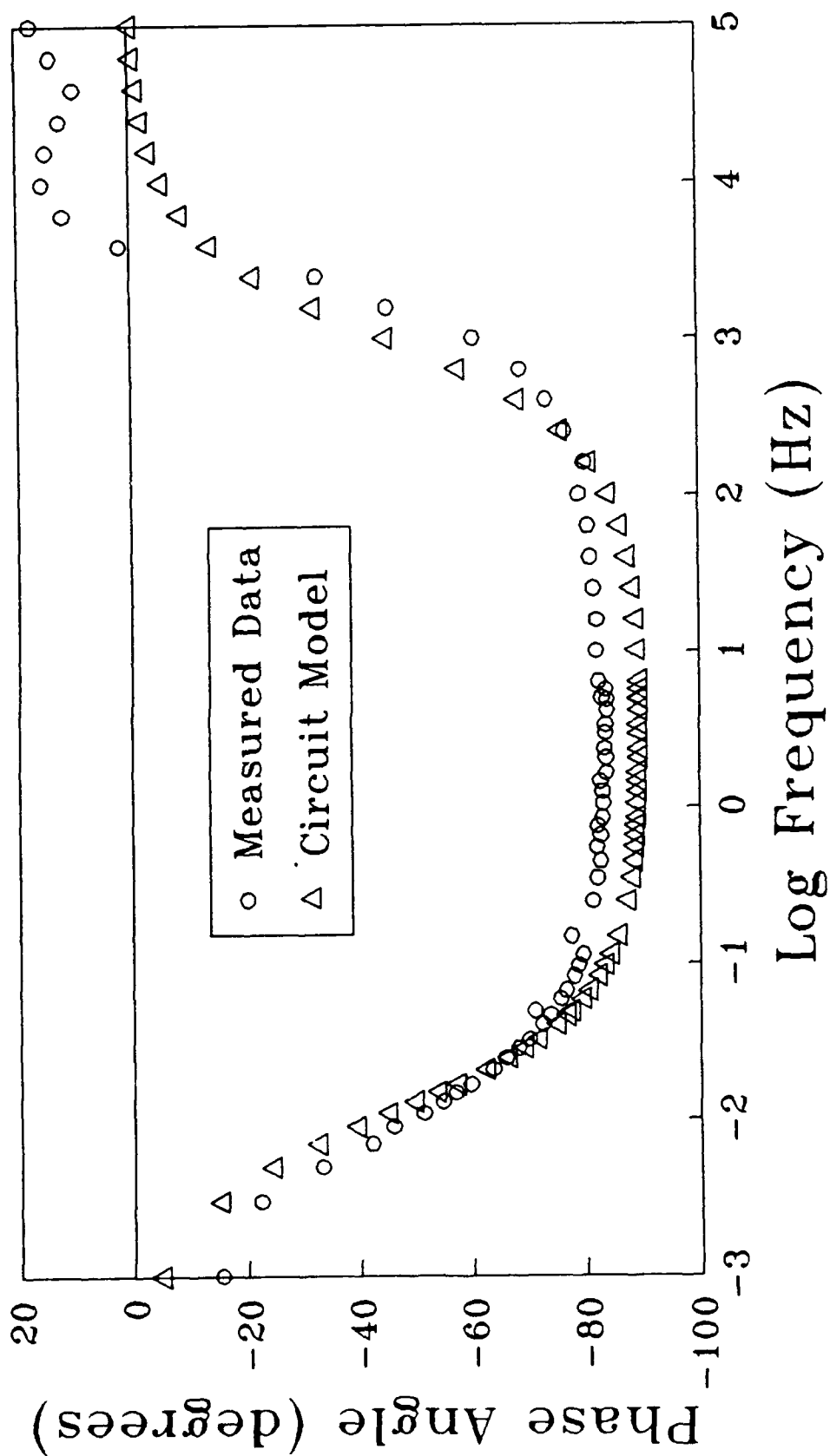


FIGURE 48b. Bode phase angle plot comparing the average measured values to the calculated equivalent circuit values for polished CP-Ti.

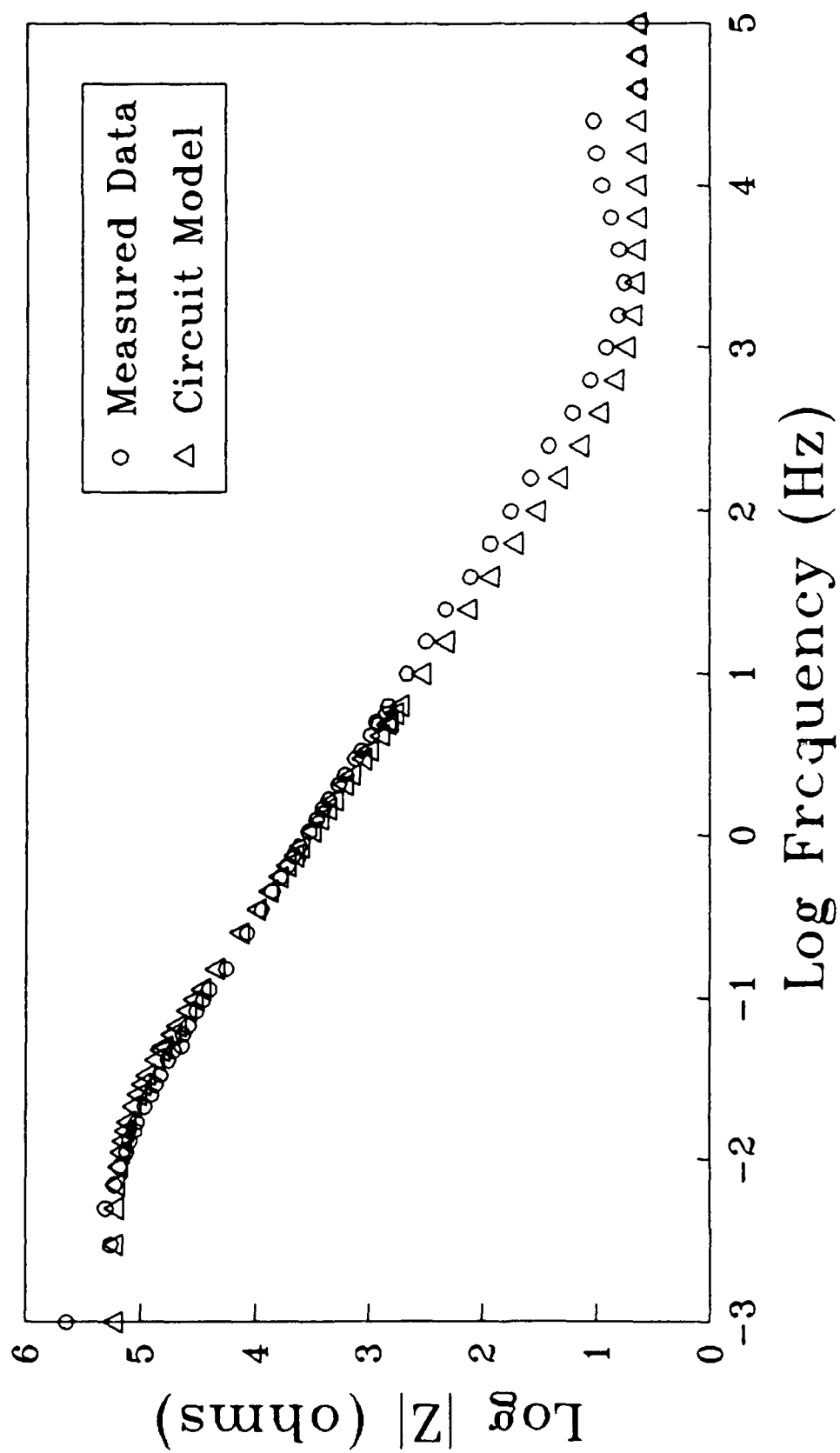


FIGURE 49a. Bode magnitude plot comparing the average measured values to the calculated equivalent circuit values for polished Ti-6Al-4V.

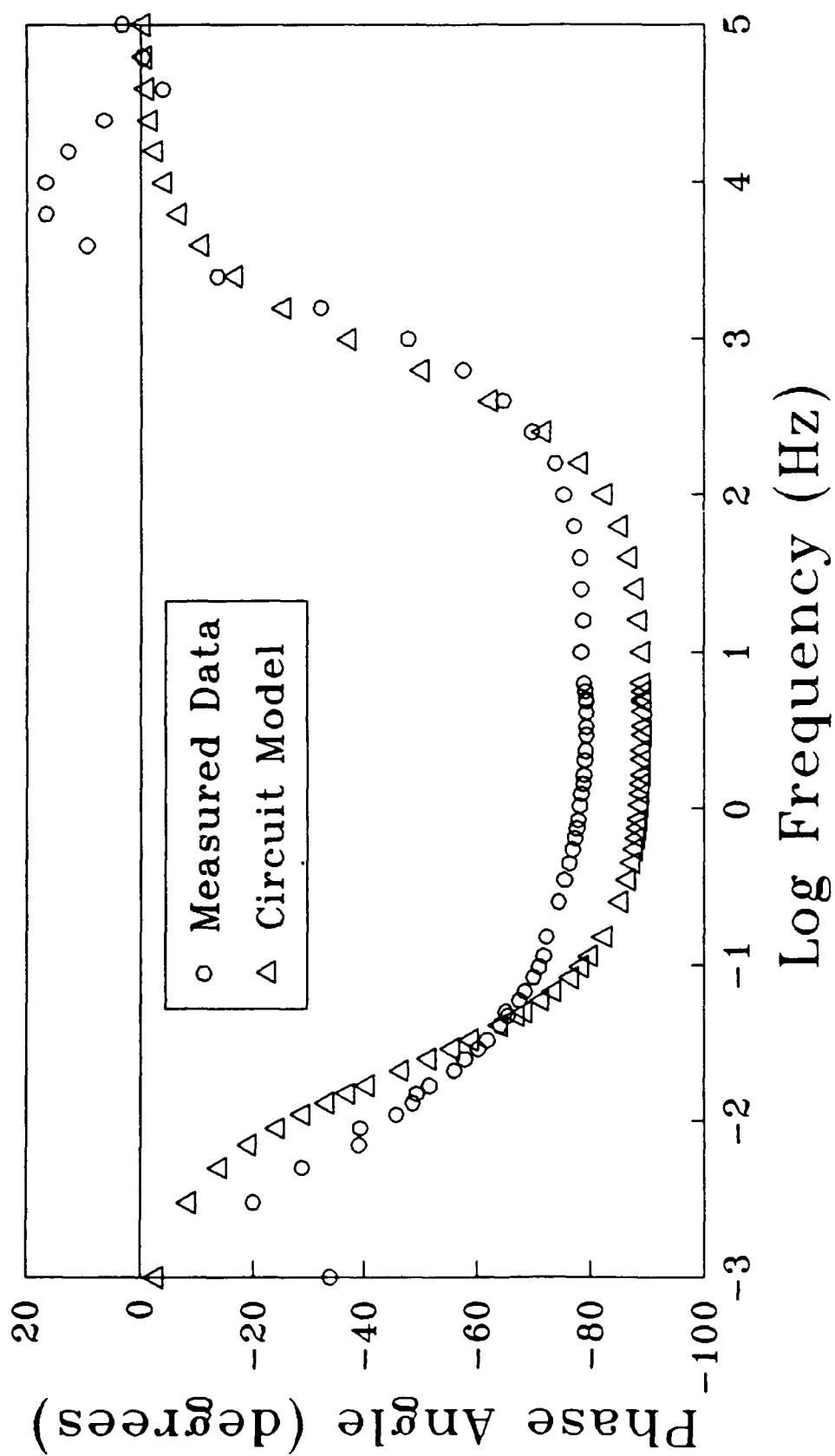


FIGURE 49b. Bode phase angle plot comparing the average measured values to the calculated equivalent circuit values for polished Ti-6Al-4V.

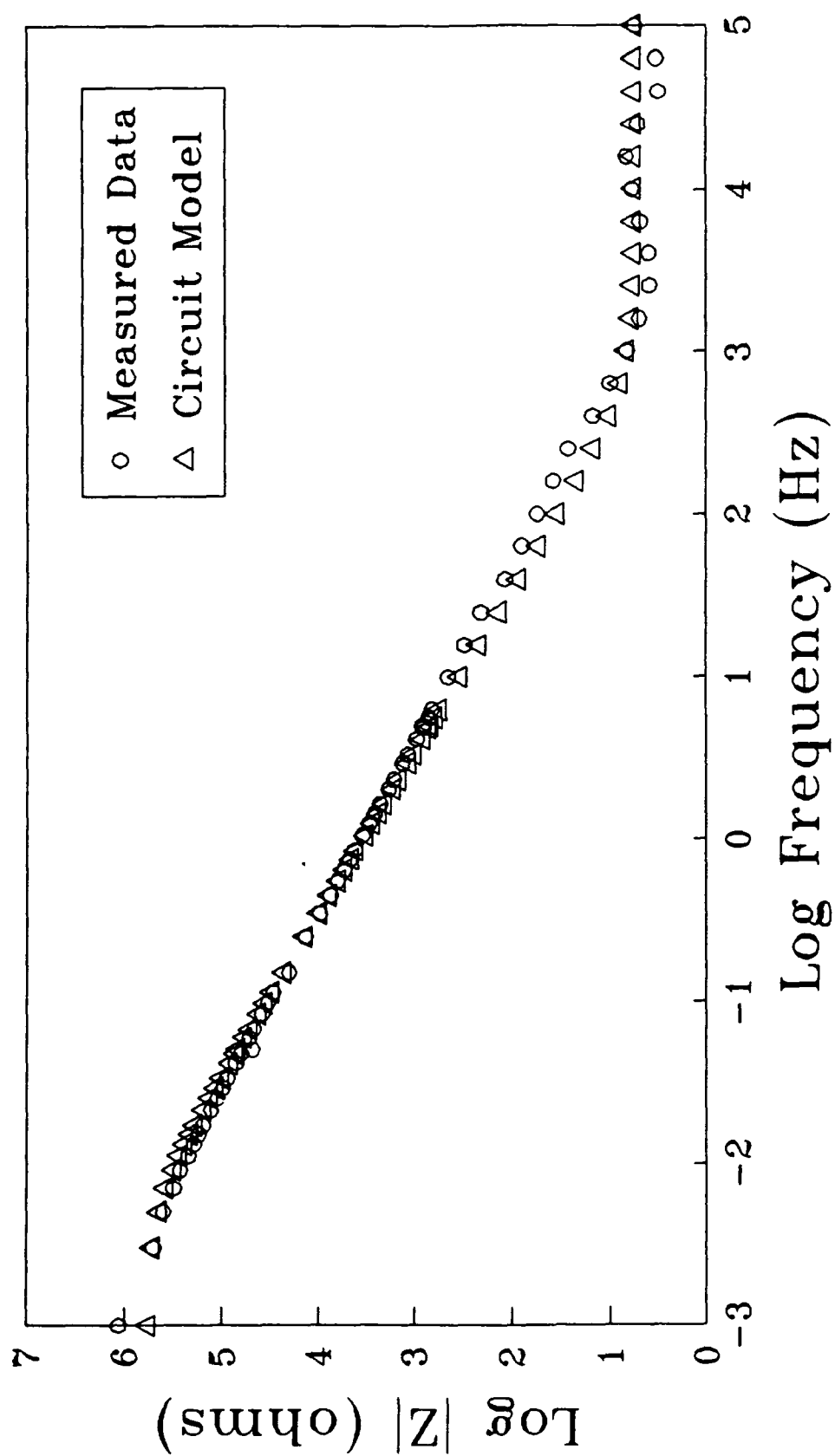


FIGURE 50a. Bode magnitude plot comparing the average measured values to the calculated equivalent circuit values for passivated CP-Ti.

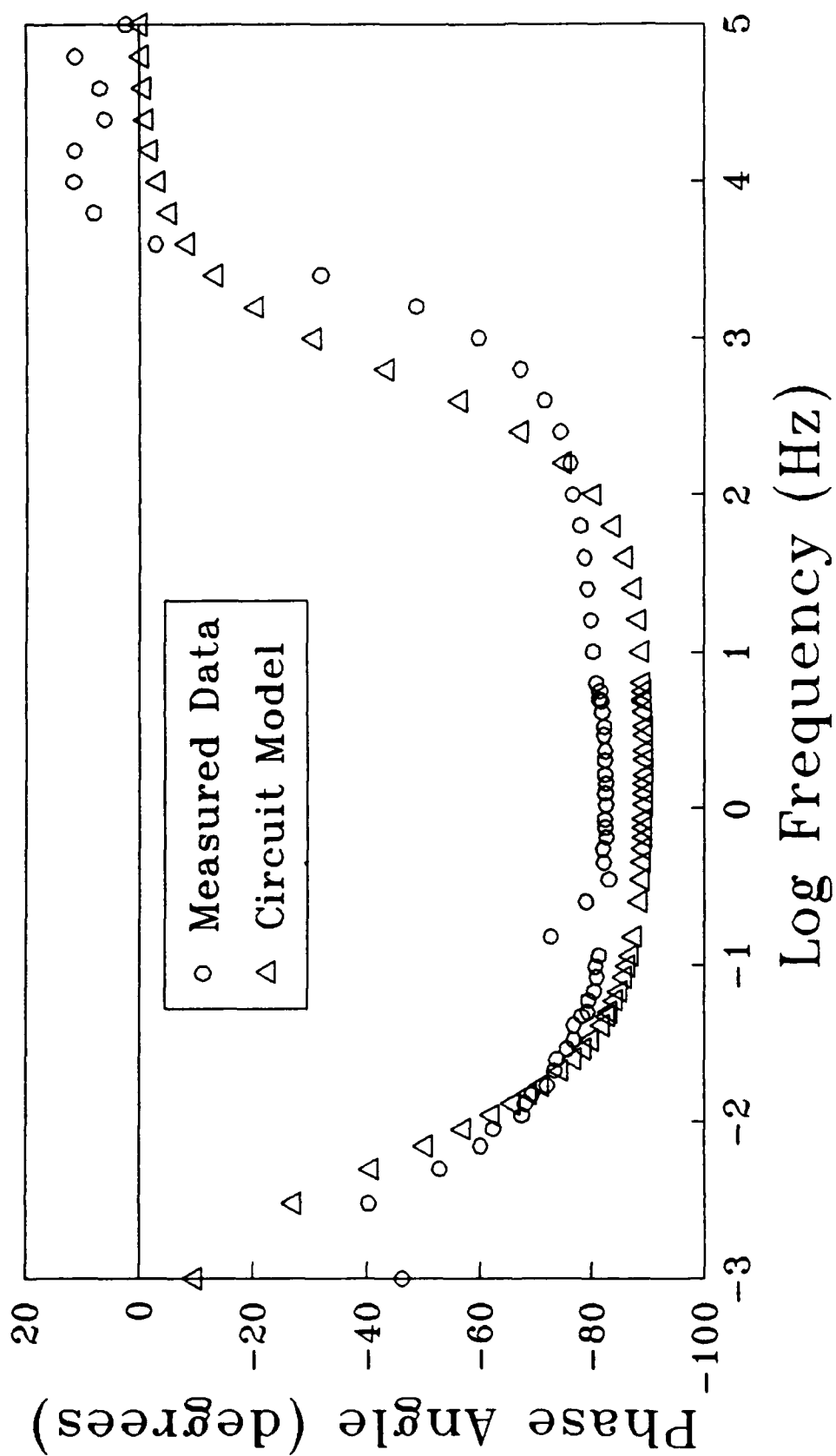


FIGURE 50b. Bode phase angle plot comparing the average measured values to the calculated equivalent circuit values for passivated CP-Ti.

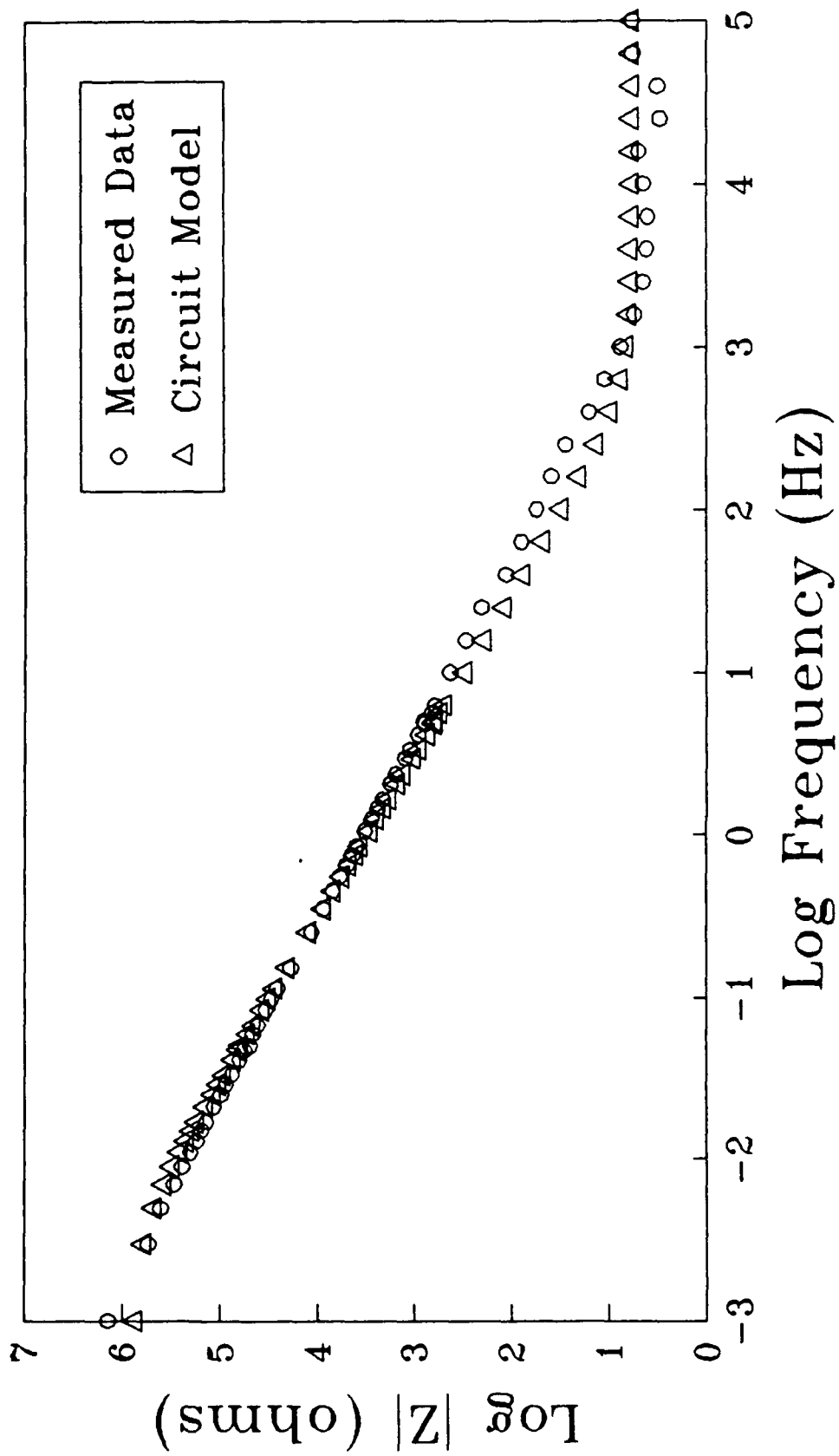


FIGURE 51a. Bode magnitude plot comparing the average measured values to the calculated equivalent circuit values for passivated Ti-6Al-4V.

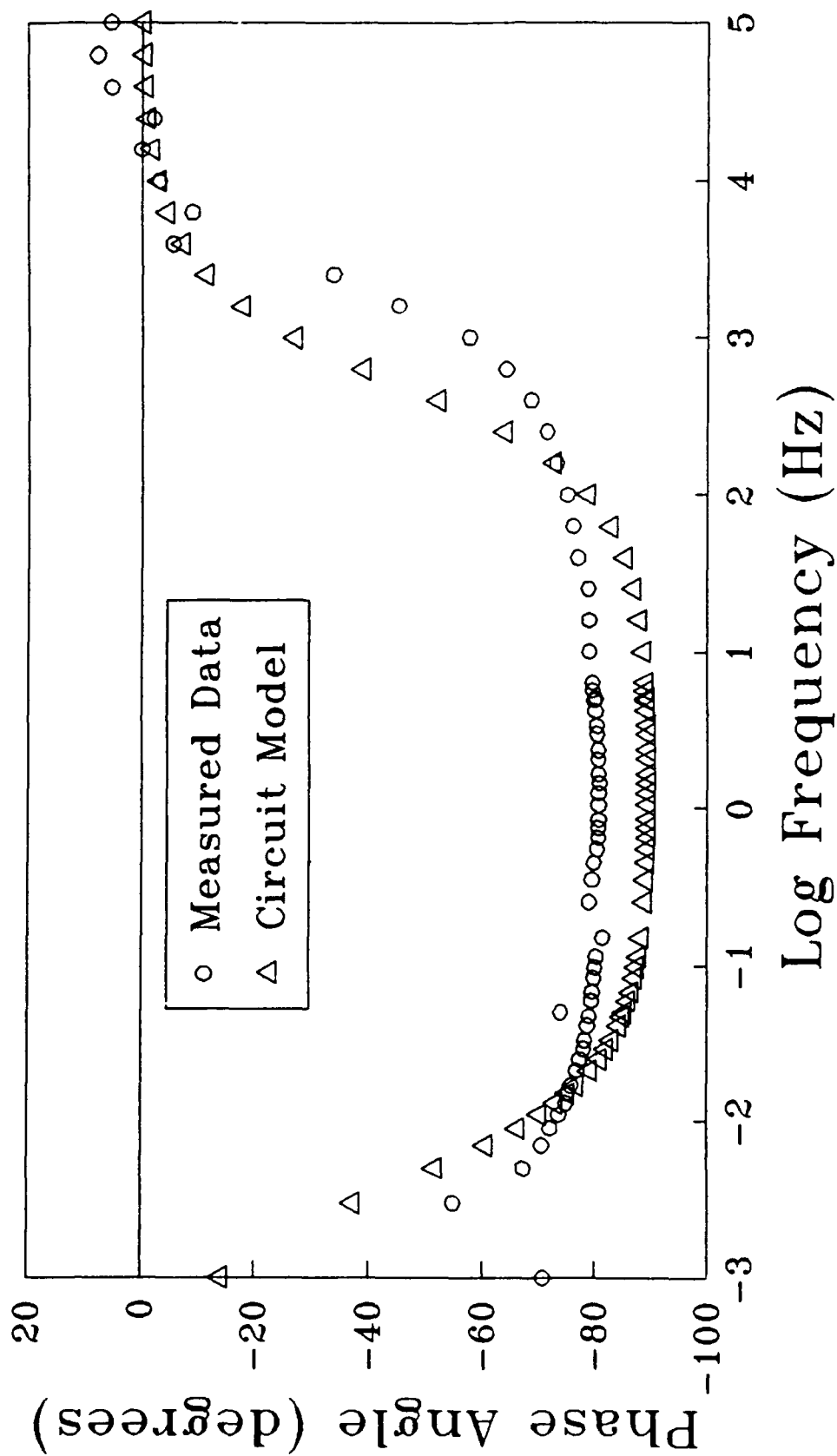


FIGURE 51b. Bode phase angle plot comparing the average measured values to the calculated equivalent circuit values for passivated Ti-6Al-4V.

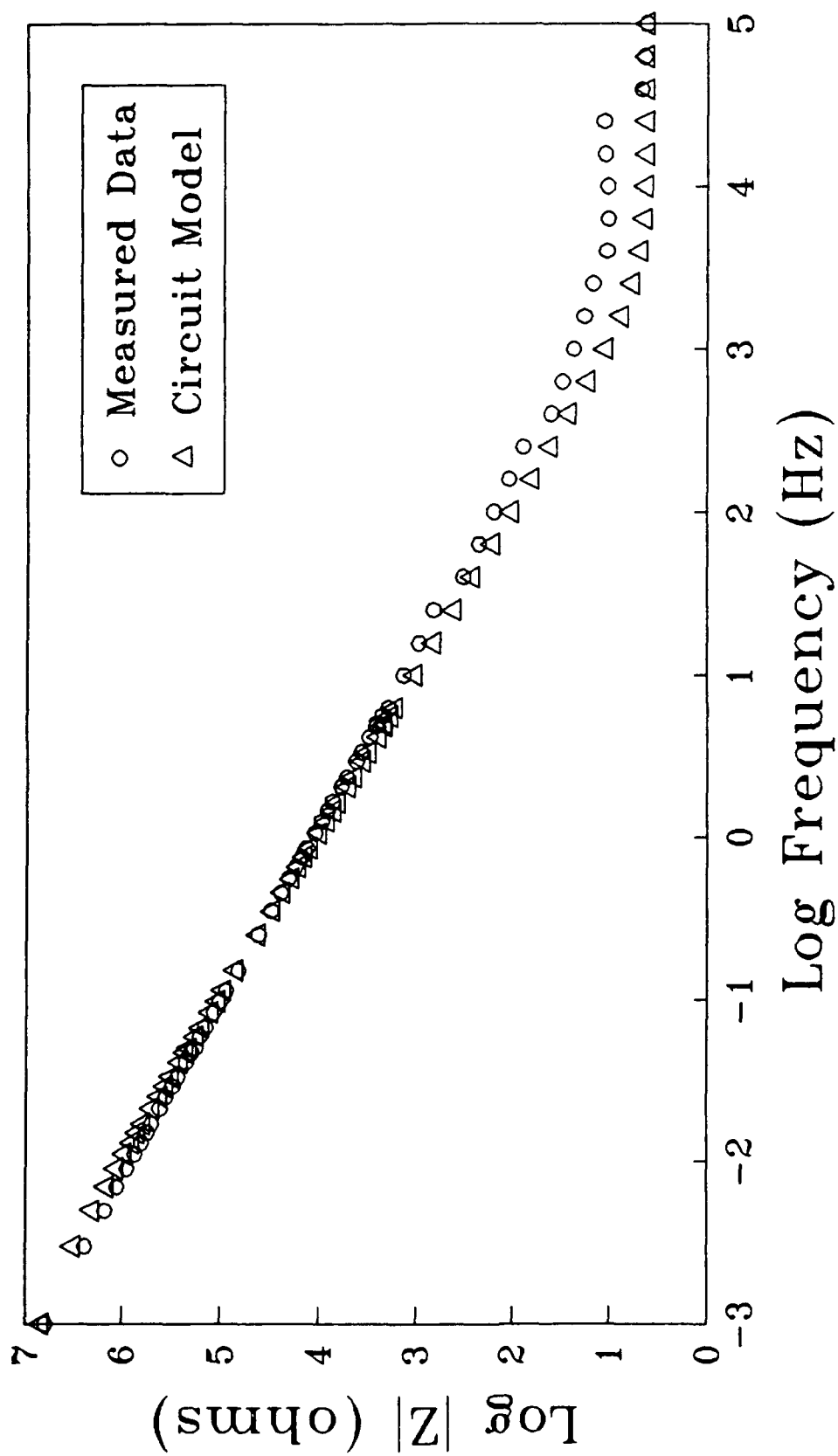


FIGURE 52a. Bode magnitude plot comparing the average measured values to the calculated equivalent circuit values for anodized CP-Ti.

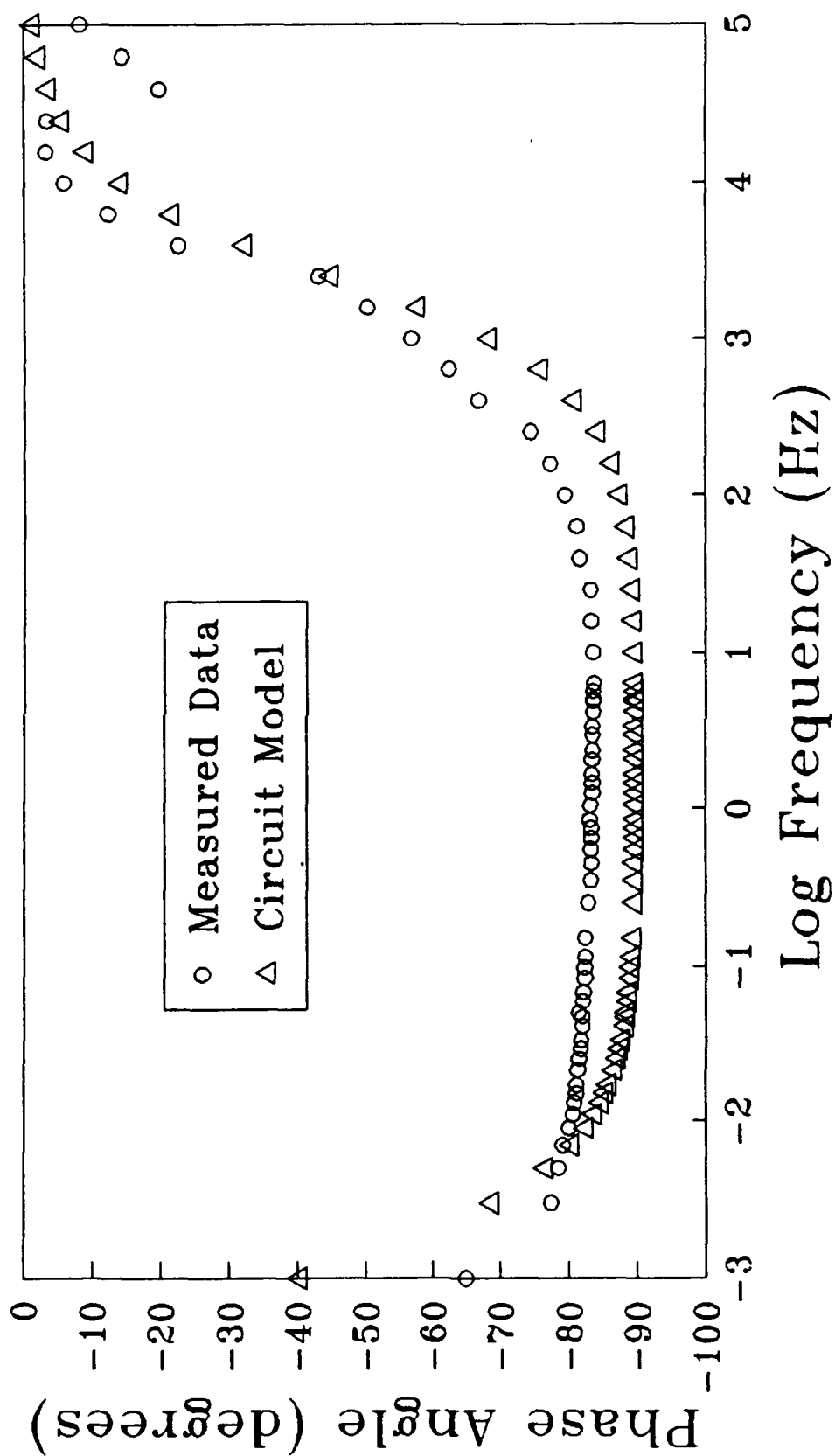


FIGURE 52b. Bode phase angle plot comparing the average measured values to the calculated equivalent circuit values for anodized CP-Ti.

The Bode magnitude plot for each of the polished surfaces in Figures 48a and 49a shows a distinct plateau at low frequencies. Therefore, for these cases, R_p can be read directly from the Bode magnitude plot. The values obtained by this method are the same as those in Table 6 which were calculated by the curve fitting routine.

The Bode magnitude plots for the passivated samples in Figures 50a and 51a, however, do not show this plateau at low frequencies. In order to determine the R_p graphically, the Bode phase angle plots in Figures 50b and 51b can be extrapolated until the point where the low frequency end reaches -30 degrees. The frequency at which this occurs can be considered to be zero and the R_p can be read off of the Bode magnitude plot at this frequency. Applying this technique yields the same values for R_p as were obtained from the circuit model and are given in Table 6.

The R_p 's for the passivated surfaces are somewhat higher than those for the polished surfaces. One trend of interest is that the R_p is lower for the Ti-6Al-4V than for the CP-Ti in the polished condition, whereas in the passivated condition the Ti-Al-4V has the higher R_p . This is evident in the Bode plots in Figures 27, 29, 33 and 35, and agrees with the slightly thicker oxide on the passivated Ti-6Al-4V, as seen in the EIS depth profiles (Figures 40 to 43). This suggests that the Ti-6Al-4V samples more readily oxidize than the CP-Ti samples.

The graphical determination of R_p that was performed for the polished and passivated samples can not be applied to the anodized CP-Ti. This is because the Bode phase angle curve, as seen in Figure 52b, does not extend to a low enough frequency to accurately extrapolate the frequency at which this curve reaches -30 degrees. It is obvious that the curve has begun to curve upward so it can be assumed that the zero frequency condition would be achieved within a short distance of the lowest frequency measured. From the trends of both the Bode phase angle and the Bode magnitude curves for the anodized CP-Ti, it is apparent that the R_p should be greater than $\log 7$. The circuit model does not support this, and merely reports the lowest value recorded. This is due to the mismatch of the phase angles for the model and the measured data at low frequencies, as is evident in Figure 52b.

Even with the above discrepancies, the R_p for the anodized CP-Ti is more than an order of magnitude greater than that for any of the other conditions discussed thus far. This is evident in the anodized CP-Ti curve in Figure 35 and correlates with the AES depth profile in Figure 44, which shows an oxide that is at least twice as thick as the oxide on any of the other samples discussed thus far. The distinctly higher R_p 's for the samples with thicker oxides indicates a definite link between R_p and oxide thickness.

The R_p 's in Table 6 that were obtained from these circuits compare quite well with the R_p 's obtained from the potentiodynamic polarization given in Table 5. This agreement

is greatest for the polished samples. For the passivated samples, however, the R_p 's obtained from the potentiodynamic polarization are somewhat higher. This is most likely due to the large variation in E_{corr} for the passivated potentiodynamic polarization samples. The R_p for the anodized CP-Ti obtained from the potentiodynamic polarization is significantly higher than that obtained by EIS. This is due to the fact that the EIS was not conducted to low enough frequencies to approach the zero frequency condition. Consequently, the R_p obtained from the potentiodynamic polarization should be considered to be more accurate.

The chi-squared values obtained for these five models suggest a reasonably good fit to the data. The plots of these models in Figures 48 through 52 confirm this. In all of these models, however, the phase angle goes to -90 degrees while the test data goes to only about -75 to -85 degrees. This is because in the model, all frequency dependent, or imaginary components of the impedance are accounted for by a pure capacitor.

The anodized Ti-6Al-4V behaved significantly different than any of the other cases, which is why it is being addressed separately. The Bode plots for this condition in Figures 31 and 35, as well as the corresponding Nyquist plots in Figures 32 and 36, reveal the presence of three time constants. This is evident in the three regions of the Bode phase angle curve that are concave up which occur at about -2, -1 and 4 on the log frequency scale. These changes in

curvature indicate that there are three frequency dependent processes occurring on the surface of the anodized Ti-6Al-4V, as opposed to only one frequency dependent process on all of the other samples.

Due to the multiple time constants, the only information that could be taken directly off of the data plots was the R_Q . Obviously the same model that was used to fit the other cases would not work here due to the multiple frequency dependent processes. Consequently, the model would have to have a minimum of three frequency dependent components.

The literature contains several models for coatings with different characteristics. As previously mentioned, during anodization, the Ti-6Al-4V samples turned a blue color before they obtained their final yellow color. This suggests that these samples formed a layer of TiO_2 first and a layer of $TiO_3 \cdot 2H_2O$ on top of that, resulting in a two layer coating. Furthermore, the AES depth profile data (Figures 44 and 45) reveals that the oxide coating is nearly twice as thick on the anodized Ti-6Al-4V as what it is on the anodized CP-Ti. The potentiodynamic polarization results for these same two cases in Table 5, however, show the anodized CP-Ti to have the better corrosion properties. Therefore, it can be concluded that the coating on the anodized Ti-6Al-4V, although thicker than that on the anodized CP-Ti, does not offer as much protection to the surface.

Assuming the blue coating that formed initially is the same as that which formed on the CP-Ti samples, the first

layer can be modeled by the same circuit used for the anodized CP-Ti samples. To account for the oxide being substantially thicker on the anodized Ti-6Al-4V than on the CP-Ti without providing substantially better corrosion protection, the second layer can be modeled as a porous layer. This model is depicted in Figure 53. This model was presented by Juettner and Lorenz²⁴ as a model for the corrosion of anodized aluminum.

In this model, C_{c1} and R_{p1} are the coating capacitance and polarization resistance for the first, non-porous layer. No matter which path taken through the porous layer, the same sub-circuit must be traversed in order to get through this first layer to the base metal. R_{p0} is the resistance through the pores. C_{c2} and R_{p2} are the coating capacitance and polarization resistance for the non-porous portion of the second layer. Again, R_0 is the solution resistance.

The values of C_{c1} and R_{p1} were initially taken to be the same as those for the anodized CP-Ti sample. The values of C_{c1} and R_{p1} were adjusted to account for a different thicknesses of oxide than what was on the anodized CP-Ti sample. Both of these values are related to the oxide thickness, however, so changes in their magnitudes must relate to the same corresponding change in thickness. Since the oxide is so much thicker on the anodized Ti-6Al-4V, and since this sample went beyond blue to yellow during anodization, the TiO_2 was considered to be thicker on the anodized Ti-6Al-4V than on the anodized CP-Ti. Consequently, the value of C_{c1} was decreased and the value for R_{p1} was increased. With these two values,

Solution $\text{TiO}_3 \cdot 2\text{H}_2\text{O}$ TiO_2 Ti-6Al-4V

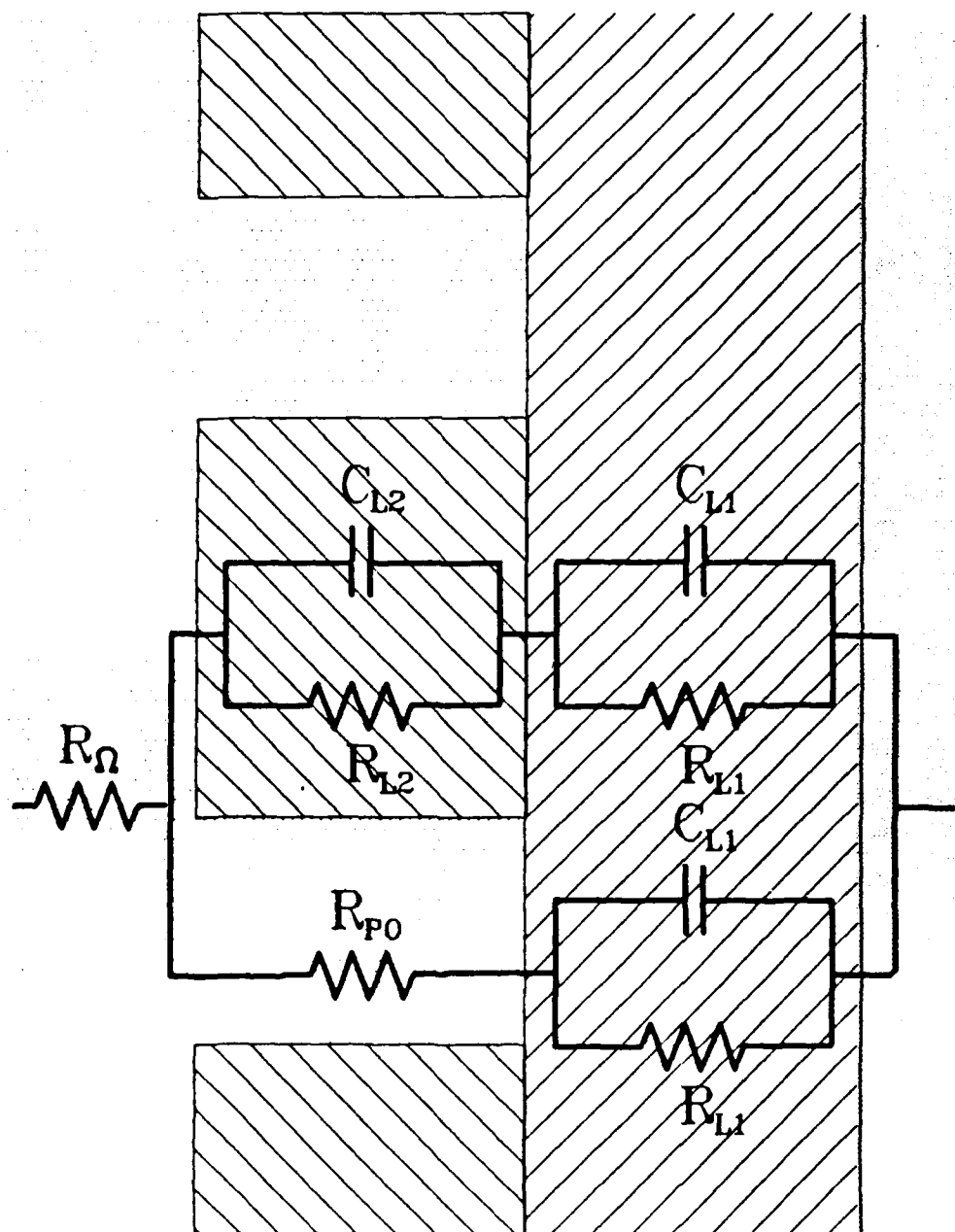


FIGURE 53. Equivalent circuit used to model the anodized Ti-6Al-4V as having a porous layer of $\text{TiO}_3 \cdot 2\text{H}_2\text{O}$ over a non-porous layer of TiO_2 .

as well as the solution resistance fixed, the software adjusted the values of the remaining circuit elements to obtain the best fit to the data.

The values obtained for the different circuit elements are given in Table 7. This circuit is plotted along with the experimental data in Figures 54a and 54b. The Chi-squared value for this fit compares well with the same value from the other tests.

TABLE 7
Circuit Element Values for the
Anodized Ti-6Al-4V Circuit Model

R_0 (Ω)	C_{c1} (F) $\times 10^{-6}$	R_{p1} (Ω) $\times 10^6$	R_{p0} (Ω) $\times 10^4$	C_{c2} (F) $\times 10^{-7}$	R_{p2} (Ω) $\times 10^5$	Chi ²
4.15	9.5	9.5	1.02	6.83	3.84	0.13

Since the Bode magnitude plot did not reach a plateau at low frequencies and since the Bode phase angle plot shows no trend toward zero, the total polarization resistance for the system $R_{p_{tot}}$ must be found another way. This can be done by assuming a zero frequency which causes all capacitors to go to an infinite capacitance. The remaining resistors can then be added to obtain the $R_{p_{tot}}$ as follows: $1/R_{p_{tot}} = [1/(R_{p0} + R_{p1})] + [1/(R_{p2} + R_{p1})]$. This gives a total polarization resistance of 4.85×10^6 or $\log 6.69 \Omega$. This value is slightly lower than that found by potentiodynamic polarization, as given in Table 5.

This value is also considerably lower than that which was determined by EIS for the anodized CP-Ti. This is reasonable since the potentiodynamic polarization also produced a lower

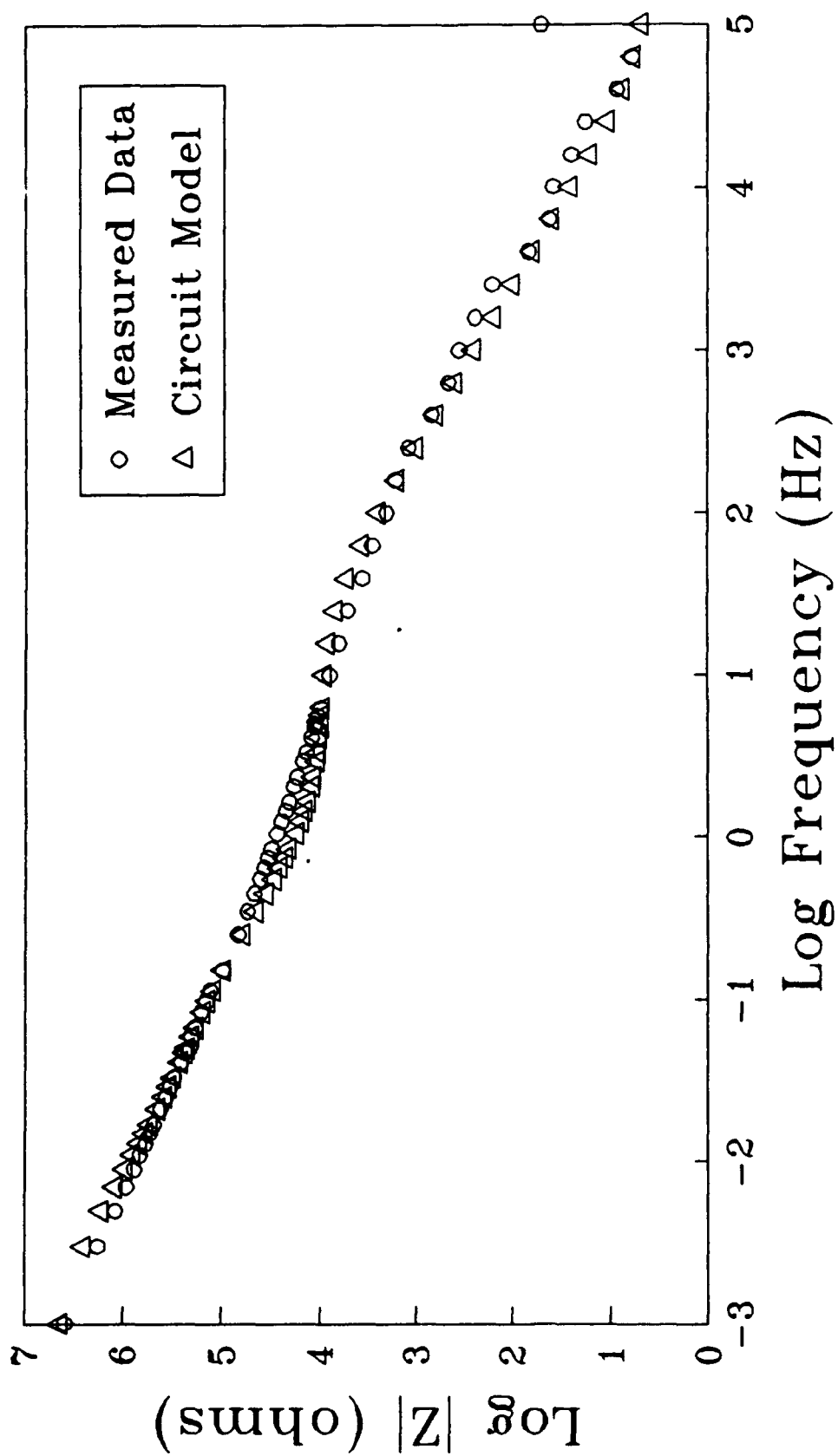


FIGURE 54a. Bode magnitude plot comparing the average measured values to the calculated equivalent circuit values for anodized Ti-6Al-4V.

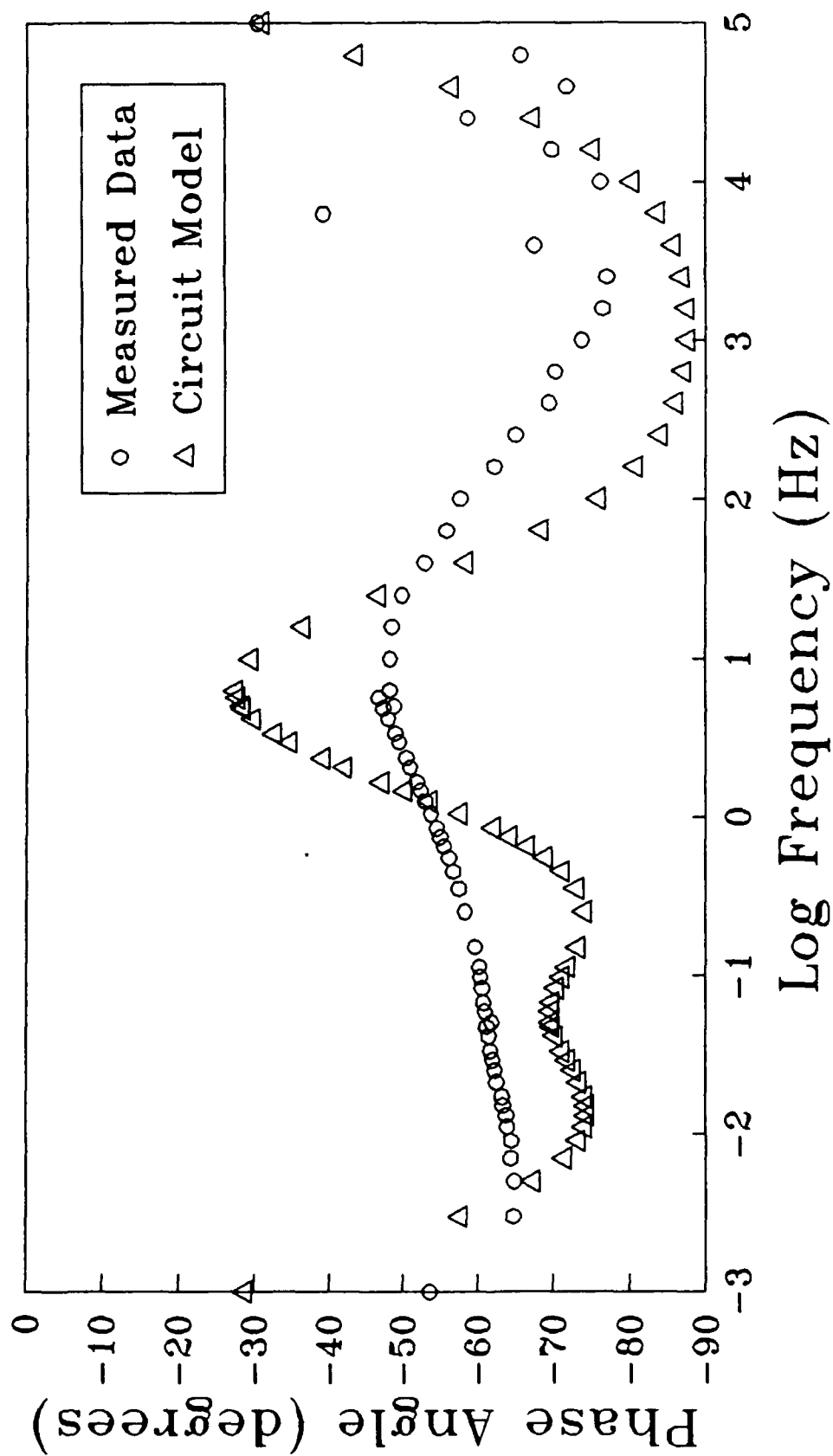


FIGURE 54b. Bode phase angle plot comparing the average measured values to the calculated equivalent circuit values for anodized Ti-6Al-4V.

R_p for the anodized Ti-6Al-4V than anodized CP-Ti. What seems unusual, however, is the fact that for the anodized Ti-6Al-4V, the TiO_2 layer was modeled as being thicker than that on the anodized CP-Ti, yet the Ti-6Al-4V has a lower R_p .

This can be partially accounted for by the faster oxidation of the Ti-6Al-4V, but more importantly it is the affect of that second layer. It would seem that the second layer, instead of offering additional protection to the material, is actually causing additional oxidation. This further supports the idea that the second, yellow layer is $\text{TiO}_3 \cdot 2\text{H}_2\text{O}$ because this substance is unstable in the presence of water and has an oxidizing power similar to that of hydrogen peroxide.²⁹ Thus, rather than offering further protection to the base material, this oxide tends to cause further oxidation. This results in the lower R_p seen for the anodized Ti-6Al-4V than would be expected by its oxide thickness. It is worth repeating that the formation of $\text{TiO}_3 \cdot 2\text{H}_2\text{O}$ is not limited to Ti-6Al-4V, as this same oxide has been produced on CP-Ti with only changes in the viscosity and the concentration of the anodizing solution.

Auger Electron Spectroscopy

Auger Electron Spectroscopy was used to correlate the EIS trends with oxide thicknesses. As previously mentioned, the AES depth profile data presented in Figures 40 through 45 and in Table 4 provide oxide thicknesses in terms of the number of sputtering cycles required for the oxygen signal to reach a plateau near zero.

Both materials have about the same oxide thickness in the polished condition due to the rapid oxidation of the surface during the one hour from the time the sample was polished to the time it was placed into the ultra-high vacuum of the AES microscope.

The passivated CP-Ti has the same oxide thickness as the polished samples, whereas the passivated Ti-6Al-4V sample has a somewhat thicker oxide. It was expected that for both samples the oxide would be noticeably thicker for the passivated condition than for the polished condition. The corrosion tests supported this by indicating lower corrosion rates for the passivated surfaces. The apparent discrepancy in the measured oxide thickness may be due to the variability of the passivation process. This variability was evident in the large deviations in the corrosion data for the passivated samples. The instability of the passivated surfaces, as discussed previously in the potentiodynamic polarization section of the discussion, may also have contributed to the apparent discrepancy in oxide thicknesses.

The most interesting case is that of the anodized surfaces. Both of these surfaces have considerably thicker oxides than the passivated samples of the same material. The Ti-6Al-4V sample, however, has a significantly thicker oxide than the CP-Ti. This further supports the notion that the Ti-6Al-4V oxidizes more rapidly than the CP-Ti. Additionally, the depth profiles for the anodized surfaces are unique in that they show a region of fairly steady composition near the

surface with phosphorous incorporated into it. This is due to the anodization process, which uses phosphoric acid as an oxidizer, and shows that some of the phosphorous is trapped in the oxide. The depth to which the phosphorous is found gives an indication of the integrity of the oxide coating.

During anodization, once the surface begins to oxidize, the phosphoric acid has to penetrate through this initial coating to attack the metal underneath. Consequently, the deeper the phosphorous is observed on the AES depth profile, the more porous the oxide. The depth profile for the CP-Ti shows that for this sample the level of phosphorous is fairly constant for about the first 5 cycles and then rapidly drops off. This suggests that this oxide is only slightly porous near the surface.

For the Ti-6Al-4V, the depth profile reveals a fairly constant phosphorous level out to about 10 cycles, which then slowly drops off. This indicates a porous layer near the surface that does little to restrict the diffusion of the phosphoric acid, while further into the oxide, the amount of porosity decreases. This porous region near the surface correlates with the suspected layer of porous $\text{TiO}_3 \cdot 2\text{H}_2\text{O}$, while the region underneath correlates with a non-porous layer of TiO_2 .

Summary

The polished samples of CP-Ti and Ti-6Al-4V produced very similar potentiodynamic polarization test results. They also produced similar EIS test results. Furthermore, there is

little difference in the R_p 's produced by the two different methods as shown in Table 8. The similarities between the two materials in the polished condition are substantiated by their nearly identical oxide layer thicknesses as shown by AES depth profiles.

TABLE 8
Summary of Corrosion Results

SURFACE	OXIDE THICKNESS (# OF CYCLES)	Log R _p (Ω)	
		Pot. Pol.	EIS
<u>POLISHED</u>			
CP-Ti	9	5.45	5.51
Ti-6Al-4V	8	5.46	5.21
<u>PASSIVATED</u>			
CP-Ti	8	6.13	5.76
Ti-6Al-4V	13	6.13	5.89
<u>ANODIZED</u>			
CP-Ti	22	7.28	6.94
Ti-6Al-4V	31	7.05	6.69

The passivated samples also produced similar potentiodynamic polarization test results. The EIS test results, however, showed a higher R_p for the Ti-6Al-4V sample as would be expected by its thicker oxide layer found by AES depth profile. The R_p 's obtained by potentiodynamic polarization are slightly higher than those obtained by EIS, as listed in Table 8. Furthermore, the passivated samples have higher R_p 's than the polished samples.

The CP-Ti formed a layer of stable adherent TiO_2 during the anodization process which gave it a blue color.

Initially, the Ti-6Al-4V formed a blue layer, but this changed to yellow before the anodization process was complete. This yellow layer is suspected to be $\text{TiO}_3 \cdot 2\text{H}_2\text{O}$ which is unstable in water.

Both of the materials produced potentiodynamic polarization results similar to those for the polished and passivated conditions. Both anodized samples had R_p 's from the potentiodynamic polarization that were higher than those of the polished and passivated conditions, with the R_p for the anodized CP-Ti being the higher of the two.

The EIS tests of the anodized CP-Ti produced the same trends as those of the polished and passivated conditions due to the same type of oxide layer. The R_p obtained from the EIS test of the anodized CP-Ti was much higher than those obtained for the polished and passivated conditions due to the much thicker oxide on the anodized CP-Ti. This value of R_p was again slightly lower than that obtained from the potentiodynamic polarization tests of the same material.

The EIS tests of the anodized Ti-6Al-4V show a trend completely different from the tests for all of the other conditions. This is due to the presence of two different oxide layers, one which is porous and another which is non-porous. This results in a R_p that is lower than that of the anodized CP-Ti even though the anodized Ti-6Al-4V has a much thicker oxide layer as shown by the AES depth profile. This R_p for the anodized Ti-6Al-4V which was obtained from EIS is

again lower than the same value as determined by potentiodynamic polarization as listed in Table 8.

CHAPTER VI

CONCLUSIONS

This study began with the aim of proving or disproving several hypotheses which were stated in the introduction. In this section, each of these hypotheses will be restated and addressed in terms of the findings of this study. Furthermore, additional conclusions will be drawn which were not foreseen when this project began.

1. For the same surface preparation, CP-Ti will be more corrosion resistant than Ti-6Al-4V.

In the polished condition CP-Ti has the better corrosion resistance as determined by EIS. In the passivated condition Ti-6Al-4V has the better corrosion resistance as determined by EIS due to its thicker oxide layer. Potentiodynamic polarization showed little or no difference between the corrosion resistance of the two metals in either the polished or passivated conditions. In the anodized condition the CP-Ti has better corrosion resistance than Ti-6Al-4V as, determined by both potentiodynamic polarization and EIS. This is due to the more protective oxide that formed on the CP-Ti.

2. For the same material, the anodized condition will be more corrosion resistant than the passivated condition,

which will be more corrosion resistant than the polished condition.

This holds true for both materials and both corrosion measuring techniques employed. The difference in corrosion resistance between the anodized and the passivated conditions is much greater than that between the passivated and the polished conditions. The passivated condition, however, shows considerable variability, and in a particular case this relation may not hold.

3. For the same material, the oxide layer on the anodized sample will be thicker than the oxide layer on the passivated sample, which will be thicker than the oxide layer on the polished sample.

The oxide layer on the anodized surface is thicker than that for either the passivated or the polished surfaces. Due to the instability of the oxide layers on the passivated surfaces, these oxide layers are not always thicker than the oxide layers on the polished samples.

4. A thicker oxide coating will correspond to a lower corrosion current density as, determined from potentiodynamic polarization.

This generally holds true as long as the two oxides being compared are the same type of oxide. That is, as long as the two oxides being compared have the same chemical makeup, then the thicker oxide will result in the lower corrosion current density.

5. The polarization resistance obtained from the EIS will be equal to the polarization resistance, as determined from the potentiodynamic polarization.

This is essentially true, although there are slight variations between the values obtained from the two different techniques. Generally, the R_p obtained from the EIS test is slightly more conservative.

6. The resistance calculated from the applied current and potential during anodization will be the same as that calculated from the equilibrium current and potential.

This is false. The resistances calculated from these two process are not even close to being the same because these are two entirely different processes and as such should not be compared.

7. The impedance data for the different materials and surface preparations will behave as similar electrical circuits.

This is true as long as the surface layers on the samples being compared have the same chemical makeup. That is, as long as the samples being compared have the same form of oxide, they will fit the same circuit model.

8. A thicker oxide coating will correspond to higher pore resistances and higher coating capacitances as determined from EIS.

The effect of oxide coating thickness on pore resistance cannot be verified in this study since only one of the conditions tested had a pore resistance. With regards to

coating capacitance, a thicker oxide will result in a lower coating capacitance due to the inverse relation between capacitors and impedance. This again is as long as the different oxide layers being compared are the same form of the oxide.

Other conclusions that can be drawn but were not foreseen at the start of this study are listed below.

Although both potentiodynamic polarization and EIS tests reveal the same information about the rate of corrosion of a material, the EIS test offers insight into the mechanisms of the corrosion.

The oxide produced on Ti-6Al-4V and CP-Ti by the passivation procedure in ASTM F86 is inconsistent in the way the oxide forms on the surface and in the way that the oxide deteriorates after the passivation process.

The oxide produced by anodization is significantly affected in both thickness and composition by small changes in conditions.

The effect of an oxide on the corrosion properties of CP-Ti and Ti-6Al-4V depends on both oxide thickness and oxide composition.

REFERENCES

1. S.B. Goodman, V.L. Fornasier, J. Lee, and J. Kei, J Biomed Mat Res 24, 11(1990): pp. 1539-1549.
2. R.A. Goyer, Metals Handbook, vol.2, 10th ed. (USA: ASM International, 1990), pp. 1233-1269.
3. ASTM F67-88 Standard Specification for Unalloyed Titanium for Surgical Implant Applications (Philadelphia, PA: American Society for Testing and Materials [ASTM], 1988), pp.7-9.
4. ASTM F136-84 Standard Specification for Wrought Titanium 6Al-4V ELI Alloy for Surgical Implant Applications (Philadelphia, PA: American Society for Testing and Materials [ASTM], 1984), pp. 23-25.
5. O.W. Siebert, ASTM STP 866 (Philadelphia, PA: American Society for Testing and Materials [ASTM], 1985), pp. 65-90.
6. EG&G Princeton Applied Research, Model 342 Softcorr Corrosion Measurement Software Operating Manual (Princeton, NJ: PARC, 1989).
7. Refresher on Electrochemical Impedance Techniques, Conference: EG&G Princeton Applied Research 5th Annual Symposium (St. Louis, MO: PARC, Dec 1990).
8. EG&G Princeton Applied Research, Basics of Electrochemical Impedance Spectroscopy, Application Note AC-1 (Princeton, NJ: PARC).
9. R. Granata, Evaluation of Organic Coatings by Electrochemical Impedance Measurements, Application Note AC-2 (Princeton, NJ: PARC).
10. D. D. Macdonald, Corrosion 46, 3(1990): pp. 229-242.
11. J.Titz, G.H. Wagner, H. Spahn, M. Ebert, K. Juttner, and W.J. Lorenz, Corrosion 46, 3(1990): pp. 221-229.
12. M. Pourbaix, Atlas of Electrochemical Equilibria in Aqueous Solution, 2nd ed. (Houston, TX: NACE, 1974).

13. ASTM F86-84 Standard Practice for Surface Preparation and Marking of Metallic Surgical Implants (Philadelphia, PA: American Society for Testing and Materials [ASTM], 1984), pp. 12-14.
14. A.A. Mazhar, F. El-Taib Heakal, and A.G. Gad-Allah, Corrosion 44, 10(1988): pp. 705-710.
15. L.C. Lucas, J.L. Ong, J.E. Lemons, T. Reddrick, and E.D. Rigney, Conference: 17th Annual Meeting of the Society for Biomaterials (Scottsdale, AZ: Society for Biomaterials, 1991), p. 201 (abstract).
16. A. Cigada, M. Cabrini, and P. Pedeferrri, Conference: 17th Annual Meeting of the Society for Biomaterials (Scottsdale, AZ: Society for Biomaterials, 1991), p. 198 (abstract).
17. M.L. Rothstein, Electrochemical Corrosion Measurements for the Metal Finishing Industry, Application Note Corr-5 (Princeton, NJ: PARC, 1986).
18. S.W. Tait, J Coatings Technol 61, 768(1989): pp. 57-61.
19. J.R. Macdonald, Impedance Spectroscopy Emphasizing Solid Materials and Systems (New York, NY: John Wiley & Sons, 1987), pp. 260-316.
20. D.D. Macdonald and M.C.H. McKubre, ASTM STP 727 (Philadelphia, PA: American Society for Testing and Materials [ASTM], 1981), pp. 110-149.
21. W.S. Tait, K.A. Handrich, and J.A. Maier, Conference: SSPC Coating Evaluation and Durability Conference (Pittsburgh, PA: SSPC, 1991), pp. 1-14.
22. H. Shih and F. Mansfeld, Corrosion 45, 4(1989): pp. 325-328.
23. F. Mansfeld, Corrosion 44, 12(1988): pp. 856-868.
24. K. Juttner and W.J. Lorenz, Materials Science Forum 44 & 45 (1989): pp. 191-204.
25. F. Mansfeld and M.W. Kendig, ASTM STP 866 (Philadelphia, PA: American Society for Testing and Materials [ASTM], 1981), pp. 122-142.
26. F. Mansfeld, S. Lin, S. Kim, and H. Shih, Materials Science Forum 44 & 45 (1989): pp. 83-96.

27. I. Epelboin, C. Gabrielli, M. Keddam, and H. Takenouti, ASTM STP 727 (Philadelphia, PA: American Society for Testing and Materials [ASTM], 1981), pp. 150-166.
28. ASTM G5-82 Standard Practice for Standard Reference Method for Making Potentiostatic and Potentiodynamic Anodic Polarization Measurements (Philadelphia, PA: American Society for Testing and Materials [ASTM], 1982), pp. 123-133.
29. J. Schmets, J. Van Muylder, and M. Pourbaix, Atlas of Electrochemical Equilibria in Aqueous Solution, 2nd ed. (Houston, TX: NACE, 1974), pp. 213-222.
30. B.A. Boukamp, Equivalent Circuit: Users Manual, 2nd ed. (Enschede, the Netherlands: University of Twente, 1989).
31. W.S. Tait, K.A. Handrich, S.W. Tait, and J.W. Martin, Conference: ASTM Symposium on Electrochemical Impedance: Analysis and Interpretation (San Diego, CA: ASTM, 1991).